IONIC COMPOSITION OF RAINWATER ON THE BLACK SEA COAST OF TURKEY

A THESIS SUBMITTED TO
THE GRADUATE SCHOOL OF NATURAL AND APPLIED SCIENCES
OF
MIDDLE EAST TECHNICAL UNIVERSITY

BY

PINAR TUNCER

IN PARTIAL FULFILLMENT OF THE REQUIREMENTS
FOR
THE DEGREE OF MASTER OF SCIENCE
IN
ENVIRONMENTAL ENGINEERING

SEPTEMBER 2019

Approval of the thesis:

IONIC COMPOSITION OF RAINWATER ON THE BLACK SEA COAST OF TURKEY

submitted by **PINAR TUNCER** in partial fulfillment of the requirements for the degree of **Master of Science in Environmental Engineering Department, Middle East Technical University** by,

Prof. Dr. Halil Kalıpçılar
Dean, Graduate School of **Natural and Applied Sciences**

Prof. Dr. Bülent İçgen
Head of Department, **Environmental Eng.**

Prof. Dr. Gürdal Tuncel
Supervisor, **Environmental Eng., METU**

Examining Committee Members:

Prof. Dr. Ayşegül Aksoy
Environmental Engineering, METU

Prof. Dr. Gürdal Tuncel
Environmental Eng., METU

Prof. Dr. İpek İmamoğlu
Environmental Engineering, METU

Prof. Dr. Gülen Güllü
Environmental Engineering, Hacettepe University

Assist. Prof. Dr. Mihriban Civan
Environmental Engineering, Kocaeli University

Date: 09.09.2019

I hereby declare that all information in this document has been obtained and presented in accordance with academic rules and ethical conduct. I also declare that, as required by these rules and conduct, I have fully cited and referenced all material and results that are not original to this work.

Name, Surname: Pınar Tuncer

Signature:

ABSTRACT

IONIC COMPOSITION OF RAINWATER ON THE BLACK SEA COAST OF TURKEY

Tuncer, Pınar
Master of Science, Environmental Engineering
Supervisor: Prof. Dr. Gürdal Tuncel

September 2019, 139 pages

Composition of rainwater is a measure of pollutant deposition to marine and terrestrial ecosystem. Soluble fraction of wet deposited pollutants are even more important because they are bioavailable to fish in the sea and plants on the land. In addition to their harmful effects on plant and animal life, inorganic ions, trace elements and organic compounds in rainwater can also be used as tracers of long-range transport to receptor. In this study, chemical composition of rainwater samples collected at Amasra (Bartın) was investigated Samples were collected by the Turkish State Meteorology Service, at the sampling station located at peripheral of the town of Amasra (41º5'8.23"N, 32º22'58.17"E), between February 2004 and July 2016 (sampling continues, but data that will be evaluated is generated by analysis of samples collected between 2004 and 2016). During this period, wet-only samples were collected using automated rain samplers. Collected samples were analyzed for major ions (SO_4^{2-}, NO_3^-, NH_4^+, H^+, Ca^{2+}, Mg^{2+}, K^+ and Na^+). Approximately 820 rainwater samples were collected in this time-period. Analysis of collected samples generated a very large data set, which is very suitable to understand dynamics of wet deposition and source regions affecting ionic composition of rainwater on the Black Sea coast of Turkey. In this study, statistical tools were employed to determine levels of ions and how those levels changed in last 10 years. This information is very important particularly for SO_4^{2-}, NO_3^- and H^+ ions, because concentrations of SO_4^{2-} and NO_3^- decreased approximately 70% in last 30 years in Western Europe, but statistically significant trend was not observed at Balkans and Eastern Mediterranean basin. Trend-analysis was performed to 12-years long data set to determine if there is a statistically significant decrease (or increase) can be seen in concentrations of ions. A source region apportionment was performed using trajectory statistics to determine source regions affecting ionic composition of rainwater at the Black Sea basin..

Keywords: Black Sea Region, Wet Deposition, Rainwater Composition, Acid Rain, Back Trajectory Analysis

ÖZ

TÜRKİYE’NİN KARDENİZ KIYILARINDAKİ YAĞMUR SUYUNUN İYONİK KOMPOZİSYONU

Tuncer, Pınar
Yüksek Lisans, Çevre Mühendisliği
Tez Danışmanı: Prof. Dr. Gürdal Tuncel

Eylül 2019, 139 sayfa

Yağmur suyunun kompozisyonu, deniz ve karasal ekosistemdeki kirletici birikiminin belirlenmesinde bir ölçüdür. Yağışla çöken kirleticilerin çözünebilir kısmı daha önemlidir çünkü denizdeki balıklar ve karadaki bitkiler için biyolojik olarak kullanabilir durumdadır. Hayvan ve bitkiler üzerindeki olumsuz etkilerine ek olarak, inorganik iyonlar, eser elementler ve organik bileşikler reseptöre uzun menzilli taşınımın izlenmesi için de kullanılır. Bu çalışmada, Amasra (Bartın)’dan toplanan yağmur suyu örneklerinin kimyasal kompozisyonu incelenmiştir. Örnekler Meteoroloji Genel Müdürlüğü tarafından Amasra İlçesi’nin yakınlarındaki örnekleme istasyonundan (41º58’8.23”N, 32º22’58.17”E) Şubat 2004 ve Temmuz 2016 tarihleri arasında toplanmıştır (örnekleme devam etmekte fakat analizle geliştirilecek veriler 2004 ve 2016 arasında toplanan örneklerden elde edilmiştir). Bu dönem boyunca yağış örnekleri otomatik yağmur örnekleyicileri ile toplanmıştır. Toplanan örnekler ana iyonlar (SO_4^{2-}, NO_3^-, NH_4^+, H^+, Ca^{2+}, Mg^{2+}, K^+ ve Na^+) için analiz edilmiştir. Bu dönem içerisinde yaklaşık 820 yağmur suyu örneği toplanmıştır. Toplanan örneklerin analizleri çok büyük veri seti oluşturmuş olup, bu veri seti ıslak çökelmenin dinamiklerini ve Türkiye’nin Karadeniz kıyılarındaki yağmur suyunun iyonik kompozisyonunu etkileyen kaynakları anlamak için oldukça uygundur. Bu çalışmada, iyon seviyelerini belirlemek ve bu seviyelerin son 10 yılda değişimini belirlemek için istatistiksel araçlar kullanılmıştır. Bu bilgi, özellikle SO_4^{2-}, NO_3^- ve H^+ iyonları için önemlidir çünkü SO_4^{2-} ve NO_3^- konstrasyonları Batı Avrupa'da son 30 yıl içerisinde yaklaşık %70 düşmüştür ama Balkanlarda ve Doğu Akdeniz Havzası'nda istatistiksel olarak çok önemli bir eğilim gözlemlenmemiştir. Bu çalışmada, 12 yıllık veri setinden iyon konsantrasyonlarında önemli bir artış (ya da azalış) olup olmadığını gözlemlemek için istatistiksel bir eğilim analizi kullanılmıştır. Kaynak bölgesinin Karadeniz Havzası'ndaki yağmur suyu kompozisyonuna etkisini belirlemek için yörünge istatistikleri kaynak bölgesi belirlemede kullanılmıştır.

Anahtar Kelimeler: Karadeniz Bölgesi, Yaş Çökelme, Yağmur Suyu Kompozisyonu, Asit Yağmuru, Geri Yörünge Analizi

For long you’ll live and high you’ll fly and smiles you’ll give and tears you’ll cry
and all you touch and all you see is all your life will ever be ..

ACKNOWLEDGEMENTS

First of all, I would like to thank my supervisor Prof. Dr. Gürdal Tuncel for his patience, guidance and insight throughout this study. I would also like to express my gratitude to Ali İhsan İlhan, Tülay Balta and Yalçın Ün from General Directorate of Meteorology for providing the rainwater measurements that is the core of this work.

I would like to thank my committee members Prof. Dr. Ayşegül Aksoy, Prof. Dr. İpek İmamoğlu, Prof. Dr. Gülen Güllü and Assist. Prof. Dr. Mihriban Civan for their attention and contributions.

I would like to thank especially Dr. İlker Balcılar for patiently teaching me the modeling tools and basically anything to do with flow climatology. Also, I would like to express my gratitude for his endless support throughout my study. I would also like to thank Assoc. Prof. Dr. Fatma Öztürk for giving me insight on trend analysis. I also would like to express my gratitude for Assist. Prof. Dr. Ebru Koçak for her endless support. Of course I would like to thank the few people I could not function without: Gizem Yücel, Hazal Aksu Bahçeci, Nazlı Barçın Doğan, Selin Özkul, Melike Kiraz and Ceren Ayyıldız. A very special thanks goes to them for picking me up when I felt low and unencouraged. The speciallest thanks of them all goes to my partner in crime Gizem Yücel for basically being my partner in crime throughout my long master study and supporting me all the way as well as constantly managing the things I forget.I would like to express my endless gratitude for my father, mother and brother for showing me that everything happens for a reason and there is light at the end of every tunnel. Also, thanks to my beloved boyfriend İbrahim İyce for putting up with me through the tough times and supporting me in everything I do. Finally, I would like to thank my dog Fox for constantly rescuing me from depression by simply just having a cute face.

TABLE OF CONTENTS

ABSTRACT v

ÖZ vii

ACKNOWLEDGEMENTS x

LIST OF TABLES xiv

LIST OF FIGURES xv

LIST OF ABBREVIATIONS xviii

CHAPTERS

1. INTRODUCTION 1
  - 1.1. Introduction 1
    - 1.1.1. Objectives of the Study 2

2. LITERATURE REVIEW 3
  - 2.1. Atmospheric Removal Mechanisms 3
  - 2.2. Acid Deposition 4
    - 2.2.1. Chemical Composition of Acid Precipitation 4
      - 2.2.1.1. Principle Precursors of Acidification 6
      - 2.2.1.2. Principle Precursors of Neutralization 7
    - 2.2.2. Studies of Acid Precipitation 7
      - 2.2.2.1. Studies of Chemical Precipitation 8
  - 2.3. Source Apportionment 9
    - 2.3.1. Source Oriented Models 10
    - 2.3.2. Receptor Oriented Models 10
      - 2.3.2.1. Trajectory Statistics 10

2.3.2.2. Potential Source Contribution Function 11

2.3.2.3. Positive Matrix Factorization 13

2.4. Geography and Climatology of Study Area.. 15

3. MATERIAL AND METHODS 17

3.1. Sampling Site 17

3.2. Longterm Meteorological Conditions of the Station 18

3.3. Collection of Wet Deposition Samples.. 20

3.4. Sample Handling.. 21

3.4.1. Determination of Volume and pH 21

3.4.2. Preparation of Samples for Ion Chromatography.. 22

3.5. Analysis of Samples.. 22

3.6. Data Quality Assurance 24

3.6.1. Field Blanks.. 24

3.6.2. Calculation of Detection Limits 24

3.6.3. Quality Assurance 25

3.7. Computation of Back Trajectories 26

3.7.1. Flow Climatology.. 28

3.8. Potential Source Contribution Function.. 33

3.9. Positive Matrix Factorization.. 34

3.10. Mann-Kendall Test for Trend Analysis 36

4. RESULTS AND DISCUSSION 39

4.1. General Characteristics of the Data 39

4.1.1. Distribution Characteristics of the Data 40

4.1.2. Comparison of the Data with Literature.. 44

4.1.2.1. Comparison with EMEP Network 44
4.1.2.2. Comparison with MGM Network 49
4.2. Flow Climatology 54
4.2.1. Residence Time Analysis...54
4.2.2. Sector-Based Flow Climatology 59
4.2.3. Cluster Analysis 61
4.3. Ionic Composition of Wet Deposition...72
4.3.1. Ion Balance 72
4.3.2. Contributions of Ions to Total Ion Mass 73
4.4. Acidity of Wet Deposition..76
4.4.1. pH of Rainwater..76
4.4.2. Neutralization of Rainwater..79
4.5. Temporal Variations 81
4.5.1. Seasonal Variations in Ion Concentrations 82
4.5.2. Interannual Variations in Ion Concentrations 87
4.6. Positive Matrix Factorization 103
4.7. Deposition Fluxes 114
5. CONCLUSION..123
6. RECOMMENDATIONS FOR FUTURE RESEARCH 125
REFERENCES..127

LIST OF TABLES

TABLES

Table 3.1. Historical Meteorological Data for Amasra 19

Table 3.2. Detection Limits of Ions (Ayaklı, 2014) 25

Table 3.3. Calculated and Measured Concentrations of the High Purity Salts (Ayaklı, 2014) 26

Table 4.1. Statistical Summary of Ionic Composition in Amasra Station (concentrations are in mg/L) 39

Table 4.2. Average Major Ion Concentrations for EMEP Network and Amasra Station 46

Table 4.3. Average Major Ion Concentrations for MGM Network and Amasra Station 51

Table 4.4. Number and Percentage of Trajectories Allocated in Each Cluster 63

Table 4.5. Median Concentration of Species (mg/L) for each Cluster 70

Table 4.6. Annual Median Concentrations of Measured Major Ions (mg/L) 90

Table 4.7. Results of the Van Belle and Hughes Homogeneity Test 94

Table 4.8. Summary of the Results of the Mann-Kendall Test 95

Table 4.9. Results of the Sen's Slope Estimator 99

Table 4.10. Summary of the Results of the Mann-Kendall Test between 2005-2015 102

Table 4.11. Results of the Sen's Slope Estimator between 2005-2015 102

Table 4.12. Categories and Signal-to-Noise Raitos (S/N) of the Ions 104

Table 4.13. Seasonal Fluxes of Major Ions and Their Winter to Summer Ratios ... 118

LIST OF FIGURES

FIGURES

Figure 3.1. Location of Amasra MGM Station 18
Figure 3.2. Annual and Seasonal Wind Roses at Amasra Station 19
Figure 3.3. Wet and Dry Deposition Sampler in Amasra Station..............................20
Figure 3.4. Trajectory Calculation Window of TrajStat 28
Figure 3.5. Study Domain for the Residence Time Analysis.....................................30
Figure 3.6. Study Domain Used in the Calculation of Contribution of Wind Sectors 31
Figure 3.7 The Schematical Description of the Trend Analysis Methodology..........36
Figure 4.1 Frequency Distribution -Anions 42
Figure 4.2 Frequency Distribution - Cations...43
Figure 4.3 Comparison of pollution-derived ions in this study with corresponding data from EMEP network. 47
Figure 4.4 Comparison of crustal and marine ions in this study with corresponding data from EMEP network..48
Figure 4.5 The location of the Station in MGM Network...49
Figure 4.6 Comparison of pollution-derived c ions in this study with corresponding data from other stations located in Turkey..52
Figure 4.7 Comparison of crustal and marine ions in this study with corresponding data from other stations located in Turkey...53
Figure 4.8 Distribution of Air Mass Residence Times in Study Domain (a) 100 m Starting Altitude, (b) 500 m Starting Altitude, (c) 1500 m Starting Altitude, (d)Segments in All Starting Altitudes 56
Figure 4.9 Seasonal Variation in Hourly Residence Times (a) Summer Residence Times, (b) Winter Residence Times, (c) Summer-Winter Difference 58
Figure 4.10 Seasonal variations of percent contributions of wind sectors.................59

Figure 4.11 Comparison of seasonal contributions of wind sectors at Dereköy and Trabzon Stations 61
Figure 4.12 The Percentage Change in.TRMSD to Cluster Numbers 62
Figure 4.13 Cluster Centroids of Clusters Calculated for Combined Trajectories 63
Figure 4.14 Trajectories Allocated to Different Clusters 65
Figure 4.15 Residence Times of Air Masses Below 500 m for each Cluster 66
Figure 4.16 Median Concentration of Species (mg/L) for each Cluster 71
Figure 4.17 The scatterplot of the equivalent sum of anions to equivalent sum of cations. 72
Figure 4.18 Contribution of Ions measured in Amasra Station to Total Ion Mass 74
Figure 4.19 Variation of Ionic Contribution to Total Ionic Mass in Time 75
Figure 4.20 Seasonal Variation in Ionic Contributions to Total Mass 76
Figure 4.21 pH Frequency Distributions of pH in Amasra Station 78
Figure 4.22 Monthly Variation of $[H^+]/([SO_4^{2-}] + [NO_3^-])$ Equivalent Ratio 79
Figure 4.23 Regression of H^+ ion against Ca^{2+} and NH_4^+ ions 81
Figure 4.24 Average Monthly Variation of Rainfall (mm) at Amasra Station (1975-2016) 83
Figure 4.25 Monthly variation of Ion Concentrations and Summer to Winter Ratio of Anthropogenic Ions 85
Figure 4.26 Monthly variation of Ion Concentrations and Summer to Winter Ratio of Natural Ions 86
Figure 4.27 The Summer to Winter Ratio of Ions in Amasra Station 87
Figure 4.28 Correlation and Annual Variation of Fertilizer Consumption in Bartın Province and Median Concentration of NH_4^+ ion. 89
Figure 4.29 Interannual Variation Concentration Pollution-Derived Ions in Amasra Station 91
Figure 4.30 Interannual Variation Concentration Crustal and Marine Ions in Amasra Station 92
Figure 4.31 Z Values Calculated for Pollution-Derived Ions 97
Figure 4.32 Z Values Calculated for Marine and Crustal Ions 98

Figure 4.33 Factor 1 Diagnostics: (a) factor loadings, (b) fractions of ion concentrations explained by factor 1 and (c) monthly variations of factor scores...106

Figure 4.34 Factor 2 Diagnostics: (a) factor loadings, (b) fractions of ion concentrations explained by factor 2 and (c) monthly variations of factor scores...108

Figure 4.35 Factor 3 Diagnostics: (a) factor loadings, (b) fractions of ion concentrations explained by factor 3 and (c) monthly variations of factor scores...110

Figure 4.36 Distribution of PSCF Values Using Factor 3 Scores............................111

Figure 4.37 Factor 4 Diagnostics: (a) factor loadings, (b) fractions of ion concentrations explained by factor 4 and (c) monthly variations of factor scores...113

Figure 4.38 Monthly variation of Deposition Fluxes for pollution-derived Ions 116

Figure 4.39 Monthly variation of Deposition Fluxes for Marine and Crustal Ions .117

Figure 4.40 Annual variation of Deposition Fluxes for pollution-derived Ions 119

Figure 4.41 Annual variation of Deposition Fluxes for Marine and Crustal Ions ...120

Figure 4.42 Episodic Nature of Wet Deposition Fluxes: Percentage of Rain Events Accounting for 90% of Wet Deposition Fluxes of Ions..121

LIST OF ABBREVIATIONS

ABBREVIATIONS	
BDL	Below Detection Limit
CMB	Chemical Mass Balance
DL	Detection Limit
EMEP	European Monitoring and Evaluation Programme
EPA	Environmental Protection Agency
FA	Factor Analysis
FC	Flow Climatology
GIS	Geographical Information Systems
HYSPLIT	Hybrid Single Lagrangian Integrated Trajectory
IC	Ion Chromatography
MGM	General Directorate of Meteorology
NOAA	National Oceanic and Atmospheric Administrtion
PCA	Principle Component Analysis
PMF	Positive Matrix Factorization
PSCF	Potential Souce Contribution Function
QA/QC	Quality Assurance/Quality Control
TRMSD	Total Root Mean Square Deviation
VWA	Volume Weighted Average

CHAPTER 1

INTRODUCTION

1.1. Introduction

Since the early stages of civilization, mankind has established facilities that utilize the Earth's natural resources in order to make their daily life easier. For example, in order to produce energy natural gasses, coal or oil are used up. These activities eventually resulted in pollution by the release of undesirable and harmful substances into the environment. While activities such as burning of fossil fuels in industries and transport sector, industrialization and urbanization makes life easier, they also have led to air pollution because of gaseous and particulate contaminants released into the atmosphere. Acid rain tends to be the most serious environmental problem emerged due to air pollution (Singh and Agrawal, 2008).

Acid rain is attributed to the washout of oxides of sulphur, nitrogen and other constituents present in the atmosphere. Sources of these oxides can be listed as coal fired power stations, smelters (producing SO_2) and exhausts of motor vehicles (containing NOx) (Singh and Agrawal, 2008). These oxides depending on their solubility dissolve in the water droplets present in the atmosphere and they are washed out by rain events that may result as acid rain (Liang, 2013).

Monitoring of components of rainwater continuously becomes very crucial in order to investigate the human contribution to atmospheric pollution, potential sources of the contaminants that contribute to the pollution levels observed around the receptor site. These investigations are important due to them leading a way to suggest some solutions or regulatory action in order to decrease the pollution levels.

1.1.1. Objectives of the Study

In this study, investigation was carried out for rainwater samples that were collected from Amasra Station by General Directorate of Meteorology. The main objectives of this study can be listed as:

- To determine components in rainwater composition.
- To evaluate the acidity and the neutralization of precipitation occurring in the study area.
- To determine the flow climatology of the region by analyzing the back trajectories between years 2004-2016.
- To identify the source regions affecting ionic composition of rainwater on the Black Sea coast of Turkey.
- To determine deposition fluxes of ions and to assess their contribution to pollution of the Black Sea.
- To determine long-term trends in ion concentrations at the Black Sea region.

CHAPTER 2

LITERATURE REVIEW

2.1. Atmospheric Removal Mechanisms

Atmospheric deposition is considered to be a major process that removes pollutants from the atmosphere and it is an important source of nutrients and contaminants for terrestrial and aquatic ecosystems. (Pan and Wang, 2015)

Atmospheric removal processes can be grouped into two categories such as dry deposition and wet deposition.

Dry deposition process refers to all phenomena of meteorological, chemical and biological nature that influence a flux of gas and particle pollutants interacting with a ground surface without involving the water in the atmosphere. (Giardina and Buffa, 2018)

Wet deposition refers to pollutants brought to ground by rainfall or snow. Wet deposition can be subdivided according to the point at which the pollutant was absorbed into the water droplets. In cloud absorption followed by precipitation is named as “rain-out”; below cloud absorption where pollutants are collected as the raindrops fall is named as “wash-out”. (Smith , et al., 2015)

By nature wet deposition events are episodic (Thibodeaux and Mackay, 2011). On the contrary, dry deposition of atmospheric particles to plant and soil is a much slower process than wet deposition, infact it acts nearly continuously and affects all exposed surfaces. (Grantza, et al., 2003).

2.2. Acid Deposition

Acid deposition or more commonly acid rain, is a broad term that includes any form of precipitation with acidic components that fall to the ground from the atmosphere in terms of wet or dry deposition. (EPA, 2017)

Wet deposition of acid refers to acids deposited on earth surface in the forms of rain, fog, snow and hail. On the other hand, acid also is deposited as dry in the absence of precipitation where particles and gases stick to the ground, plants or other surfaces. (Bhargava and Bhargava, 2013)

Acid deposition mainly contains sulfur dioxide, nitrogen oxides, and their derivative acids (Yu, et al., 2017). Increasing levels of atmospheric NO_3^- and SO_4^{2-} produced by anthropogenic sources, such as fossil fuel combustion, agriculture fertilizer applications, and vehicle exhaust emissions, may result in severe acid deposition. (Jia and Gao, 2017)Precipitation is considered to be acid rain when pH value is below 5. (Jacob, 1999)

2.2.1. Chemical Composition of Acid Precipitation

Precipitation chemistry involves various physical and chemical mechanisms of atmospheric constituents, and therefore can reflect the transport/transformation of anthropogenic pollutants related to regional precipitation acidification (Özsoy, et.al., 2008).

The chemical composition of rain, influenced by natural and anthropogenic sources, is the result of the incorporation of pollutants and particles in the air into the raindrops.

In general, rainwater tends to be slightly acidic with a pH value that is approximately 5.6. This is the result of Carbon dioxide (CO_2) naturally being present in the atmosphere. CO_2 is the anhydride of carbonic acid (H_2CO_3), which is formed when CO_2 dissolves in the rainwater droplets. At an extend which is determined by pKa (acid dissociation constant) of H_2CO_3 releases acidic hydronium ions (H_3O^+) into rainwater indicated in the following sequence of reactions (Aron and Patz, 2001):

$$CO_2(g) + H_2O\ (l) \leftrightarrow CO_2(aq) + H_2O\ (l)$$
$$CO_2(aq) + H_2O\ (l) \leftrightarrow H_2CO_3\ (aq)$$
$$H_2CO_3\ (aq) + H_2O\ (l) \leftrightarrow HCO_3{}^{-}(aq) + H_3O^{+}\ (aq)$$

Like CO_2, there are other major acidic oxides that influence and contribute to the formation of acidic precipitation such as sulfur and nitrogen oxides. These acidic oxides arise from burning of fossil fuels such as coal and gasoline. Resulting gaseous oxides from these emissions, mix with water and other chemicals present in the troposphere and the rain that falls to the surface is more acidic than rain containing only dissolved CO_2 (Kotz, et al., 2009) .

Sulfur dioxide (SO_2) arising from human and natural sources, reacts with oxygen to form sulfur trioxide (SO_3) which then reacts with water and becomes sulfuric acid. Related reactions are (Kotz, et al., 2009):

$$2SO_{2(g)} + O_{2(g)} \rightarrow 2SO_{3(g)}$$

$$SO_{3(g)} + H_2O_{(l)} \rightarrow H_2SO_{4(aq)}$$

Similarly, nitrogen dioxide (NO_2) reacts with water and forms nitrous and nitric acids. The reaction is as follows (Kotz, et al., 2009):

$$2NO_{2(g)} + H_2O_{(l)} \rightarrow HNO_{2(aq)} + HNO_{3_{(aq)}}$$

On the contrary, compunds such as calcium carbonate ($CaCO_3$) and gaseous ammonia (NH_3) are bases that are present in the atmosphere which also influences the pH of the precipitation. The reactions for these compounds are provided as follows (Jacob, 1999):

$$NH_{3(aq)} + H^+ \rightarrow NH_4^+$$

$$CaCO_3 + H^+ \rightarrow Ca^{2+} + HCO_3^-$$

Compounds influencing the pH both acids and bases given in this section will be discussed in the following parts of the manuscript.

2.2.1.1. Principle Precursors of Acidification

As stated in the previous sections of the manuscript the principle precursors that cause acidification are SO_2 and NO_x. While nitric oxide and sulfur dioxide are produced biogenically, there are also major anthropogenic sources of both these polluting gases. (EPA, 2004).

Emission of SO_2 is responsible for 60-70 % of the acid rain that takes place globally. More than 90% of the sulfur content present in the atmosphere is of anthropogenic origin. Sources of this precursor can be listed as (Eldin and Ramadan , 2004; Menz and Seip, 2004):

- Coal (fossil fuel) burning (typically sulfur content of coal is 2-3 % therefore when it is burned SO_2 is released)
- The smelting process of metal sulfide ores in order to obtain pure metals. Metals such as zinc, nickel, and copper can be given as examples to metals which are obtained by this process.
- Majority of SO_2 is produced by industrial combustion.
- Approximately 4% of SO_2 is produced by transportation
- The remaining minor portion originates from organic decay, sea spray, plankton, rotting vegetation, volcanic eruptions.

Additionally, 95% of emissions of NO_x in the atmosphere come from anthropogenic sources. Sources of this precursor can be listed as (Eldin and Ramadan , 2004):

- Firing process of extreme high temperature (automobiles, utility plants)
- Fertilizer production
- The remaining minor portion comes from various natural processes such as bacterial action in soil, forest fires, volcanic action and lightning.

These precursors may be transported over tens to hundreds of kilometers from their source by air masses before they reach the earth as their acidic counterparts (Rodhe H. , 1972; Eldin and Ramadan , 2004; Bricker and Rice, 1993).While the transit period, the sulfur and nitrogen compounds are oxidized and combine with water vapor and sulfuric and nitric acids, sulfate aerosols, and particulate sulfate are formed. Majority of the NOx emissions are closer to the ground level than SO_2 emissions. Also, NO_x compounds are generally oxidized more rapidly than SO_2. Therefore, NOx is generally deposited closer to its source (Bricker and Rice, 1993).

2.2.1.2. Principle Precursors of Neutralization

The degree of acidity depends on the neutralization process derived by various rainwater components such as NH_3, $CaCO_3$ and hydroxide (Al-Khashman, 2005; Flues, et al., 2002; Migliavacca, et al., 2005)

Similar to precursors of acidification explained in the previous part, alkaline species in the atmosphere are originated from both anthropogenic and natural sources. Natural sources can be listed as wind erosion of arid soils, volcanic eruptions and natural forest-fires (Hüttl and Schaaf, 1997). Whereas, anthropogenic sources can be listed as industrial and agricultural activities. The ammonium, arises from agricultural applications, livestock breeding and biomass burning (Migliavacca, et al., 2005).

2.2.2. Studies of Acid Precipitation

Acid rain is one of the major environmental threats since 19th century. The impact of acidic precipitation has been globally (Sivaramanan, 2015). Many pioneering scientists have linked the sources of acidification to industrial emissions and documented the deleterious environmental impacts such as acidification of surface waters and toxic effects on terrestrial and aquatic biota (Smith R. A., 1872; Gorham, 1961; Likens and Bormann, 1974). By the work done by these scientists the attention of governments, the media and awareness of the public were raised. This led to stricter air pollution legislations and regulations in North America and Europe regions. In Asian countries the situation was recognized later than North America and Europe.

Many studies are still conducted to continue to observe deposition levels as well as the status of recovery of the ecosystem in many areas (Burns, 2016).

2.2.2.1. Studies of Chemical Precipitation

Precipitation has a complex form of chemical composition because it alters place by place and differentiates between seasons in the same geographical region. Rainwater includes constituents of originating from local sources as well as constituents that are transported by wind from other regions. Chemical constituents both from dry and wet deposition are added to earth's crust continuously (Carroll, 1962). Therefore, rainwater has become an important topic in environmental studies. A lot of studies have been conducted about the chemical composition of rainwater and its long-term trends (Al-Khashman, 2005; Al-Momani, et al., 1997; Alagha and Tuncel, 2003; Ayaklı, 2014; Yücel, 2019).

A global study was established in 2014, where assessment of precipitation chemistry and deposition has been done under the influence of the World Meteorological Organization (WMO) Global Atmosphere Watch (GAW) Scientific Advisory Group for Precipitation Chemistry (SAG-PC). To have an understanding on a global scale the regionally representative measurements were gathered for the years 2000-2002 and 2005-2007. The study states that concentrations and deposition of sulfur and nitrogen have decreased in significant amounts in North America and Europe due to emission reduction policies. The lowest pH values are observed in North America, Europe, Eastern Asia and Central Africa where SO_2 and NO_x emissions are high resulting in highly acidified areas. Although Northeast Canada and Northern Scandinavia are associated with low emissions of SO_2 and NO_x, the precipitation observed in these areas are found to be relatively acidic due to the fact that S and N coming from high emitting areas located in the south by long-range transport (Vet, et al., 2014).

In another more local study conducted in Europe at the west coast of Portugal between September months of 2008 and 2009 rainwater was analyzed for parameters such as pH, conductivity, and Cl^-, NO_3^-, SO_4^{2-}, and NH_4^+. The outcomes of the study were also compared to outcomes obtained at the same area in 1986 and 1989. The results stated that in both collection periods oceanic air masses dominated the rainwater composition (80%). The hydrogen concentrations remained approximately same throughout 20 years whereas in sea salt sulfate (NSS-SO_4^{2-}) concentration there was a significant decrease in 2008-2009 relative to 1986-1989 period. Samples originating from Atlantic Ocean and Mediterranean also showed the similar trend as those originating from Central and Northern Europe. The declining trend was attributed to low content of sulfur in oil by-products in the study (Santos, et al., 2011).

In contrast, in Eastern Asia a conducted study in a semi-rural site located at China showed severe acidification the pH values obtained at the site raged from3.36 to 6.68 with approximately 70 % of the pH values being in the 3 - 4.5 range. The pH values obtained on the site was found to be lower than other areas in China. The reasoning for the situation is given as lack of Ca^{2+} ion in composition of rainwater which is an neutralizing agent and significant anthropogenic impact on the semi-rural site (Zhao, et al., 2013).

Another study was carried out in 5 different states of India. In this study, the rainwater was analyzed for pH and major anions and cations in monsoon season in 2006. The obtained pH during this period was alkaline and varied from 6 to7.3. the alkaline pH was further investigated by calculating neutralization factors of neutralizing agents. The results were followed a sequence of $NF_{Ca}>NF_{Mg}>NF_{NH4}$ which is an indication that crustal species are responsible for the neutralizing effect (Salve, et al., 2008).

2.3. Source Apportionment

A source apportionment study on the air pollutants is a key factor for framing and determining an effective air quality management. (Kalaiarasan, et al., 2018). Source Apportionment (SA) is conducted in order to identify ambient air pollution sources and their contribution to pollution levels. This task can be accomplished by two approaches which are source-oriented (forward) models and receptor-oriented (backward) models (Claudio, et al., 2014).

2.3.1. Source Oriented Models

Source-oriented approaches start from the source of the emission of the pollutant and work forward in time in order to estimate the contribution of a source at a receptor site. Source-oriented methods involve advanced mathematical and modelling systems for the description of the fate of the related emissions between the source and the receptor site. "Chemical Transport Models (CTMs)" are the most advanced version of source-oriented modelling system. CTMs are composed of three major components which are, an emission model, a meteorological method and an atmospheric process model (National Academy of Engineering and National Research Council, 2008).

Despite the fact that source-oriented models are capable of assessing the impact of specific sources, none can describe the random nature of dispersion in the atmosphere adequately. Therefore, related uncertainties are high with these types of models and the results can only be considered as approximate (Cooper and Watson Jr., 2012).

2.3.2. Receptor Oriented Models

Receptor models in contrast with source-oriented models, start with observations at the receptor site and work backward in time (Brook, et al., 2008).

Several receptor models are used by researchers in the literature, such as principal component analysis (PCA), enrichment factors (EFs), chemical mass balance (CMB), positive matrix factorization (PMF) and empirical orthogonal functions (EOF), multiple linear regression, neural networks, edge detection, cluster analysis, fourier transform time series and a number of other multivariate data analysis (Amato, et al., 2009; Gugamsetty, 2012; Pant and Harrison, 2013; Yatkın and Bayram, 2008; Kalaiarasan, et al., 2018).

For this study, PMF and PSCF receptor-oriented models are used to identify sources of measured pollutants.

2.3.2.1. Trajectory Statistics

The time integration of the position of an air mass while it is transported with the wind is defined as a trajectory. Trajectory models have been applied to understand dynamical processes occurring in the atmospheric environment (Yılmaz, 2010). They have a wide range of application in the literature such as investigating the air parcel flow around mountains (Steinacker, 1984), identifying pathways of desert dust (Chiapello, et al., 1997) and forming source-receptor relationships of atmospheric pollutants (Stohl A., 1996).

In recent trajectory modeling, measured pollutant concentrations are combined with back-trajectories of air masses which is done in order to obtain information on the source regions (Yücel, 2019).

Majority of the trajectory models considers observed or analyzed winds as horizontal component. On the other hand for the calculation of the vertical components several assumptions are used such as isobaric, isentropic, kinematic. Description of these assumptions are further explained below (Yılmaz, 2010; Doğan, 2005):

- Isobaric is where the trajectory is assumed to follow constant pressure.
- Isentropic is where the trajectory is assumed to follow constant potential temperature
- Kinematic is where the trajectory is assumed to migrate with the vertical velocity wind fields formed by diagnostic or prognostic model.

Two calculations which are based on back-trajectories are carried out for this study to identify the potential source regions and compare their contribution to the pollutant concentrations at Amasra Station. These two trajectory statistics are flow climatology (FC) and potential source contribution function (PSCF).

2.3.2.2. Potential Source Contribution Function

In flow climatology approach, trajectories are classified without taking air pollution data into account. Unlike FC, potential source contribution function analysis includes the air pollution data. PSCF is the conditional probability that a parcel with a certain level of pollutant concentration reaches a receptor site after having passed through a specific upwind source region (Wang, et al., 2012).

The analysis is developed by Ashbaugh et al. (1985) and Malm et.al. (1986). PSCF has been used widely in the literature in over a variety of geographic regions (Wang, et al., 2012; Gao, et al., 1993; Biegalski and Hopke, 2004).

Back trajectories of air masses which intercept at a receptor site are represented with segment endpoints. Each of the end points have two coordinates such as latitude and longitude that show the central location air mass at a certain time. In PSCF calculation, entire geographic region which is covered by the back trajectories should be parted into certain size of grid cells depending on the geographical scale of the problem. By doing this the PSCF becomes a function of locations as represented by the cell indices *i* and *j* (Hopke, 2009).

Assuming that N represents the total number of endpoints of the trajectory segments during the entire study period, T and n represents the endpoints of segments which are positioned in *ij*th (illustrated as n_{ij}), the probability related with event A is given as (Hopke, 2009):

$$P[A_{ij}] = \frac{n_{ij}}{N} \qquad \text{(Equation 2.1)}$$

In equation 2.1 $P[A_{ij}]$ represents the measurement of the residence time of an air mass in the *ij*th which is randomly selected relative to the study period, T (Hopke, 2009).

Additionally, for the same *ij*th cell there is a subgroup of segment endpoints that corresponds to trajectories which intercept at the receptor site at the time that measured concentrations are higher than a predefined standard value. The probability related with this event of high concentration is represented by the following Equation 2.2 (Hopke, 2009):

$$P[B_{ij}] = \frac{m_{ij}}{N} \qquad \text{(Equation 2.2)}$$

Probability B is similar to probability A, but it represents only the contaminated air parcels. The PSCF is formulized as the ratio of $P[B_{ij}]$ to $P[A_{ij}]$ and represented in the following Equation 2.3 (Hopke, 2009):

$$P_{ij} = \frac{P[B_{ij}]}{P[A_{ij}]} = \frac{m_{ij}}{n_{ij}} \qquad \text{(Equation 2.3)}$$

P_{ij} represents the conditional probability in which an air mass that passes through the *ij*th cell had a high concentration at the trajectory endpoint. Cells that contain emission sources would have conditional probabilities that are close to one when the trajectories that cross the cells effectively bring the emitted pollutant to the receptor site. Therefore, for geographical areas PSCF allows a means to map the potential sources. Consequently, the model does not provide information on the apportionment of the contribution of the source regions to the measured data at the receptor site (Hopke, 2009).

2.3.2.3. Positive Matrix Factorization

Positive Matrix Factorization (PMF) is an advanced type of receptor model, developed by Dr. Pentti Paatero Department of Physics, University of Helsinki (Paatero and Tapper , 1994; Comero, et al., 2009).

The method was developed in order to eliminate some limitations of Factor Analysis (FA) and Principle Component Analysis (PCA) which are other receptor-oriented tools used to analyze multivariate data (Comero, et al., 2009). The method has been used as alternative of FA in many studies in the literature including wet deposition (Anttila, et al., 1995) and sources of aerosols (Polissar, et al., 1996).

The advantage that PMF has over PCA is that non-negativity of both factor loadings and scores of factors are built-in inside the model. Furthermore, the model is not dependent on correlation matrix information, instead it uses a minimization scheme of point by point least squares. Thus, the input matrix can be compared to the produced profiles without transformation (Lee, et al., 1999).

The ultimate aim in PMF is based on the solution of problems by means of bilinear model given in Equation 2.4. Also, it can be expressed in the component form given in Equation 2.5.

$$X = GF + E \qquad \text{(Equation 2.4)}$$

$$X_{ij} = \sum_{p=1}^{p} g_{ip} f_{pj} + e_{ij} \qquad i = 1 \ldots m; j = 1 \ldots n \qquad \text{(Equation 2.5)}$$

Where, X is the data matrix, F symbolizes the source profiles, G stands for the contribution of sources and E represents the unmodeled part. G and F matrices are the ones that are aimed to be determined. Because of the logic that no sources are able to emit negative quantities, the elements of G and F are forced to have positive value (Comero, et al., 2009).

The main objective is to minimize the object function which is composed as a function G and F. The object function is represented in Equation 2.6.

$$Q(E) = \sum_{i=1}^{m} \sum_{j\_1}^{n} \left(\frac{e_{ij}}{\sigma_{ij}}\right)^2 \qquad \text{(Equation 2.6)}$$

Where, σij is the uncertainty for data value xij, therefore, optimum weight in the least square fit is 1/ σij. In this means the PMF problem is then determined as a minimization of Q(E) according to G and F, and under the constraint that G and F matrices are to be non-negative (Comero, et al., 2009).

Q is a critical parameter for PMF and there are two Q values displayed for each model run which are Q(true) and Q(robust). The first one Q(true) is calculated including all data points and represents the goodness-of-fit. The second one Q(robust) represents the goodness-of-fit as well but it is calculated by excluding the samples with the uncertainty-scaled residual greater than 4. Q(true) and Q(robust) should be closer to each other in a successful run.

2.4. Geography and Climatology of Study Area

The Black Sea is a semi-enclosed sea and it's the only connection to the ocean is through a narrow Bosphorus. The coordinates of the sea is 40º55' to 46º32' N and 27º27' to 41º32' E. Black Sea is connected to the Mediterranean to its south and to the North it is connected to Sea of Azov by Kerch Strait. Six countries which are located in Europe and Asia sorrounds the Black Sea. These surrounding countries can be listed as: Bulgaria, Georgia, Romania, Russia, Ukraine and Turkey. The 2nd, 3rd and 4th major rivers located in Europe flows into the Black Sea so it is under the influence of approximately one third of the whole land area of continental Europe (Bakan and Büyükgüngör, 2000).

Meteorological conditions of the Black Sea region differentiate in east-west as well as north south directions. During winter time Siberia which is the maximum pressure center dominates the region. The average wind speed is highest in January and February being approximately 16 knots. The highest average temperatures for the central northern and southern parts are 24ºC, 24ºC and 22ºC, respectively. Along the southern coast where Turkey is located, the regional variations in temperature of air can reach 8ºC (Bakan and Büyükgüngör, 2000).

The Black Sea coast of Turkey is approximately 1695 km long starting from the Bulgarian border in the west and ending at Georgia border in the east. The area of the region is about 141 000 km^2 corresponding to approximately 18% of the total surface area of Turkey. The topography of the area has a significant impact on the population distribution and consequently it has an indirect effect on pollution sources along the coast. The Ponthic mountains lie parallel to the coastline and rises severely within 30 km of the shore and therefore large cities cannot be developed easily. The coastal zone supports extensive agriculture and contains some of the most productive lands located in Turkey (Bakan and Büyükgüngör, 2000).

CHAPTER 3

MATERIAL AND METHODS

3.1. Sampling Site

General Directorate of Meteorology (MGM) operates a network of 10 rainwater monitoring stations which they called “Acid Rain Network”. Ten stations in this network are located at Çatalca, Marmaris, Amasra, Hatay, Trabzon, Çamkoru (Ankara), Antalya, Yatağan, İzmir and Balıkesir. All of these stations, except for Yatağan, are located rural areas outside the cities.

Data generated in one of these stations, the one located at Amasra, were used in this study. The data is generated by MGM. The exact coordinates of the station are 41°45'09" N and 32°22'58" E. The altitude of the station is 73 m. The location of Amasra station is given in Figure 3.1. The station is located outside the Amasra district (population 15000) of the city of Bartın (population 72000). The location of Amasra station is given in Figure 3.1.

Figure 3.1. Location of Amasra MGM Station

3.2. Longterm Meteorological Conditions of the Station

In Amasra district a rainy mid-zone climate is dominant that is unique for the Black Sea coast. The average historical data from 1975 to 2016 for temperature and precipitation data of Amasra is given in Table 3.1

According to Table 3.1 in Amasra between the years 1975 and 2016 the annual average temperature is 13.7ºC. Highest precipitation is seen in December as 119.6 mm and the annual average precipitation amount is 990.3 mm. Highest wind speed is observed in December as 4.7 m/s whereas lowest wind speed is observed in May and June as 3.2 m/s. The wind roses for annual and seasonal average wind speeds are given in Figure 3.2.

Table 3.1. *Historical Meteorological Data for Amasra*

	Average Temp. (ºC)	**Monthly Average Precipitation (mm)**	**Average Relative Humidity (%)**	**Wind Speed (m/s)**
Jan	6.4	104.1	69.6	4.5
Feb	6.0	70.7	70.1	4.5
Mar	7.5	68.8	71.1	4.2
Apr	10.9	47.5	72.7	3.5
May	15.0	42.0	76.0	3.2
Jun	19.6	63.3	73.6	3.2
Jul	22.0	63.0	75.2	3.4
Aug	22.3	73.6	74.9	3.4
Sep	19.2	103.3	71.8	3.8
Oct	15.5	118.0	72.4	3.9
Nov	11.7	116.4	68.5	4.4
Dec	8.3	119.6	68.0	4.7
Annual	13.7	990.3	72.0	3.9

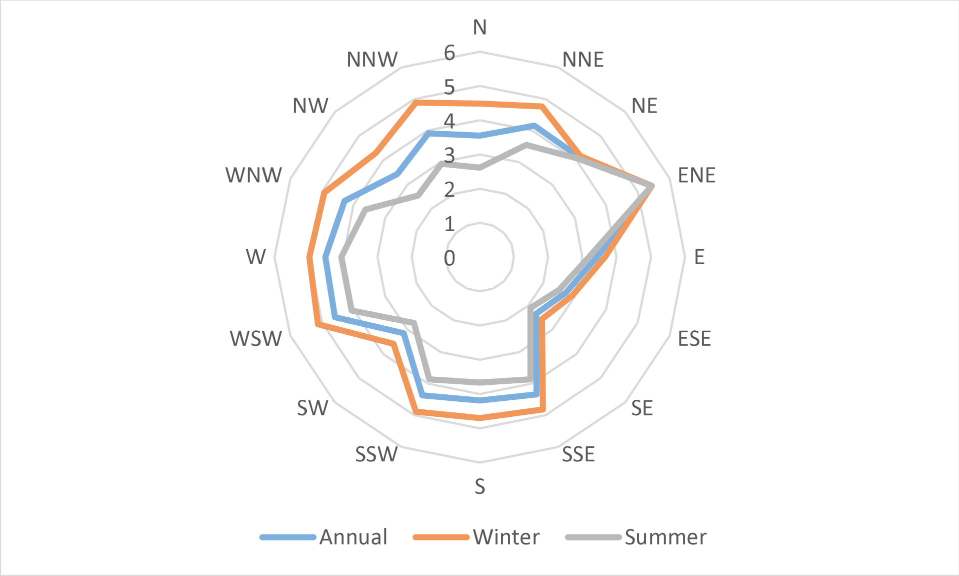

Figure 3.2. Annual and Seasonal Wind Roses at Amasra Station

3.3. Collection of Wet Deposition Samples

Both rainwater and dry deposition samples are collected using the same procedure at every station in MGM network, including in Amasra station. However, dry deposition samples are not included in this study. Total of 820 samples were collected between the years 2004 and 2016. In collection of these samples, an automated wet-and-dry sampler, which, is shown in Figure 3.3, was used.

Figure 3.3. Wet and Dry Deposition Sampler in Amasra Station

The sampler consists of two buckets with 30 cm diameter, one for collecting dry and the other one is to collect wet deposition samples, a cap that automatically moves from one bucket to other when start and end of a rain event is sensed and a rain sensor. There is an activated rain sensor attached to the buckets. One of the buckets is used for collecting wet deposition samples while the other one is used for the collection of dry deposition samples. The cap closes the bucket that is not in use depending on the presence of rain detected by the rain sensor. The sensor controls the movement of the cap. If it is a wet period the precipitation is sensed by the rain sensor and the cap covers the dry deposition bucket and wet deposition sample is collected. On the other hand, if it is a dry period cap covers the wet deposition bucket allowing the sampler to collect the dry deposition.

Polyethylene bags having 10 L capacity are placed in each bucket. The bags provided an easy and contamination free collection system for the samples once the collection period is finished. Dry deposition samples are collected weekly therefore, at the end of each week the polyethene bag inside the dry deposition bucket is taken for analysis and it is replaced with a new one. Collection of wet deposition samples is event-based, which means that wet deposition, samples are collected at the end of each rain event. The wet deposition bucket is checked daily and if rain is observed in the bucket the bag is removed for analysis and replaced by a new one. If there is no rain event the bag is left on the sampler.

3.4. Sample Handling

At the station after at the end of each sampling period, the bags that contain deposition samples are taken off from the sampler with use of polyethylene bottles. The bottles are then sealed and they are put in another polyethylene bag and sent to the laboratory.

When the samples arrive to the laboratory, they are poured to high density polyethylene bottles with the use of a high-density polyethylene funnel. Then analysis of the sample is done for major ions.

3.4.1. Determination of Volume and pH

Volume and pH were measured by the use of calibrated sampling bottles in the laboratory. Sampling bottle heights were compared by the calibrated bottle. Before measurements were done the pH meter was calibrated using standard buffer solutions of pH 4.0 and pH 7.0. In pH measurements, a Radiometer PHM 80 portable pH meter which had a combination glass electrode was used. pH measurements were done immediately when the samples arrived to the laboratory.

3.4.2. Preparation of Samples for Ion Chromatography

The collected samples are directed to MGM laboratory for analysis. Extensive sample treatment is not necessary for the measurement of ion concentrations. However, there might be fine particles in the collected rainwater samples. Therefore, only treatment that is done is the removal of fine particulate matter by filtration process. In order to remove fine particulate matter, the samples are passed through cellulose acetate membrane filters with 0.2 µm pore size. Additionally, by this treatment, the clogging of IC column is prevented. In all collected precipitation samples ions such as SO_4^{2-}, NO_3^-, NH_4^+, Na^+ and Cl^- are almost 100% soluble. Therefore, these ions are not affected by the filtration process. On the other hand, solubility of ions such as Ca^{2+}, K^+ and Mg^{2+} varies between samples depending on the acidity of rainwater. Therefore, for this study only the soluble fraction of these ions is considered.

3.5. Analysis of Samples

In this study, to determine the major ion composition in the collected rainwater samples ion chromatography (IC) method is used.

IC can be considered to encompass liquid chromatographic techniques which can be used to determine ionic solutes such as: inorganic anions; inorganic cations including alkali metal, alkaline earth, transition metal, and rare earth ions; low-molecular-weight (water soluble) carboxylic acids as well as organic phosphonic and sulfonic acids, including detergents; carbohydrates; low-molecular-weight organic bases; and ionic metal complexes. (Jackson, 2000)

In IC method, separation of ions is done based upon their interactions with resin which is the stationary phase and the eluent which is the mobile phase. These phases can differ between an anion column that attracts anions, and a cation column that attracts cations. Each column is only able to measure the conductivity of the specific type of ion that it attracts. According to the ions affinity for the specific resin, they will travel through the columns of the ion chromatographer at different speeds. Additionally, the separation will also be affected by the ion charge and size. While the eluent passes through the column, the ions having weaker affinity for the specific resin will travel through the faster thus they will be eluted first. Whereas, ions having stronger affinity towards the resin will travel through the column much more slowly. When the ions exit the column, they are measured with an electrical conductivity detector. The output of this detector is a chromatogram which plots conductivity versus time. On this plot, each ion produces a peak where the height of the peak is based on the relative ion concentration in the injected solution. Then these measurements are used in order to determine analyte concentrations in an unknown sample. To prevent interferences that can be caused by ions in the eluent, a suppressor can be used to eliminate the undesired electrolyte before the conductivity measurement takes place. The logic is that as the solution travels through the suppressor, ions present in the mobile phase are replaced with nonionic species. If the eluent has a low conductivity or is dilute then there is no need to use a suppressor. (OSU, 2011)

In Amasra Station the soluble portion of the ions in the collected samples were analyzed by a Dionex 120 Ion Chromatograph in MGM laboratories. To different columns were used for anions (SO_4^{2-}, NO_3^-, Cl^-) and cations (NH_4^+, Mg_2^+, Na^+, Ca^{2+}, K^+) which are Dionex model AS9-HC and CS12A respectively. Moreover, in addition to the separation columns, suppressor columns were used. The suppressor used for anion analysis was ASRS-ULTRA whereas the suppressor used for cation analysis was CSRS-ULTRA. The eluents used for anion and cation analysis were 10 mM Na_2CO_3 and 18 mM methane sulfonic acid (MSA) solutions, respectively. Batch of 100 samples were selected and anions were analyzed. Then the column was changed to cation column and the cations were measured. Injection volumes for anions and cations were 75 μL and 10 μL, respectively whereas the flowrate of the eluent for both of them was 1.0 mL.

3.6. Data Quality Assurance

3.6.1. Field Blanks

Wet deposition samples consist of very low concentrations of dissolved components. The representativeness of the samples must be monitored and controlled by a strict quality control process since rainwater samples are very dilute by nature (Peden, et al., 1986).

Careful handling of precipitation samples from the field to the final destination (laboratory) is critical to obtain precise data. Mishandled or compromised samples can easily become contaminated. (National Atmospheric Deposition Program, 2019).

The primary purpose of these blanks is to detect sampling and analytical bias caused by contamination from equipment, supplies, and ambient environmental conditions. (United States Environmental Protection Agency, 2009; Francy, et al., 1998). Both field and laboratory blanks are collected. Field blanks are blank solutions used to check the potential contamination that can occur throughout all stages of sampling process including; the collection of samples, processing, preservation, transportation, and handling. Similarly, laboratory blanks are blank solutions utilized in order to evaluate bias from laboratory contamination taking into account entire sample preparation and analytical procedures (Francy, et al., 1998).

Field blanks were collected by pouring distilled deionized water in the polyethylene bags after they have been placed in the sampler. These prepared field blanks are treated exactly like the other precipitation samples collected during the study period. On the hand, laboratory blanks are used to evaluate the contaminations resulting from the acid washing, filter digestions and other processes.

3.6.2. Calculation of Detection Limits

The International Union of Pure and Applied Chemistry (IUPAC) defines a method's detection limit or limit of detection (LOD) as the smallest concentration or absolute amount of analyte that has a signal significantly larger than the signal from a suitable blank (IUPAC, 1995).

Commonly, the definition of detection limit is the concentration that corresponds to three times the standard deviation (σ) of ten replicate blank measurements. Similarly, detection limits for ions of concern for this study was determined by introducing one of the blank samples into the IC ten times and the concentration that corresponds to 3σ of the 10 measurements were detected from the calibration curve and finally this concentration was given as the limit of detection. Detection limits are given in Table 3.2 for each major ion. (Ayaklı, 2014)

Table 3.2. *Detection Limits of Ions (Ayaklı, 2014)*

ION	**DETECTION LIMIT (µg/L)**
SO_4^{2-}	0.0215
NO_3^-	0.0227
Cl^-	0.0764
NH_4^+	0.0812
Mg^{2+}	0.0077
Na^+	0.0185
Ca^{2+}	0.0448
K^+	0.0207

3.6.3. Quality Assurance

Quality Assurance (QA) for an analytical laboratory is an essential tool to ensure good comparability of data (Rauf and Hanan, 2009). Calibration check is considered to be a key component of QA.

By this means, in this study, Dionex-120 ion Chromatograph calibrated by Dionex Seven Anion Standard-II and Dionex Six Cation-II Standard which are commercially available. Seven Anion Standard-II was used for anions whereas Dionex Six Cation-

II Standard was used for cations. The calibration accuracy was tested by the analyzing known concentration of ions from Merck high purity salts (NaCl, K_2SO_4, $NaNO_3$, KCl, $CaCl_2$ and NH_4Cl) that are prepared using nanopore water. This testing process was carried out occasionally in order to test the calibration. The obtained results of this process are given in Table 3.3 (Ayaklı, 2014). In comparison, the calculated and measure concentrations indicate that the calibration of the instrument was reliable.

Table 3.3. *Calculated and Measured Concentrations of the High Purity Salts (Ayaklı, 2014)*

IONS	**Calculated Concentration (mg/L)**	**Measured Concentration (mg/L)**
SO_4^{2-}	6.00±0.30	6.25±0.10
NO_3^-	6.00±0.30	6.36±0.12
Cl^-	6.00±0.30	6.26±0.05
NH_4^+	2.94±0.15	3.10±0.28
Ca^{2+}	3.10±0.16	3.04±0.24
K^+	3.05±0.15	2.93±0.30
Na^+	3.01±0.15	2.96±0.27

3.7. Computation of Back Trajectories

Trajectories are the paths of infinitesimally small constituents of air with respect to time and space (Dutton, 1986). Forward trajectories represent where the air particles are headed and describes the future conditions whereas back trajectories show where the air masses are travelling from and describes the past conditions. By this means, back trajectories are generally used in order to demonstrate measurements of trace substances present in the atmosphere to evaluate relationships between their sources and their receptors (Stohl A. , 1998; Stohl, et al., 2002). In order to calculate trajectories, commonly used softwares are HYSPLIT (Draxler and Hess, 1998) and FLEXTRA (Stohl, 1999) (Wang, et al., 2008).

In this study, the back trajectories were calculated according to HYSPLIT model which stands for Hybrid Single Particle Lagrangian Integrated Trajectory. This model is a 3D isentropic model developed by National Oceanic and Atmospheric Administration (NOAA). This trajectory model is included in a GIS based software called TrajStat version 1.2.2.6. which is also available at NOAA's website. TrajStat is also capable of performing other trajectory related analysis such as cluster analysis, potential source contribution function (PSCF) and concentration weighted trajectory (CWT) analysis.

Five-day (120 hours) back trajectories starting from the Amasra station at 12:00 UTC at three different altitudes (100 m, 500 m and 1500 m) were calculated daily for every year between 2004 and 2016. Isentropic vertical motion method type was selected in TrajStat where air parcel is assumed to travel at a potential temperature. The format of the latitude and longitude values describing the receptor location is converted from degree-minute-second to decimal degree. Monthly meteorological data which introduced to the software is downloaded from the NOAA database. The interface of TrajStat software for trajectory calculation is given in Figure 3.4.

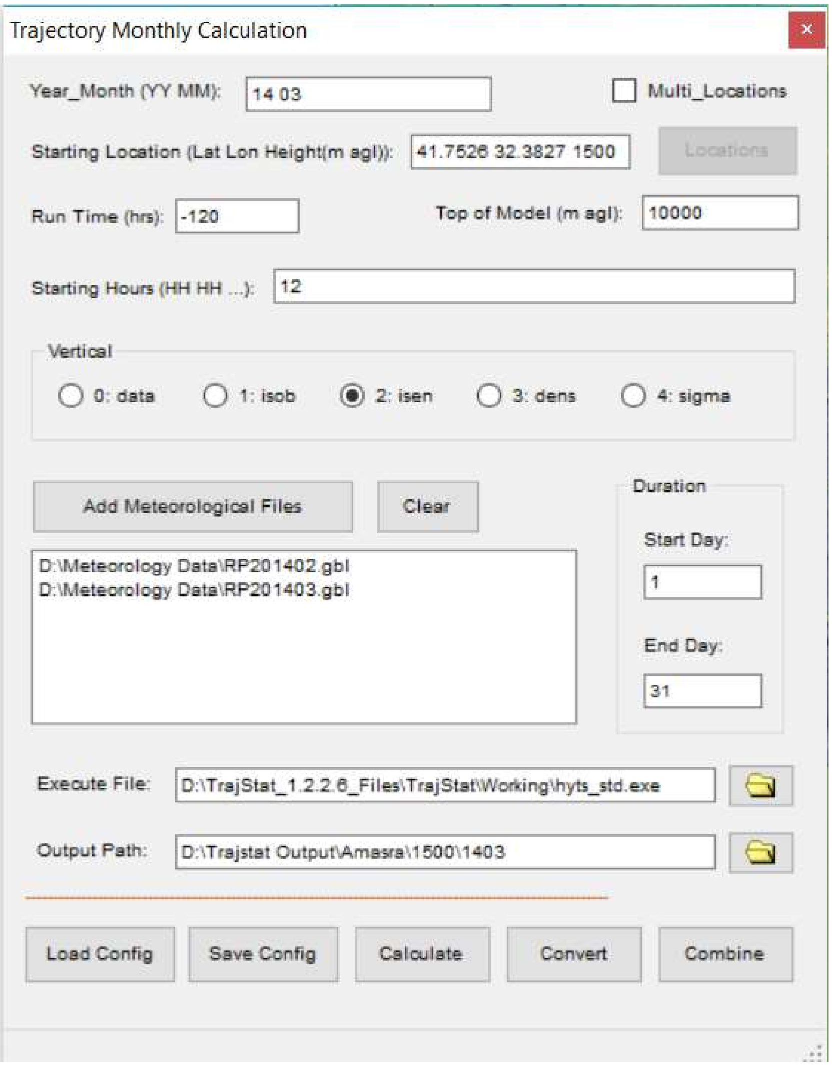

Year_Month (YY MM): 14 03

☐ Multi_Locations

Starting Location (Lat Lon Height(m agl)): 41.7526 32.3827 1500

Run Time (hrs): -120

Top of Model (m agl): 10000

Starting Hours (HH HH ...): 12

Vertical: ○ 0: data ○ 1: isob ● 2: isen ○ 3: dens ○ 4: sigma

D:\Meteorology Data\RP201402.gbl
D:\Meteorology Data\RP201403.gbl

Duration
Start Day: 1
End Day: 31

Execute File: D:\TrajStat_1.2.2.6_Files\TrajStat\Working\hyts_std.exe

Output Path: D:\Trajstat Output\Amasra\1500\1403

Figure 3.4. Trajectory Calculation Window of TrajStat

3.7.1. Flow Climatology

Flow climatology is concept that refers to the understanding of the air flow patterns impacting the study area. Such analysis is a type of trajectory statistics and provides insight on source areas of pollutants. Back trajectories that are calculated according to HYSPLIT model included in TrajStat software. The computed back trajectories were then introduced to MapInfo GIS Software Version 16.0 in order to create thematic maps that emphasize the patterns in the trajectory data.

Flow climatology was represented in this study by incorporating two different approaches, namely residence time analysis and wind sector analysis. Residence time analysis is an approach developed by our team whereas wind sector analysis is a more conventional method used widely in different studies in the literature.

In the first method (residence time analysis), the study domain was divided into 1ºx1º grids and it is shown in Figure 3.5. As can be seen from Figure 3.5 the study domain extends from west of UK (20ºW) to Center of Asia (60ºE) in West-East direction and from Siberia (75ºN) to middle of Africa (15ºN) in North-South direction. Then the segments of the back trajectories were assigned to grids according to their coordinates (longitude and latitude). Segments in each grid are counted in Map Info software. Segments are 1-hour part of a trajectory hence the count of segments in each grid represents the amount of hours air masses spend in that grid through the years 2004 to 2016. The distribution maps of residence times are done for each starting altitude (100 m, 500 m, 1500 m) and combination of these altitudes, also they are prepared for summer and winter seasons separately.

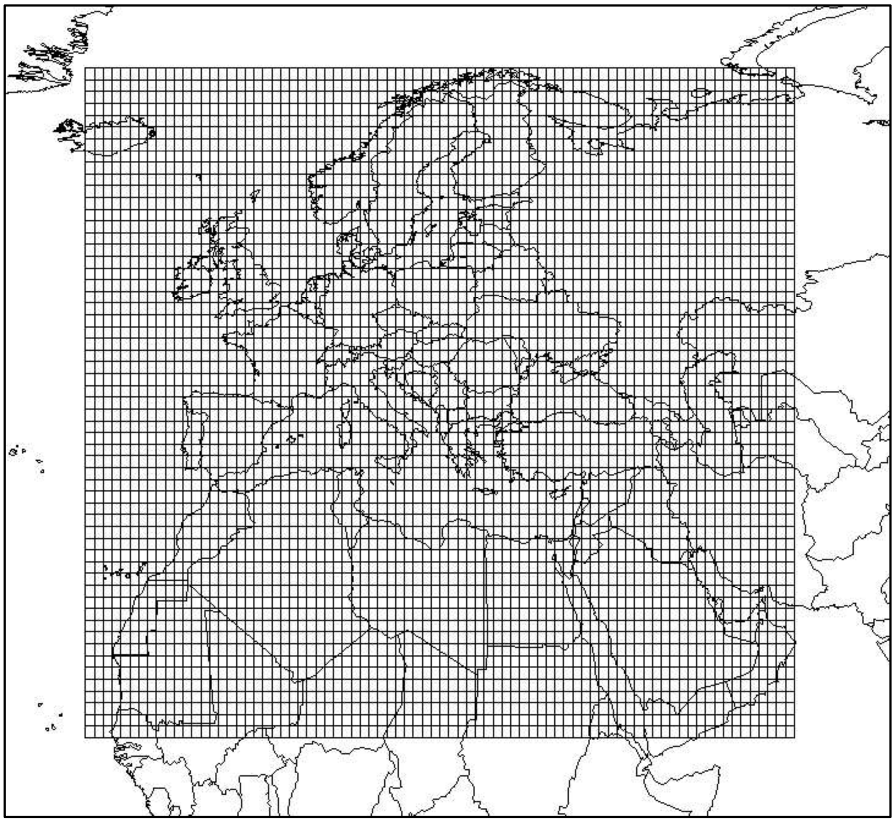

Figure 3.5. Study Domain for the Residence Time Analysis

Second method is the wind sector analysis which widely used in the literature and this method is analyzed in this study in order to compare the results with other studies done outside of our group. For the second method, the study domain is divided into total of 8 wind sectors, namely N, NE, E, SE, S, SW, W, NW. In a similar manner to the first approach, this time number of segments dedicated to each wind sector is counted. The dedication of trajectories to wind sectors are always a problematic issue in this conventional method since trajectories can pass through more than one sector before they arrive to the receptor site. To overcome this issue, number of segments were counted for each wind sector. Study domain used for the calculation of contribution of wind sectors is given in Figure 3.6.

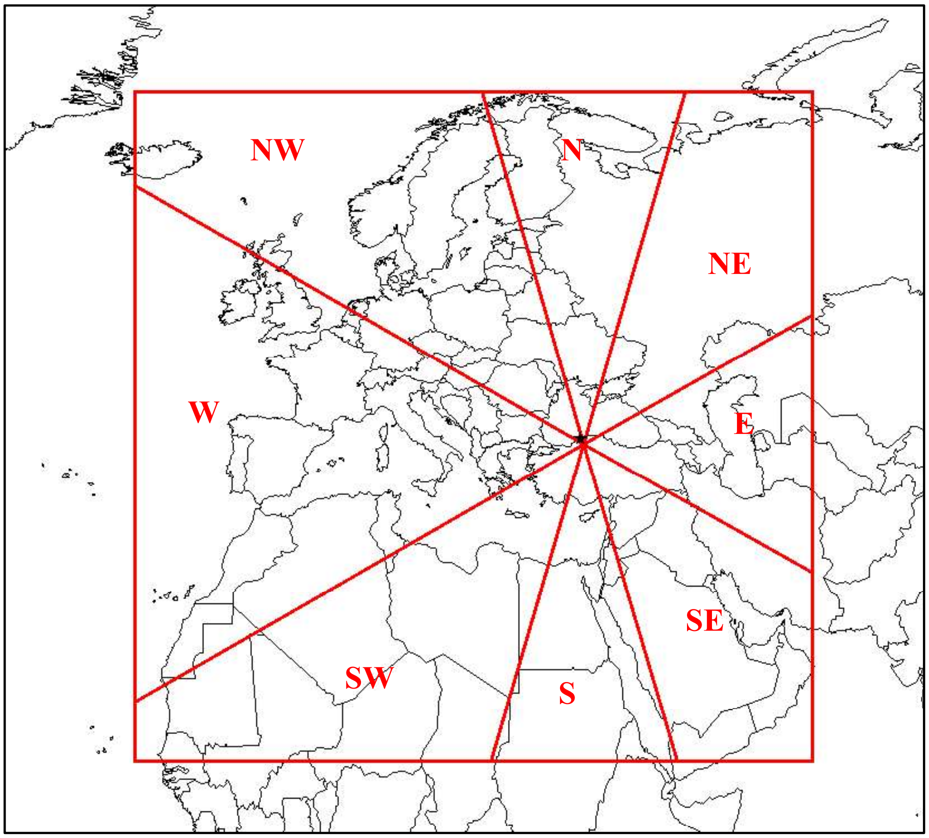

Figure 3.6. Study Domain Used in the Calculation of Contribution of Wind Sectors

Final assessment for flow climatology was performed in TrajStat software in order to group the trajectories into clusters. In the past air trajectories were frequently used in order to interpret individual flow situations whereas nowadays, statistical methods have been developed in order to evaluate large sets of trajectory data. Cluster analysis which is a multivariate statistical technique is a method that is used frequently in air pollution studies to identify trajectory groups that can bring anthropogenic and natural species to receptor.

In cluster analysis technique, the logic is to split the trajectory set of trajectory groups that are as homogeneous as possible in themselves and as different as possible between the groups. Grouping of trajectories bases on co-variation in transport speed and direction of trajectories, resulting in clusters of trajectories with similar curvature and length (Abdulmogith and Harrison, 2005; Moody and Samson, 1989). Moody and Galloway (1988) were the first ones to use trajectory coordinates as variables to group trajectories into cluster. After that, clustering was applied in many studies (for example Brankov et al. 1998; Harris and Kahl, 1990; Sirois and Bottenheim, 1995; Cape et al., 2000; Buchanan et al., 2002).

The TrajStat software forms clusters by combining nearest trajectories according to Ward's hierarchical method (Ward, 1963). In TrajStat, distance between two trajectories is determined by Euclidean distance formula which uses the latitude and longitude data as variables. The related formula is given in Equation 3.1 (Wang et.al, 2008).

$$d_{12} = \sqrt{\sum_{i=1}^{n}((X_1(i) - X_2(i))^2 + (Y_1(i) - Y_2(i))^2)} \qquad \text{(Equation 3.1)}$$

where d_{12} represents the distance between back trajectories and X_1 (Y_1) and X_2 (Y_2) are the reference backward trajectories 1 and 2, respectively.

In order to determine the optimum number of clusters a method that bases on variation in total root mean square deviation (TRMSD) with number of clusters was used (Brankov et al., 1998). In this approach, number of clusters was calculated from 3 to 20. Percent change in total root mean square (TRMSD) is computed every time. TRMSD decrease as number of clusters increase. The point where increasing cluster number by one results in 5% change in TRMSD is considered as the optimum number of clusters.

Determining number of clusters using statistical approach described above should be supplemented by visual inspection because, sometimes, increasing number of clusters by one does not generate a new cluster, but splits one of the existing clusters into two or more different clusters. In such a case, the last number of clusters before splitting occurs should be chosen as optimum number.

3.8. Potential Source Contribution Function

To find out the potential regions which are source of pollutants the measured concentrations must be combined with geographical information. In order to combine this information potential source contribution function is used which is another method of trajectory statistics. PSCF analysis describes areas that contributed to high concentrations of pollutants at the receptor site.

The study domain used for PSCF is the same as the domain represented in Figure 3.4. The segments are counted within each grid in a similar manner as described in previous flow climatology section of the manuscript.

The trajectory files corresponding to the measured days are selected. From the selected trajectories a group that corresponds to 30% of the polluted concentration is extracted and this extracted group of trajectories are referred as “polluted”. Similarly, segments forming these polluted trajectories are referred as “polluted segments”. The value for each grip in PSCF analysis is calculated according to Equation 3.2.

$$PSCF_{ij} = \frac{m_{ij}}{n_{ij}} \qquad \text{(Equation 3.2)}$$

Where m_{ij} is number of polluted segments in grid i and n_{ij} represents number of all segments (polluted + unpolluted) in the same grid. “j” is the segments counter.

PSCF value of grid ranges between 0 and 1. If the value is 1 at certain grid this means that every segment in that grid corresponds to high concentration of a specie or a factor. Thus, regions corresponding to those grids are considered as potential source regions. In contrast, grids having PSCF value of 0 indicate that the grid is not likely to be a potential source region.

There are uncertainties associated with PSCF analysis similar to all models. If the total number of segments in a grid is small then the PSCF value will only be depending on a few segments and the value obtained for the grid may be high. Statistically these values may not be significant and regions corresponding to these grids may not be a strong potential source region. Therefore, PSCF value obtained for these kinds of cells will have high uncertainties. In order to prevent these misleading outcomes a weighting method was developed by Zhao and Hopke (2006) is used and it is given in Equation 3.3.

$$W(n_{ij}) = \begin{cases} 0{,}15 & n_{ij} \le {}^{n_{avg}}\!/_{2} \\ 0{,}5 & {}^{n_{avg}}\!/_{2} < n_{ij} \le n_{avg} \\ 0{,}75 & n_{avg} < n_{ij} \le 2 * n_{avg} \\ 1.0 & n_{ij} > 2 * n_{avg} \end{cases} \qquad \text{(Equation 3.3)}$$

Where $W(n_{ij})$ is the weighting function and n_{avg} is the average number of segments in each grid.

As can be seen from Equation 3.3, when the total number of grids less than half of the average number of segments then the PSCF value was multiplied by 0,15. If the number of segments in a grid lies between half of average number of segments and average number of segments then the value is multiplied by 0,5. Additionally, when the number of segments are between the average number of segments and twice of the average number of segments, the PSCF value is multiplied by 0,75. Finally, if the segment number is more than twice of the average number of segments then the PSCF value is multiplied 1.0. This method clearly reduces the uncertainties arising from grids having few segments as the values of those grids are multiplied with lower coefficients.

3.9. Positive Matrix Factorization

In this study, PMF version 5.0 which is available for download at EPA’s website is used for source apportionment. PMF requires two input files which are a file containing measured concentrations and another file for their related uncertainties. Receptor models do not allow missing data points in terms of concentrations of the species. In order fill the missing data in concentration and values that are below the detection limit of the method (BDL) the methodology described by Reff et. al. (2007) is used. According to this methodology the missing concentration data is replaced by the geometric mean of the specie whereas the values that are below the detection limit are replaced with half of the method detection limit. The related detection limits are given in Table 3.2.

The concentration data and associated uncertainty calculations are summarized in Equation 3.4:

$$\left.\begin{array}{l} If\ C_i > DL_i \rightarrow Use\ C_i\ as\ concentration\ value\ and\ UNC_i = DL_i + 0{,}1 * C_i \\ If\ C_i \leq DL_i \rightarrow Replace\ C_i\ with\ \frac{DL_i}{2}\ and\ UNC_i = DL_i * \frac{5}{6} \\ If\ C_i\ is\ missing \rightarrow Use\ geometric\ mean\ as\ C_i\ and\ UNC_i = 4 * Geo.mean \end{array}\right\} \quad \text{(Equation 3.4)}$$

Where;

C_i: Concentration of ion,

DL_i: The detection limit of the ion

UNC_i: Uncertainty of the ion.

In each run PMF software calculates 2 Q values which are Q_{true} and Q_{robust}. In addition, $Q_{theoretical}$ value should be calculated by using Equation 3.5.

$$Q_{theoretical} = (k * m) - t(k + m) \qquad \text{(Equation 3.5)}$$

Where;

k: Number of elements

m: Number of days

t: Number of factors.

Various number of runs should be done in order to determine the number of factors and each run gives a Q_{robust} and Q_{true} data. After obtaining these values they should be compared with the calculated $Q_{theoretical}$. $Q_{true}/Q_{theoretical}$ ratio should be approximately 1 to 1.5 in order for number of factors to be feasible.

After the selection of number of factors, by evaluating the outputs such as correlation between species and factor profiles, the decision can be made about which factor represents which source.

3.10. Mann-Kendall Test for Trend Analysis

Schematics of methodology in trend analysis is given in Figure 3.7. Every step of the trend analysis is conducted using the software MYSTAT (Student version of SYSTAT).

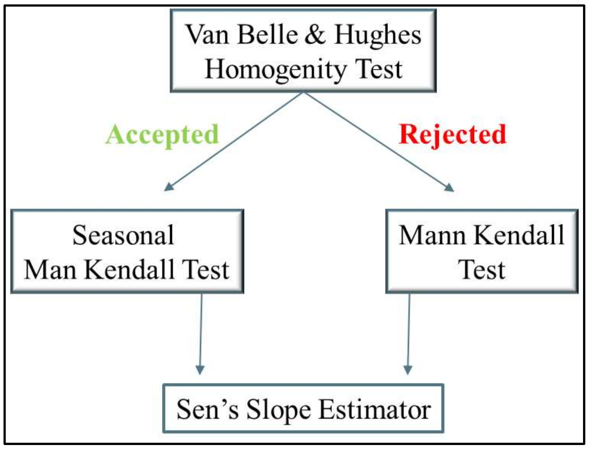

Figure 3.7 The Schematical Description of the Trend Analysis Methodology

If in all seasons the trends are in the same direction (upward or downward) then it meaningful to say there is a global trend. Therefore, homogeneity test was applied to see whether there is a global trend among the seasons. This test helps to decide whether to apply Seasonal Mann Kendall Test or Mann Kendall Test. If the homogeneity test is verified, then it is logical to use Seasonal Mann Kendall Test. Consequently, if the test is not positive then it is appropriate to use Mann Kendall Test.

Mann-Kendall statistic S for the data set xi of length 'n' is given as in Equation 3.6:

$$S = \sum_{k=1}^{n-1} \sum_{j=k+1}^{n} sgn(x_j - x_k) \qquad \text{(Equation 3.6)}$$

Where;

$$sgn(x_j - x_k) = \begin{cases} +1 \ if \ (x_j - x_k) > 0 \\ 0 \ if \ (x_j - x_k) = 0 \\ -1 \ if \ (x_j - x_k) < 0 \end{cases} \qquad \text{(Equation 3.7)}$$

The normal test statistics Z can be calculated, thereafter, first estimating the variance (S) as shown in the Equation 3.8:

$$z = \begin{cases} \frac{S-1}{\sqrt{Var\ (S)}} \ if \ S > 0 \\ 0 \qquad if \ S = 0 \\ \frac{S+1}{\sqrt{Var\ (S)}} \ if \ S < 0 \end{cases} \qquad \text{(Equation 3.8)}$$

Positive Z values are the indication of an increasing trend while negative values suggest a decreasing trend. An increasing or decreasing trend (two tailed test) can be tested at the α level of significance against the null hypothesis of, H_0, no trend. H_0 is rejected if the absolute value of Z is greater than the $Z_{1-\alpha/2}$, where $Z_{1-\alpha/2}$ is obtained from the standard tables.

To determine the global trend, as mentioned in the previous paragraphs, the seasonal trends should be in the same direction and magnitude or to put it another way, they should be homogenous. To evaluate whether there is homogeneity between the seasons Homogeneity Test originally developed by Van Belle and Hughes (1984) was applied. The corresponding test statistic χ^2_{homog} can be computed by using the Equation 3.9:

$$X^2_{homog} = X^2_{Total} - X^2_{Trend} = \sum_{i=1}^{m}(Z_i)^2 - m(\bar{Z})^2 \qquad \text{(Equation 3.9)}$$

Where;

$$Z_i = \frac{S_i}{\sqrt{Var(S_i)}}, \ \overline{Z} = \frac{1}{m}\sum_{i=1}^{m} Z_i \qquad \text{(Equation 3.10)}$$

The computed $\chi^2_{homogen}$ value was compared to the standard value at 11 degrees of freedom ($d_f = 11$) and at the α level significance to test the null hypothesis, H_0, of homogenous seasonal trend over a time period. If the computed value exceeds the standard one, then the null hypothesis is rejected. If that is the case it is not suitable to use seasonal Kendall test and slope estimate, rather than that Mann-Kendall test and Sen's Slope Estimator should be used for each individual season (Gilbert, 1987). In the case of $\chi^2_{homogen}$ not exceeding the critical value, χ^2_{Trend} is compared to the chi square distribution with 1 d_f to test if there is a common trend among all seasons.

Sen's Slope Estimator is another non-parametric tool used to calculate the rate of change per time. This tool avoids outliers and allows missing values. The equation of the method is given below (Equation 3.11):

$$Q_i = \frac{x_j - x_k}{j-k} \quad for \quad i = 1, \dots, n \qquad \text{(Equation 3.11)}$$

Where x_j and x_k represent the data values at times j and k (j>k). median of the n values of Q_i is taken as Sen's Slope Estimator. Then, median value obtained from Q_i is tested by two-sided test at the confidence interval of 100(1-α) % and true slope is obtained as a result.

CHAPTER 4

RESULTS AND DISCUSSION

4.1. General Characteristics of the Data

In this study, a total of 820 samples were collected by MGM between the years 2005 to 2016. Collected samples were analyzed and concentrations of nine major ions were determined. Ions measured in the study include, H^+, Cl^-, SO_4^{2-}, NO_3, $^-NH_4$, Ca^{2+}, Mg^{2+}, K^+ and Na^+. Volume weighted averages (VWA), arithmetic means and associated with standard deviations, median, maximum and minimum concentrations of ions as well as number of data available for each ion are given in Table 4.1.

Table 4.1. *Statistical Summary of Ionic Composition in Amasra Station (concentrations are in mg/L)*

Major Ions	**Volume Weighted Average**	**Mean**	**Median**	**Range**	**N**
H^+	0.003	0.018±0.034	0.002	$4.07x10^{-6}$-0.275	820
SO_4^{2-}	0.880	3.711±4.797	2.470	0.020-66.430	812
NO_3^-	0.499	2.446±4.323	1.380	0.030-57.330	798
Cl^-	1.114	4.167±6.902	2.130	0.010-85.220	809
NH_4^+	0.282	1.145±1.778	0.660	0.010-22.000	722
Ca^{2+}	0.552	2.944±6.202	0.990	0.010-72.960	731
Mg^{2+}	0.089	0.639±1.192	0.270	0.010-10.460	749
K^+	0.055	0.430±1.391	0.150	0.010-26.770	741
Na^+	0.514	2.773±4.213	1.400	0.010-33.850	757

Concentrations of ions in precipitation is inversely proportional to the rainfall amount (Al-Momani et. al, 1998). In intense rain events concentration of the constituents are lower. On the contrary, higher concentrations are observed with low precipitation.

This situation is due to dilution effect. Volume weighted average (VWA) concentrations of measured parameters are used to avoid such variability in ion concentrations due to precipitation amount (Alagha and Tuncel, 2003; Valenta et.al., 1986).

Volume weighted average (VWA) is calculated using the following Equation 4.1:

$$C_{xp}=\frac{\Sigma(C_x*V_p)}{\Sigma V_p} \qquad \text{(Equation 4.1)}$$

Where;

C_{xp}: Volume weighted concentration of specie x,

C_x: Concentration of specie x in the given sample,

$V_{p:}$ Precipitation volume of the sample.

Volume weighted average concentration of ions varies between 0.003 mg/L for H^+ ion and 1.1 mg/L for Cl^-. Concentrations of most of the measured ions cover a very wide range of values, which is typical for environmental data in general. Number of data points for ions vary between 720 for NH_4^+ ion and 820 for H^+ ion. Such large number of samples is the most important strength of this data set.

4.1.1. Distribution Characteristics of the Data

The frequency distribution of ion concentrations is computed and presented as frequency in Figures 4.1 and 4.2 for measured anions and cations, respectively. If the right end of the plot in a frequency histogram has a longer tail and the mean exceeds the median value, the data is considered to be right skewed (positively skewed). Atmospheric data tend to always show positively skewed distribution. Among all right skewed distributions, log-normal distribution is the most commonly observed in environmental data sets (Ayaklı, 2014; Balcılar et.al., 2014; Yücel, 2019).

In this study, The Kolmogrov Simirnov (K-S-DN) statistics is used to test the "goodness of the fit" of the data to log-normal distribution. Statgraphics Centurion

Version 18.1.02 Software was used to carry out the related statistical analysis. Kolmogrov Simirnov test computes the maximum distance between the cumulative distribution of the variable and the cumulative distribution of the fitted log-normal distribution. The software tests the null hypothesis assuming the specie of selection comes from a log-normal distribution with a confidence interval which is initially defined and displays a p-value. If the p-value is greater than the initially defined confidence interval, then the data can be assumed to show a log-normal distribution. For this study, a 95% confidence interval was determined for the test and all species that have a p-value smaller than 0.05 were assumed to show a log-normal distribution. All ions in this study have a right-skewed distribution; however, distributions of only NH_4^+, Ca^{2+}, Na^+ are log-normal with 95% statistical significance. Although distributions of remaining ions are also right-skewed, they are not log-normally distributed. The frequency distributions of anions and cations are given in Figure 4.1 and Figure 4.2.

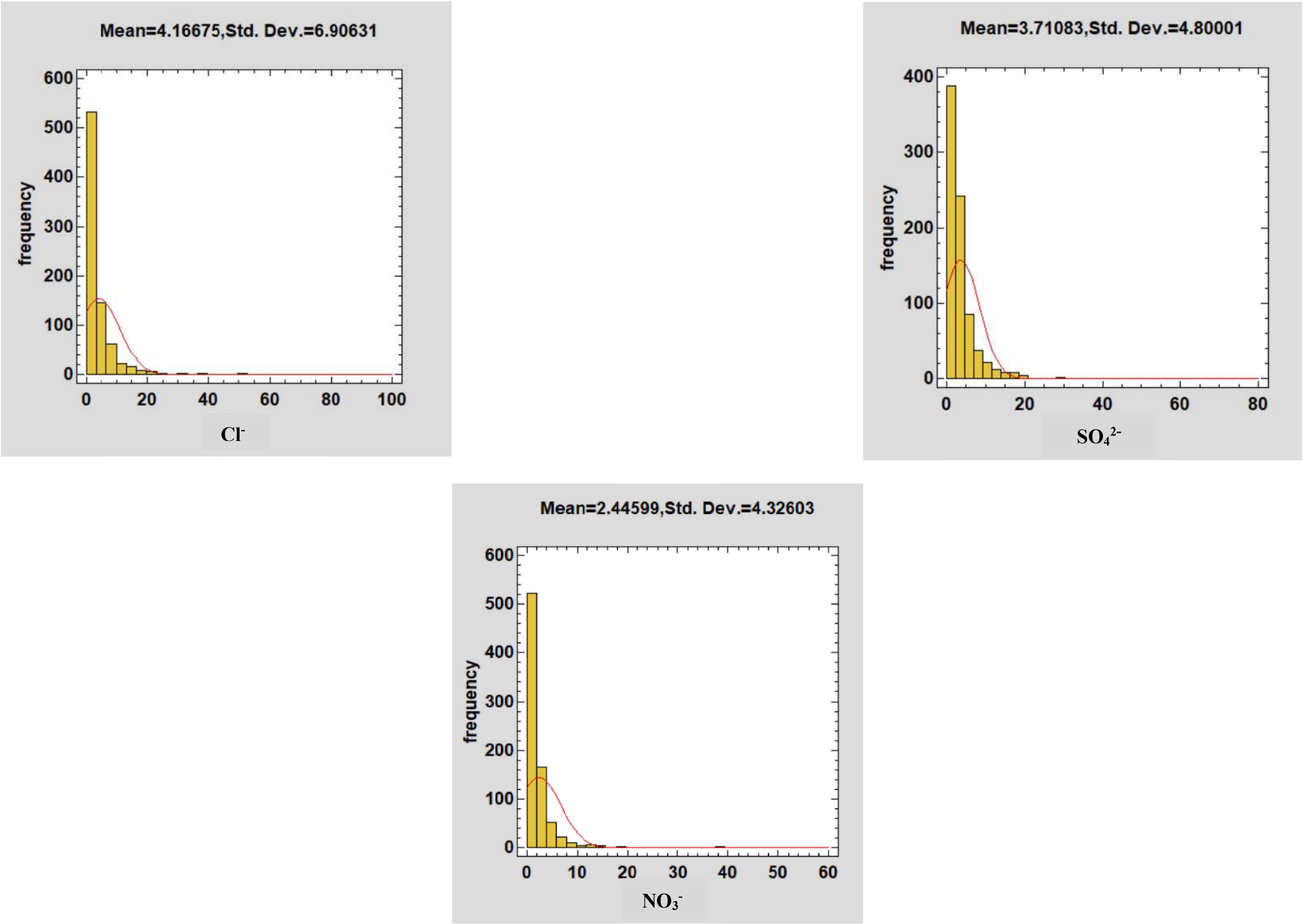

Figure 4.1 Frequency Distribution -Anions

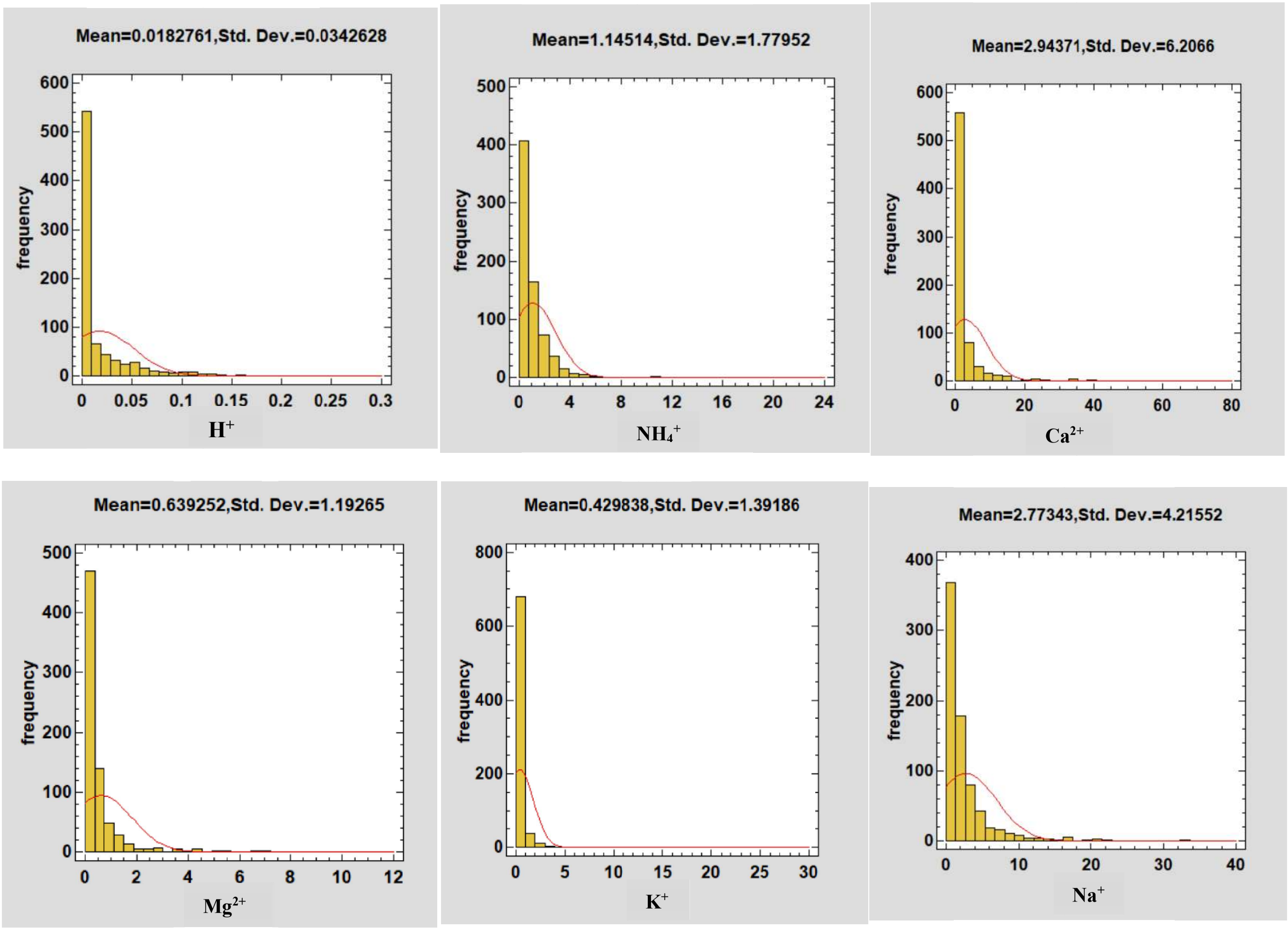

Figure 4.2 Frequency Distribution - Cations

4.1.2. Comparison of the Data with Literature

In urban and industrial zones air quality is evaluated by comparing the measured data with the air quality standards. The situation is not the same in studies performed in a rural area, which is not under direct influence of anthropogenic sources. The measurements conducted at rural sites gives lower concentrations than those measured at industrial or urban sites. The reason for lower concentrations observed in rural areas is that they are not impacted directly by industrial activities, vehicle emissions and residential emissions. Although measured concentrations at rural sites are low, they are still important as they are indicators of health of the ecosystem. Since standards set by regulations are not applicable to evaluate air quality at rural sites, the only option is to compare concentrations obtained in rural stations with the measurements for rural areas conducted by others and reported in literature.

The measurements in this study were first compared with similar data obtained in EMEP (European Monitoring and Evaluation Program) network. Secondly, they are compared with similar data obtained in other stations located in Turkey.

4.1.2.1. Comparison with EMEP Network

Within the framework of UNECE Convention on Long-range Transboundary Air Pollution (CLRTAP), the EMEP is responsible for monitoring and evaluating the long-range transport of air pollutants. The network consisted of approximately 170 rural and suburban stations and it is operational since 1977. 170 stations do not operate continuously, but approximately 100 stations are operational every year. Main objectives in operating such a large network is (a) to assess urban air quality with high resolution, (b) to determine long term trends in pollutant concentrations and (3) to validate EMEP models (or to provide data for validation of non-EMEP models).

EMEP is the co-operative program for monitoring and evaluation of the long-range transmission of air pollutants in Europe. It is a program under the Convention on Long-range Transboundary Air Pollution (CLRTAP) aiming international collaboration in order to solve problems on transboundary air pollution (EMEP, n.d.).

There is only one EMEP station located in Turkey, which is at Çubuk, Ankara. The Station was initially founded by Ministry of Health. It was under operation between the years 1993 and 2006. After that period, the station was transferred to the Ministry of Environment and it is not operating since then.

The EMEP network, which were compared with data generated at Amasra is separated to six groups based on their location in Europe (all, northern, southern, western, eastern, central and islands). Data generated at stations in these regions are expected to have some common features, which are different from data generated in stations located in other regions. Related rainwater data was downloaded from EMEP database and the average concentrations of major ions in EMEP network between the years 2004 to 2015 is calculated. This period is chosen to be comparable with the period when Amasra station was operational. Average concentrations of ions measured in these stations are given in Figure 4.3 for anthropogenic ions and Figure 4.4. for crustal and marine ions. Average concentrations of ions are also summarized in Table 4.2.

All of the pollution-derived ions (SO_4^{2-}, NO_3^- and NH_4^+) are higher at Amasra Station when compared with EMEP network data. This is an important point showing polluted nature of Amasra region. These high concentrations measured in this work is probably due to high proximity of the station to high emission areas in Ukraine and Russia, as will be discussed later in the manuscript.

As can be seen from Figure 4.4, ions that originate from sea salt, namely Na^+ and Cl^- are close to the average concentration observed in all Europe. Islands in Europe have the highest concentrations for Na^+ and Cl^- as expected. Since the station is located close to the Black Sea, the concentration of sea salt originated ions is expected to be higher in Amasra than EMEP stations, except for “Island” group. Although concentrations of Na^+ and Cl^- at Amasra are slightly higher than their corresponding concentrations reported for Eastern, Central and Northern Europe, they are lower than averages reported for Western and Islands groups.

Another point that is important to note in Figure 4.4. is the high concentration of Ca^{2+} concentration at Amasra. Average of long years data at Amasra station is approximately 3 mg L^{-1}, which is factors of 3-6 higher than Ca^{2+} concentrations reported for entire Europe. High Ca^{2+} concentrations at Amasra is probably due to alkaline nature of the soil in that region.

Table 4.2. *Average Major Ion Concentrations for EMEP Network and Amasra Station*

	All	Eastern	Western	Southern	Central	Nothern	Islands	Amasra
H^{+}*	10.39	13.29	7.90	7.04	10.61	15.22	5.44	18.28
SO_4^{2-}	1.22	1.85	0.74	1.54	1.16	1.28	0.32	3.71
NO_3^{-}	1.44	1.65	1.27	1.55	1.65	1.43	0.60	2.45
Cl^{-}	6.24	0.94	10.29	1.52	1.17	1.70	40.74	4.17
NH_4^{+}	0.56	0.67	0.48	0.62	0.62	0.50	0.37	1.15
Ca^{2+}	0.67	0.85	0.60	1.08	0.27	0.53	1.10	2.94
Mg^{2+}	0.46	0.13	0.69	0.20	0.09	0.15	2.70	0.64
K^{+}	0.28	0.29	0.28	0.31	0.09	0.19	0.85	0.43
Na^{+}	2.92	0.57	4.75	0.93	0.64	0.99	17.69	2.77

H^{+} concentrations are given in µg/L.

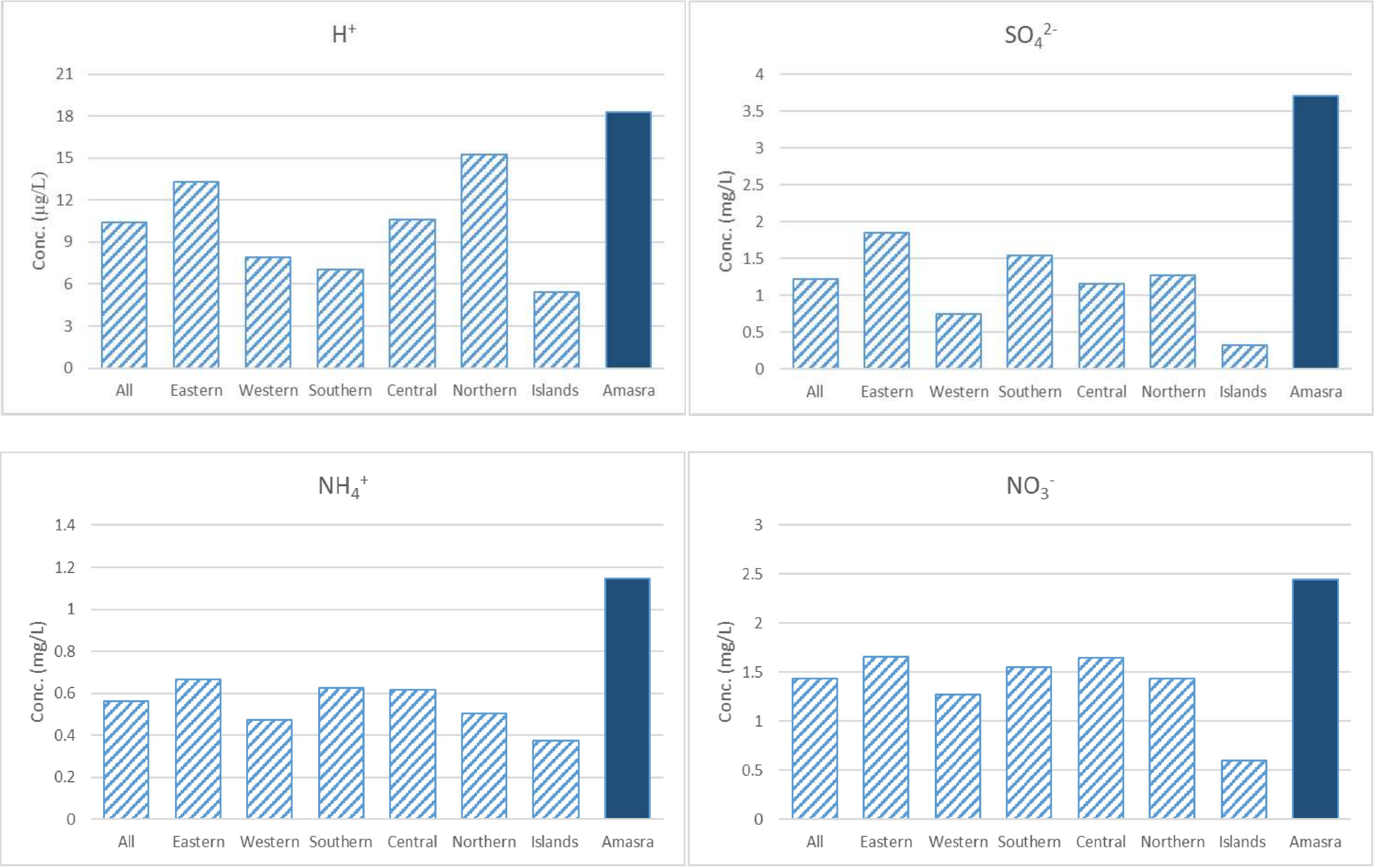

Figure 4.3 Comparison of pollution-derived ions in this study with corresponding data from EMEP network.

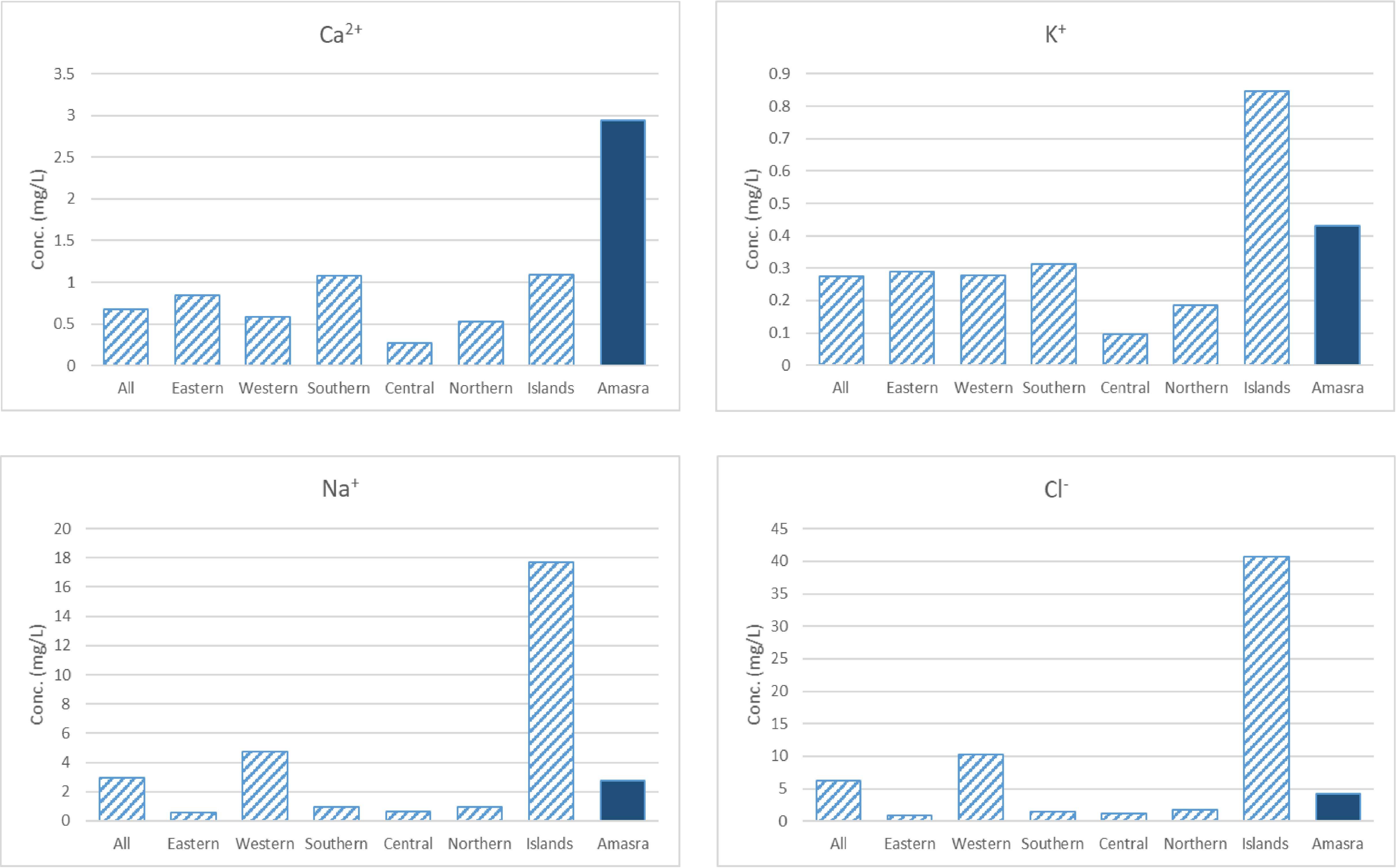

Figure 4.4 Comparison of crustal and marine ions in this study with corresponding data from EMEP network.

4.1.2.2. Comparison with MGM Network

There are 10 stations, which are currently operational, in Turkey, where composition of precipitation is monitored (MGM network). These stations are located at Antalya, Amasra, Balıkesir, Çamkoru, Çatalca, Hatay, İzmir, Marmaris, Trabzon and Yatağan. The locations of the stations in MGM Network is given in Figure 4.5. Please note that although stations are identified with the cities and villages where they are located none of these stations, except for Yatağan, are located in cities. They are >10 km away from the settlement centers.

Figure 4.5 The location of the Station in MGM Network

The network started with a bulk sampling station at Çamkoru in 2004. Among the 10 stations operated by MGM, Çamkoru is the only one that is equipped with bulk samplers. An automated wet-and-dry sampler was also installed at Çamkoru in 2014. Other stations are equipped only with automated wet-and-dry samplers. Amasra and Balikesir stations were also commissioned in 2004. After a year, in 2005 two other stations became operational at Antalya and Çatalca. Following these, stations in İzmir and Marmaris were activated in 2011. Yatağan, Hatay and Trabzon stations were commissioned in 2012, 2013 and 2014, respectively. Among these stations only

Amasra is approximately 10 km away from the urban site. Others are installed to Meteorological Doppler radar sites, which are always more than 10 km away from urban areas.

Average concentrations of major ions observed in this study and in other stations in MGM network the stations that are located in Turkey is represented in Figure 4.6 and 4.7. Average concentrations of ions are also summarized in Table 4.3.

As can be seen from Figure 4.6, pH values among stations does not show any significant changes throughout the stations in Turkey including this work. In all stations pH vary between 5,7 and 7.0. They are all above the range that is considered as acidic (pH<5). This is observed in all rainwater studies performed in Turkey and in Eastern Mediterranean and Black Sea region and attributed to calcareous nature of soil in Turkey and Mediterranean region in general. High level of $CaCO_3$ in soil neutralizes acids, such as H_2SO_4 and HNO_3, in rainwater. Rainwater neutralization will be discussed in more detail in the following sections of the manuscript.

Another striking difference observed in Figure 4.6 is very high SO_4^{2-} concentration observed at Yatağan Station. Such unusually high concentration of SO_4^{2-} observed at Yatağan is probably due to the presence of the thermal power plant located near this station.

Following Yatağan, Çatalca and Amasra has the highest concentrations of SO_4^{2-} and NO_3^-. Çatalca Station is located very close to İstanbul, which is a very strong urban and industrial source. Çatalca is also close to Kocaeli province, which is a very strong industrial source area. Probably high concentrations of most of the anthropogenic ions at Çatalca represent relatively high regional background concentrations in that region.

Concentrations of pollution derived ions at Amasra station is higher than concentrations measured in most of the MGM stations, except for Yatağan and Çatalca stations. Relatively high concentrations of anthropogenic ions and trace elements are also observed in particle (Balcılar et al., 2014; Tokgöz and Tuncel, 2015) and rainwater (Alagha and Tuncel, 2003) samples collected at other stations on the Black

Sea coast; indicating that regional concentrations of anthropogenic species are also high on the Black Sea coast. The sources contributing high regional concentrations in the Black Sea region is probably located at industrial areas at the Eastern Ukraine and the Black Sea Coast of Russia (Balcılar et al., 2014)

In Figure 4.7, the concentrations of crustal and sea salt ions are represented for stations in Turkey. From the figure it can be seen that the of sea salt ions are the highest in Hatay Station. Concentrations of Na^+ and Cl^- are also high at Amasra station. Both stations are very close to the coast.

Another interesting point observed from Figure 4.7 can noted as the unusually high concentration of Ca^{2+} observed in Yatağan Station. The reason is probably higher $CaCO_3$ content of soil at Yatağan area.

Following Hatay Station, in Amasra the K^+ content was found to be relatively high. Again, the reason for this can be given as proximity to the coastline because K^+ concentration can also be introduced with the contribution of sea salt. It is important to note that both Na^+ and Cl^- is very high in Amasra Station as well.

Table 4.3. *Average Major Ion Concentrations for MGM Network and Amasra Station*

	Antalya	Balıkesir	Çamkoru	Çatalca	Hatay	İzmir	Marmaris	Trabzon	Yatağan	Amasra
pH	6.31	6.05	6.82	5.86	6.21	6.26	5.90	6.72	6.53	5.70
SO_4^{2-}	1.57	3.34	2.61	4.39	3.18	3.47	3.11	1.87	9.73	3.71
NO_3^-	1.60	2.91	1.12	3.27	2.59	1.97	1.45	2.04	1.76	2.45
Cl^-	1.14	1.85	0.36	5.03	9.53	3.87	4.05	1.94	2.58	4.17
NH_4^+	1.25	1.30	0.75	1.31	1.95	2.61	1.09	2.24	3.37	1.15
Ca^{2+}	2.79	3.22	4.06	2.68	2.99	2.75	2.34	2.34	6.94	2.94
Mg^{2+}	0.28	0.28	0.55	0.48	1.49	0.41	0.57	0.61	0.43	0.64
K^+	0.25	0.29	0.15	0.34	0.54	0.36	0.35	0.28	0.29	0.43
Na^+	0.71	1.10	0.36	3.05	5.31	1.82	2.24	1.54	1.09	2.77

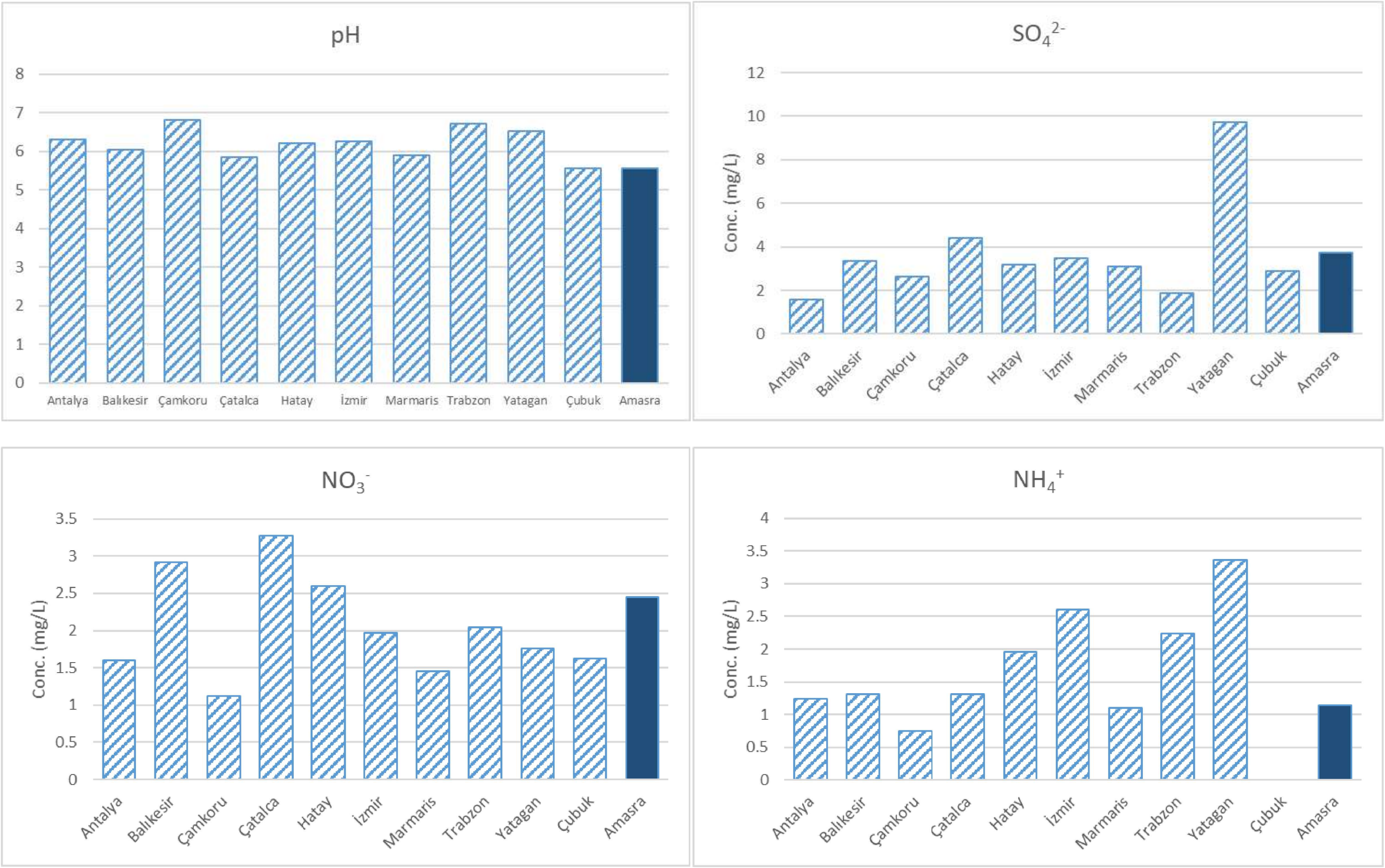

Figure 4.6 Comparison of pollution-derived c ions in this study with corresponding data from other stations located in Turkey

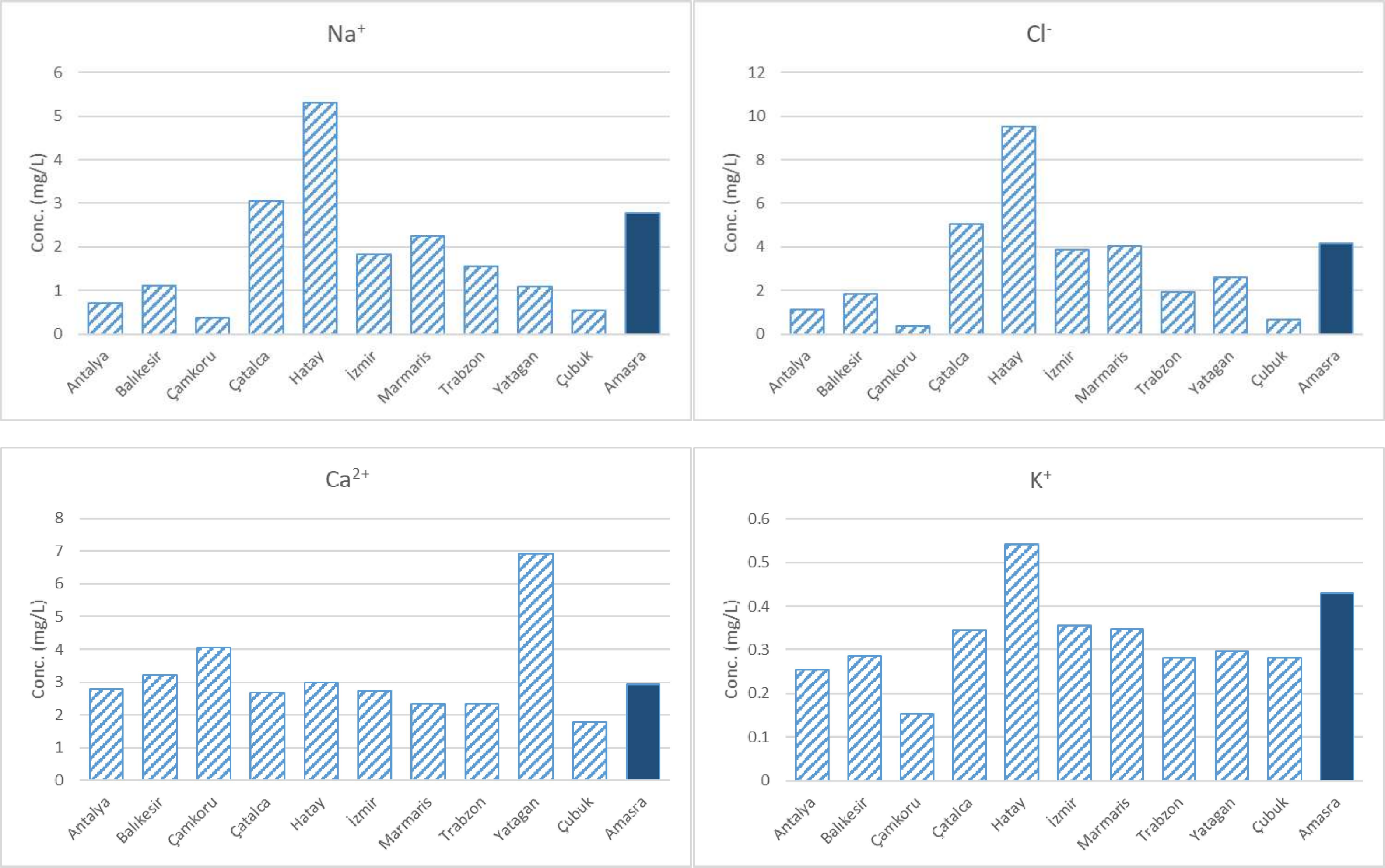

Figure 4.7 Comparison of crustal and marine ions in this study with corresponding data from other stations located in Turkey.

4.2. Flow Climatology

Flow climatology is an important concept that is presented in this study, as it shows the travel of air masses and the time that they spent in those locations until they reach the receptor site which is Amasra Station in this study. Data obtained by flow climatology provide insight about potential source areas of pollutants which are intercepted at Amasra Station. For this study, flow climatology is applied using two approaches, which bases on counting of trajectory segments in grids and in wind sectors. Trajectory analysis is conducted for a 13-yr period, between 2004 and 2016. Backtrajectories were 5-day long with starting altitudes of 500 m, 1000 m and 1500 m. One backtrajectory at these starting altitudes were calculated for each day. Trajectories consists of "segments". Each segment represent 1-hr potion of the backtrajectory. Segments indicate latitude, longitude and altitude of the air parcel at that particular1-hr period. Additional meteorological information, such as rainfall, winds etc. are also provided for the location and altitude where segment resides during that hour. Each back trajectory calculated for 5 days backwards in time consisted of 105 segments. In 13 years duration of the study 4700 backtrajectories, consisting of approximately 500,000 segments were modeled, using 3D Hysplit model, which was developed in NOAA, USA.

4.2.1. Residence Time Analysis

In the study, residence time analysis is based on segment counts in grids. All calculations were performed for the study domain which extends from west of UK and East of Caspian Sea in East – West direction and from North of Scandinavia to South of Algeria in North - South direction. This domain is divided to 1^o x 1^o grids and most of the segment counting was performed in these grids.

Segment density in grids are presented as distribution maps, which are prepared using a GIS software (Map Info). Distribution maps illustrate distribution of time air masses spend around the study domain before they were intercepted at the station. The related distribution maps of residence times in the study area for 100 m, 500 m and 1500 m starting altitudes and distributions obtained by combining segments at all starting altitudes are given in Figure 4.8.

In Figure 4.8, it can be clearly seen that no striking differences are observed between the different starting altitudes. Since all trajectories eventually converge to the station, having longer annual residence times close to the station is not surprising. The figure also demonstrates that annual residence times of air masses are longer in W, NW and North sectors, compared to E and S sectors. This can be interpreted as sources in W, NW and N sectors have higher probability of affecting chemical composition of rainwater (and aerosol) at central Black Sea region. Enlarged red area in Figure 4.8d is due to increased number of segments (by a factor of three) when trajectories at all starting altitudes are included in analysis. However, the sectors where air masses spent most of their time did not change by adding all segments into counting.

The figure also demonstrates that the air masses spend majority of their time over western half of Turkey, Balkan countries which have a coast on the Black Sea such as Bulgaria and Romania and other countries that have coast on the Black Sea particularly Ukraine and Russia. Which means that as a result of air masses source areas in these countries are more likely to influence atmospheric composition observed in Amasra Station.

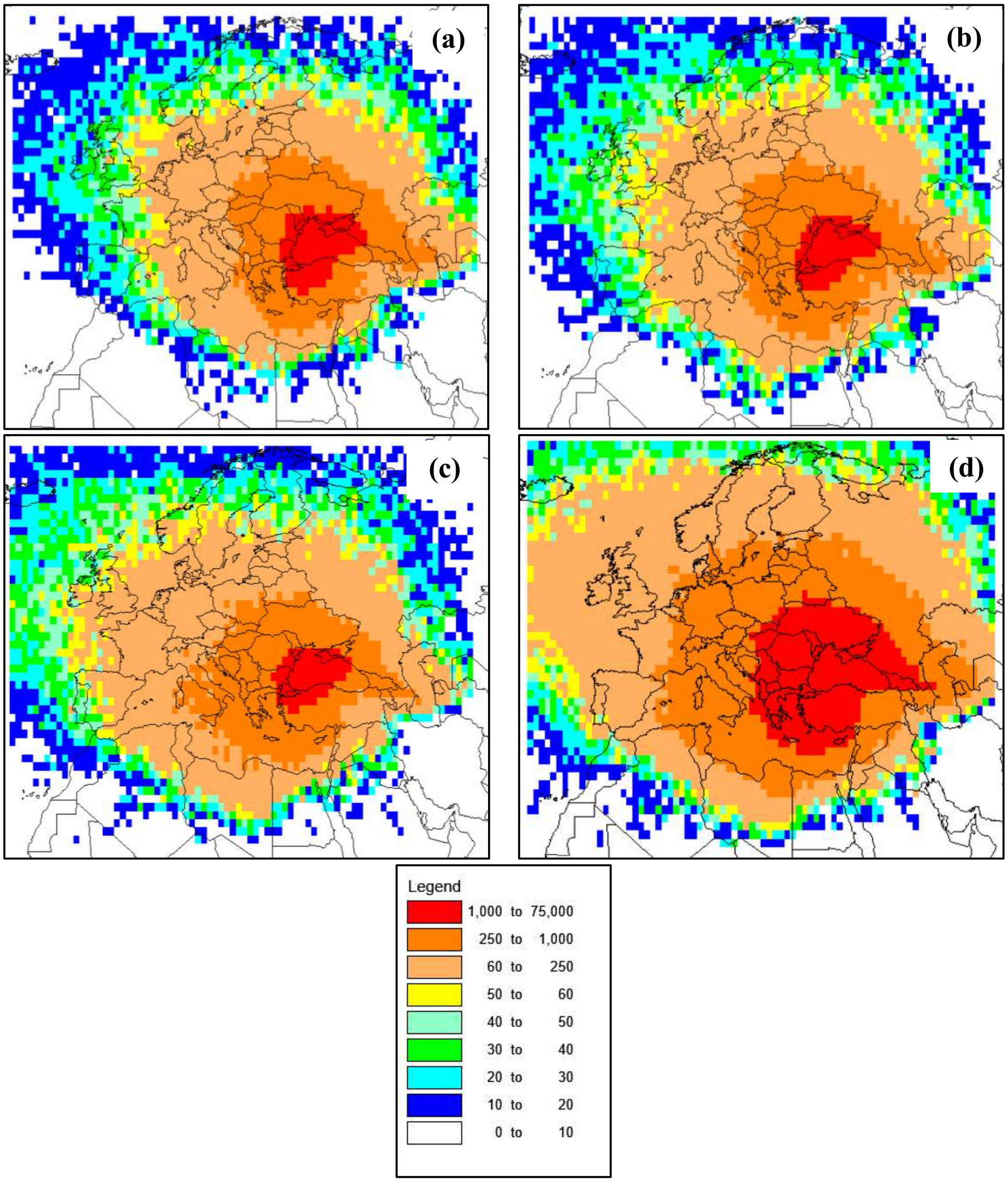

Figure 4.8 Distribution of Air Mass Residence Times in Study Domain (a) 100 m Starting Altitude, (b) 500 m Starting Altitude, (c) 1500 m Starting Altitude, (d)Segments in All Starting Altitudes

Residence times are evaluated for seasonal variations as well. The period from April to September is considered as summer, whereas the rest of months are considered as winter season. Partitioning between seasons are made according to the rainfall. Nearly 60% of the rainfall occurs during winter and the remaining 40% is observed in summer months as can be seen from Table 3.1 in the material and method section of the manuscript.

The summer, winter season distributions and summer-winter difference distribution of residence times are represented in thematic maps provided in Figure 4.9. In Figure 4.9 (c) difference between summer winter distributions is depicted. It is prepared by counting segments in each grid, in summer and winter seasons. Then for each grid, number of segments found in winter is subtracted from number of segments in summer and distribution of this difference is shown in the figure. Positive values in grids indicate that air masses spend more time in summer season in that particular grid. On the contrary, negative values indicate that air masses reside more in winter season than summer. It can be concluded that in summer air masses spend more time in North and North as sectors. On the other hand, in winter, Western half of Turkey and Western Europe are the regions where the air masses spend the majority of the time.

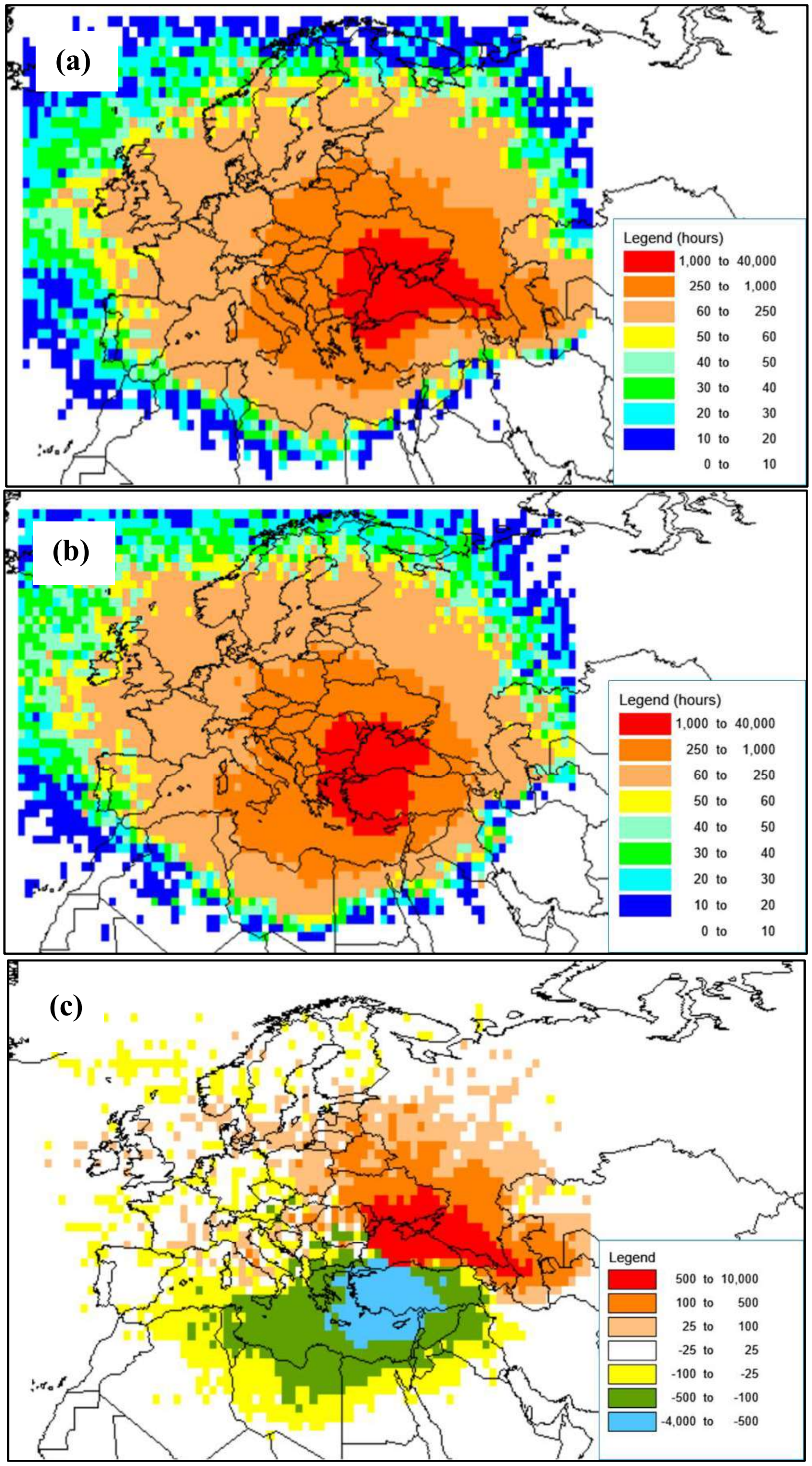

Figure 4.9 Seasonal Variation in Hourly Residence Times (a) Summer Residence Times, (b) Winter Residence Times, (c) Summer-Winter Difference

4.2.2. Sector-Based Flow Climatology

Grid-based analysis of climatology is shown in the previous section of this study. This way of looking at flow climatology is developed and used in our group. Since it is not conventional, it is difficult to compare the flow climatology found for Amasra region with other flow climatology, reported for Eastern Mediterranean and Black Sea regions. Flow climatology found in this work is also presented in more conventional way, which can be found in literature. In this second method the segments in each wind sector is counted and divided by total number of segments for each season, showing seasonal variations of percent contributions of wind sectors. Results are depicted in Figure 4.10.

The results obtained from sector-based method is similar to the results obtained by the first method. As can be seen from Figure 4.9, sectors that the air masses spend longer time are N, NE, W and NW. During summer, significantly longer residence times are observed in N, NE and E sectors whereas in winter significantly longer residence times are observed in SE, S, SW and W. In sector NW the results are similar for both seasons.

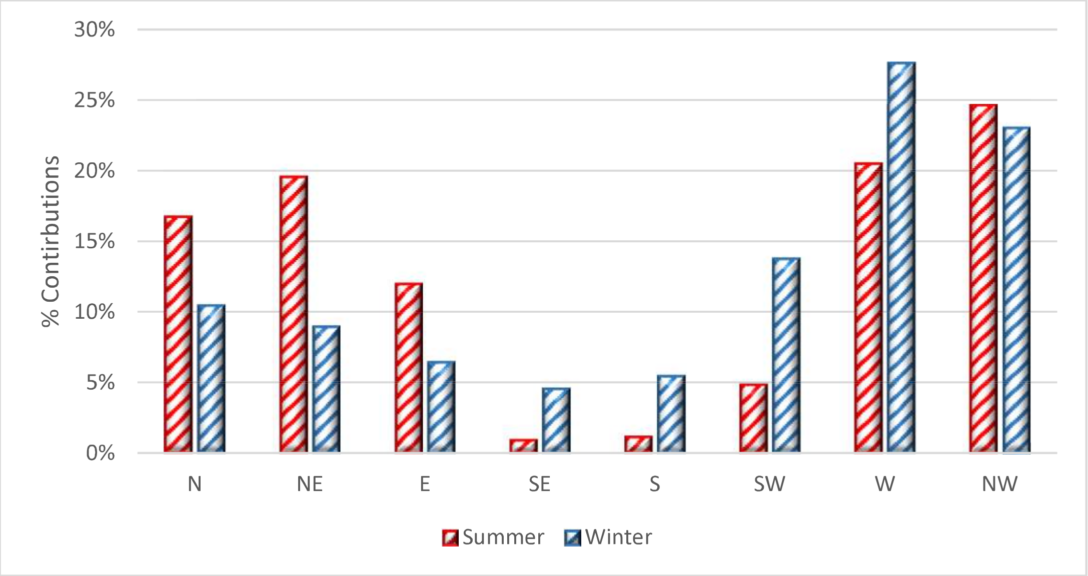

Figure 4.10 Seasonal variations of percent contributions of wind sectors

Sector-based climatology results were compared with the results of other flow climatology studies performed in Eastern Black Sea (Torul, Gümüşhane) (Balcılar et al., 2014) and Western Black Sea (Dereköy, Kırklareli – 10 km to Bulgarian border) (Tokgöz and Tuncel, 2015). Amasra Station is located in between these locations. The comparison is illustrated in Figure 4.11. In general, there no significant differences between flow climatology in different parts of the Black Sea. North, NE and E sectors have more contribution in summer. On the contrary, SE, S, SW and W sectors have more contribution in winter. In all stations, the air masses spend majority of their time in NE, N, W and NW sectors. These patterns observed in Eastern and Western Black Sea is similar with the results obtained at our station. It can be concluded that the flow patterns are similar in the entire Black Sea region.

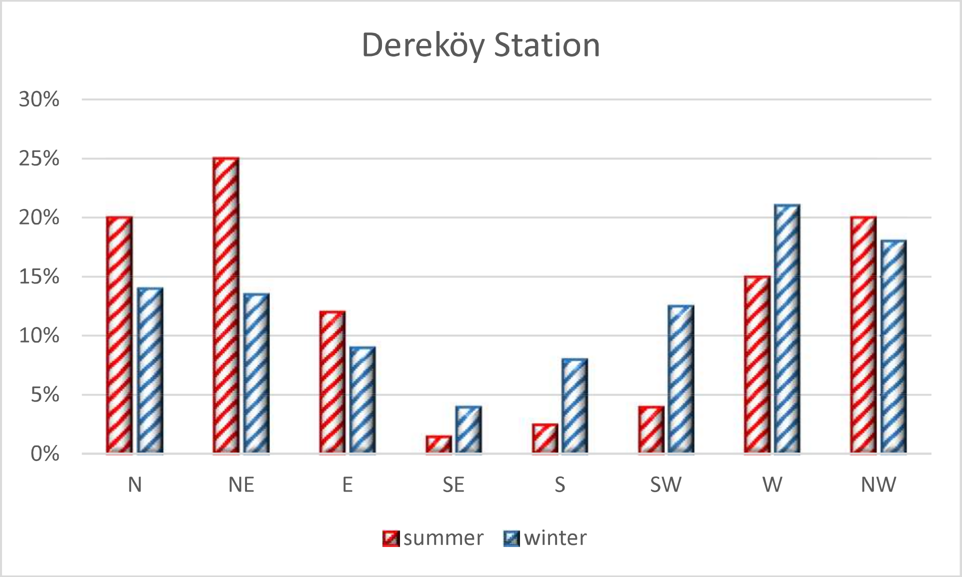

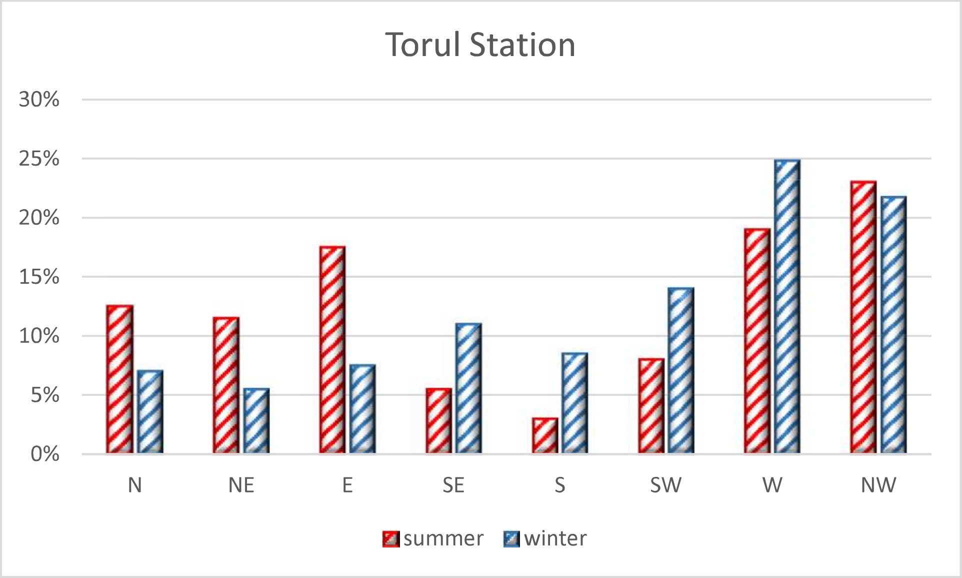

Figure 4.11 Comparison of seasonal contributions of wind sectors at Dereköy and Trabzon Stations

4.2.3. Cluster Analysis

Determination of optimum number of clusters were explained in the material and methods part of the manuscript under the flow climatology section. Variation of TRMSD with cluster number in this study is depicted in Figure 4.12. In this study, 5% change in TRMSD corresponded to 7 clusters. Visual inspection demonstrated that none of these seven clusters were generated by splitting of previous ones. Thus, 7-cluster is selected as optimum in this work.

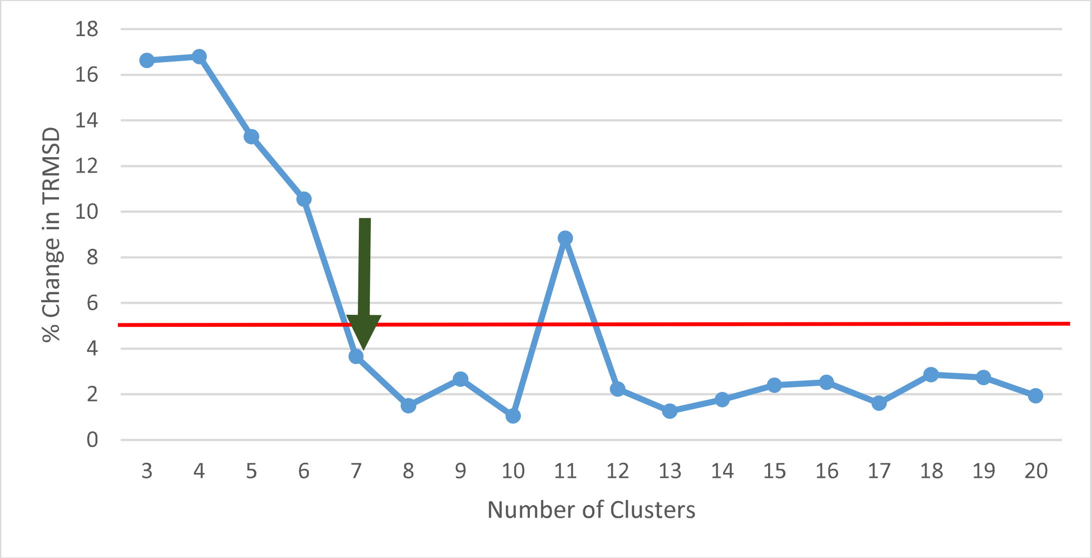

Figure 4.12 The Percentage Change in.TRMSD to Cluster Numbers

In Figure 4.13, the centroids for each cluster is shown. Centroid calculations for each cluster are carried out in TrajStat software. Centroids represent the center of mass of all trajectories in a single cluster. Number and percentage of trajectories allocated in each cluster is represented in Table 4.4.

As can be seen from Figure 4.13, there are two clusters from NW (3 and 6) and one cluster in each of the sectors N, NE, E, SW and W which are clusters 5, 7, 1, 4 and 2, respectively.

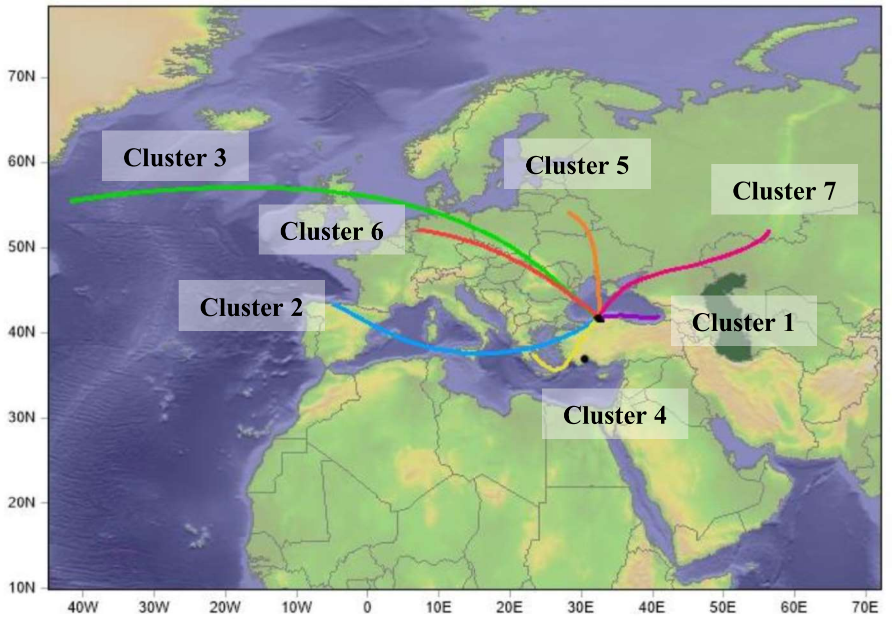

Figure 4.13 Cluster Centroids of Clusters Calculated for Combined Trajectories

Table 4.4. *Number and Percentage of Trajectories Allocated in Each Cluster*

Cluster	Number of Trajectories in Clusters	Percentage of Trajectories in Clusters
1	2519	17.7%
2	1423	10.0%
3	1532	10.8%
4	1507	10.6%
5	2861	20.1%
6	3099	21.8%
7	1306	9.2%

In this study, particular attention was paid to trajectory segments with altitude < 500 m, because these are the segments that have high probability of picking up pollutants if they pass over a source area. For example, if there are two trajectory segments over Dilovası, one at 100 altitude from the surface and the other one is at 3000 m. Among these the one occurring at 100 m altitude from stacks have much higher probability of picking up pollutants emitted from stacks compared to the one occurring at 3000 m. That is why low-lying segments are more important in terms of pollution transport from source regions. Please note that, transport of pollutants to receptor depends both on frequency of transport and presence of sources. There are very strong sources at Dilovası, but if there are no air masses passes there before they arrive to the receptor at Amasra, there will be no effect of strong sources at Dilovası on rainwater an aerosol composition at Amasra. Similarly, if there is very frequent flow of air parcels from Dilovası to Amasra, you will not see any effect of Dilovası on atmospheric composition at Amasra, if there are no sources there. These are the primary factors determining pollutant transport. If these conditions are fulfilled, then altitude of segments becomes important.

Residence time distribution of trajectory segments having altitude lower than 500 m is also calculated and presented in the form of thematic map in Figure 4.15. Not all trajectories and the segments dedicated to them have the same probability of collecting pollutants when passing a source area. Trajectory segments crossing a source area at higher altitudes are less likely to pick up pollutants that are emitted at the surface than trajectory segments passing a source area at lower altitudes. Thus, with this logic more low-lying segments are taken into account by computing segments below 500 m in order to gain relevant information on potential source areas affecting the clusters.

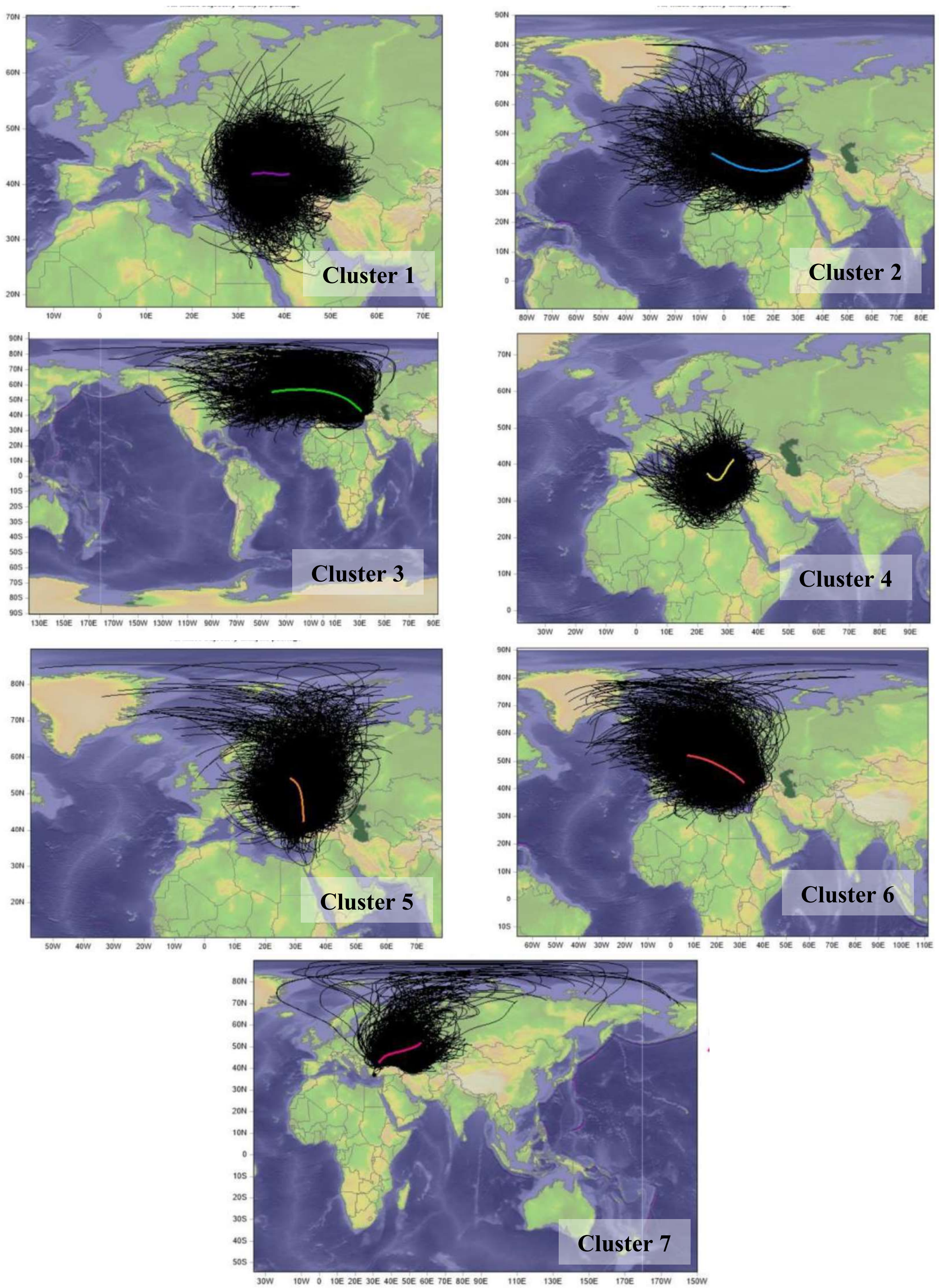

Figure 4.14 Trajectories Allocated to Different Clusters

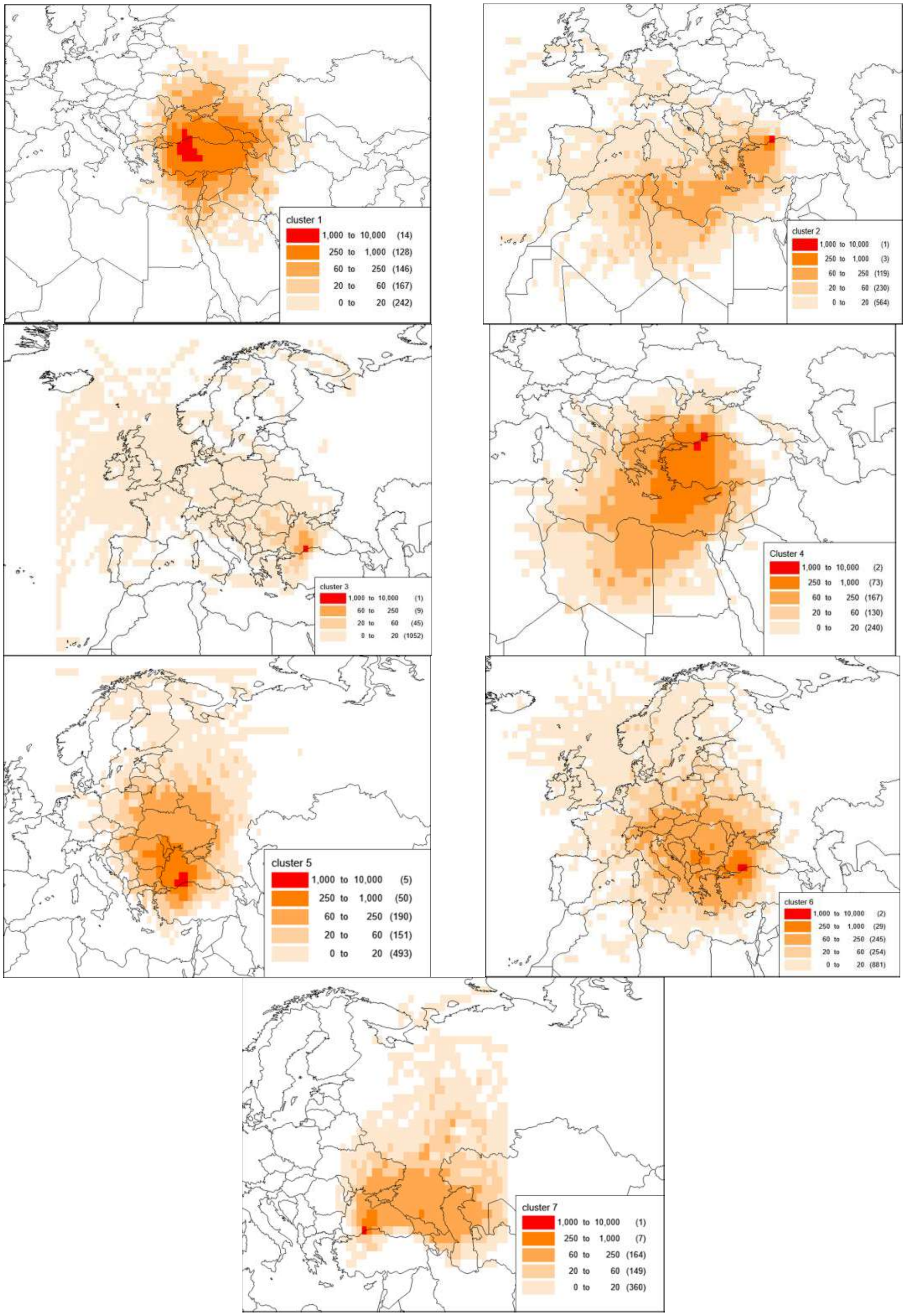

Figure 4.15 Residence Times of Air Masses Below 500 m for each Cluster

Cluster 1 consists of short trajectories from E sector. This cluster accounts for 2519 trajectories (17.7% of the whole trajectory set). This group of trajectories passes through Eastern part of Turkey as well as Eastern neighbors of Turkey. Since these trajectories are short, they can only bring emissions from local sources and do not expected to have regional significance. Distribution of low-lying segments in Figure 4.15 shows that air masses in this cluster can bring pollutants from Central and Eastern Turkey, Eastern part of Ukraine and Russian Coast of the Black Sea. Please note that Western Turkey, Ukraine and Black Sea coast of Russia are found to be important source areas affecting atmospheric composition, not only at the Black Sea, but also at the Eastern Mediterranean basin (Balcılar et al., 2014; Tokgöz and Tuncel, 2015; Öztürk, et al., 2012; Güllü et.al., 2005). Consequently, air mass transport represented by cluster 1 have potential to bring pollutants to our station at Amasra.

Cluster 2 represents flow coming from W sector. The cluster is composed of 1423 trajectories that accounts for approximately 10 % of the whole trajectory data. The centroid of Cluster 2 passes close to Africa and extends all the way up to Spain. Since the cluster centroid passes near Africa the potential transport from Sahara dust will coming from the trajectories of this cluster. Air flow represented by this cluster can also bring pollutants to Amasra as trajectories in this cluster passes over Southern European countries.

Clusters 3 and 6 includes trajectories from NW sector. Cluster 3 is composed of 1532 trajectories whereas cluster 6 is composed of 3099 trajectories which accounts for 10.8% and 21.8% of the whole set, respectively. It can be said that, when taking account these sectors together with 32.6% majority of the trajectories are coming from NW sector. Cluster 6 consists of group of trajectories which have moderate length whereas cluster 3 consists of trajectories having longer length. Cluster 3 trajectories extend from North America to Amasra Station. In this study 5-day back trajectories were calculated. Taking this aspect into consideration the air masses in cluster 3 travel quite fast to the receptor site. This kind of cluster is observed in other studies in the Black Sea region (Tokgöz & Tuncel, 2015; Balcılar et.al., 2014). Cluster 6 is important because, trajectories in this cluster comes from most of the Europe before they are intercepted at Amasra. Low lying segments in Cluster 6 mostly occurs in Balkan countries and central Europe, which is another indication for the potential of this cluster to bring pollutants from sources in Balkans and Europe.

Although air masses associated with cluster 3 can also bring pollutants, as trajectories in this cluster crosses Europe as well; low lying segments in this category are concentrated in the immediate vicinity of the station, indicating that air masses in cluster 3 travel at high altitudes until they are advected to surface when they reach to Black Sea region. Transport of forest fires emissions in Canada to Europe with such trajectories were reported in literature (Sarkodie et al., 2019; Worthy, et al., 2009).

Cluster 4 represents the flow from SW. this cluster is composed of 1507 trajectories which accounts for 10.6 % of the entire data set. This cluster of trajectories have relatively shorter length and the centroid extends to South coast of Greece. Residence times of air masses below 500 m for this cluster (Figure 4.15) are high at western part of Turkey, Greece and Egypt and other countries on the Mediterranean coast of Africa.

There is a potential that air masses in this cluster can transport pollutants to Amasra, because western parts of Turkey turned out to be important source regions in a number of studies in our group (Balcılar et al., 2014: Tokgöz et al., 2015; Güllü et al., 1998; 2005; Al-Momani et al., 1998).

Cluster 5 represents flow from N sector. This cluster consists the largest number of trajectories after cluster 6 which is 2861. It corresponds to 20.1% of the entire trajectory data. Cluster 5 centroid, which is shown in Figure 4.13, direction of trajectories, which are shown in Figure 4.14 and trajectory segments with $z < 500$ m demonstrated in Figure 4.15, shows that this set of trajectories spend most of their time around countries such as Ukraine, Romania and Bulgaria that have a coast to the Black Sea. Because the air masses spend more time in industrial zones like Ukraine and Balkan countries this set of trajectories can be the most important cluster in terms of pollution transport to central Black Sea region.

Cluster 7 represents the flow from NE sector. the cluster consists of the smallest number of trajectories which is 1306. It corresponds to 9.2% of the whole trajectory data. Low-lying segments shown in Figure 4.15 demonstrates that the air masses spend moderate amount of time at the NE bank of the Black Sea at Russia, Azerbaijan and Caspian Sea.

This analysis of clusters can explain why ions measured at Amasra station is the highest among most of the stations in MGM network. Unlike Mediterranean, Black Sea is surrounded by high emitting industrial regions in all directions, such as Eastern Parts of Ukraine and Black Sea coast of Russia at the North, Balkan And European countries at the west, Western Parts of Turkey at the south. Air masses in all clusters has to cross these high emission areas before the reach to Black Sea. This demography results in relatively high concentration of pollution derived ions at the Amasra station.

Median concentrations of the ions for each cluster is represented in Table 4.5 and Figure 4.16. Median concentrations of anthropogenic ions, except for H ion, do not change significantly from one cluster to another, because as pointed out before, no matter from which direction the air mass comes, it has to cross certain industrial regions where emission are expected to be high.

Hydrogen ion concentration is more variable between clusters, because unlike other pollution-derived ions, H^+ ion concentration does not depend only on transport of acidifying species like SO_4^{2-} and NO_3^-, but it also depends on the concentration of bases, particularly concentration of $CaCO_3$ in our case, in the air. Both of these parameters, particularly $CaCO_3$ are separately variable between clusters.

Concentrations marine ions, namely Na^+ and Cl^- are high in cluster 3. It is not surprising because, air masses associated with cluster 3 crosses Atlantic Ocean, which means they spent more time over the sea and thus pick up more sea salt than air masses associated with other clusters.

The only truly crustal ion measured in this study is Ca^{2+}, because although main source for K^+ and Mg^{2+} is also soil particles in atmosphere, these two ions are significantly contributed from sea salt. Concentration of Ca^{2+} is higher in Cluster 2. Please note that Cluster 2 is the only cluster that can bring Saharan Dust to our station.

Table 4.5. *Median Concentration of Species (mg/L) for each Cluster*

	Cluster 1	**Cluster 2**	**Cluster 3**	**Cluster 4**	**Cluster 5**	**Cluster 6**	**Cluster 7**
pH	5.84	6.02	5.45	5.86	5.32	5.39	5.49
H^{+*}	1.45	0.96	3.55	1.38	4.27	4.07	3.24
SO_4^{2-}	2.56	3.08	2.42	2.87	2.05	2.57	1.99
NO_3^-	1.60	1.53	1.38	1.37	1.19	1.26	1.34
Cl^-	1.56	1.97	2.80	1.53	2.20	2.33	2.00
NH_4^+	0.77	0.39	0.65	0.52	0.39	0.52	0.71
Ca^{2+}	0.94	1.39	0.91	1.00	0.55	0.78	0.61
Mg^{2+}	0.22	0.23	0.32	0.21	0.21	0.23	0.25
K^+	0.14	0.12	0.16	0.14	0.12	0.14	0.13
Na^+	1.09	0.96	2.02	1.02	1.14	1.35	1.40

**H^+ concentrations are given in µg/L.*

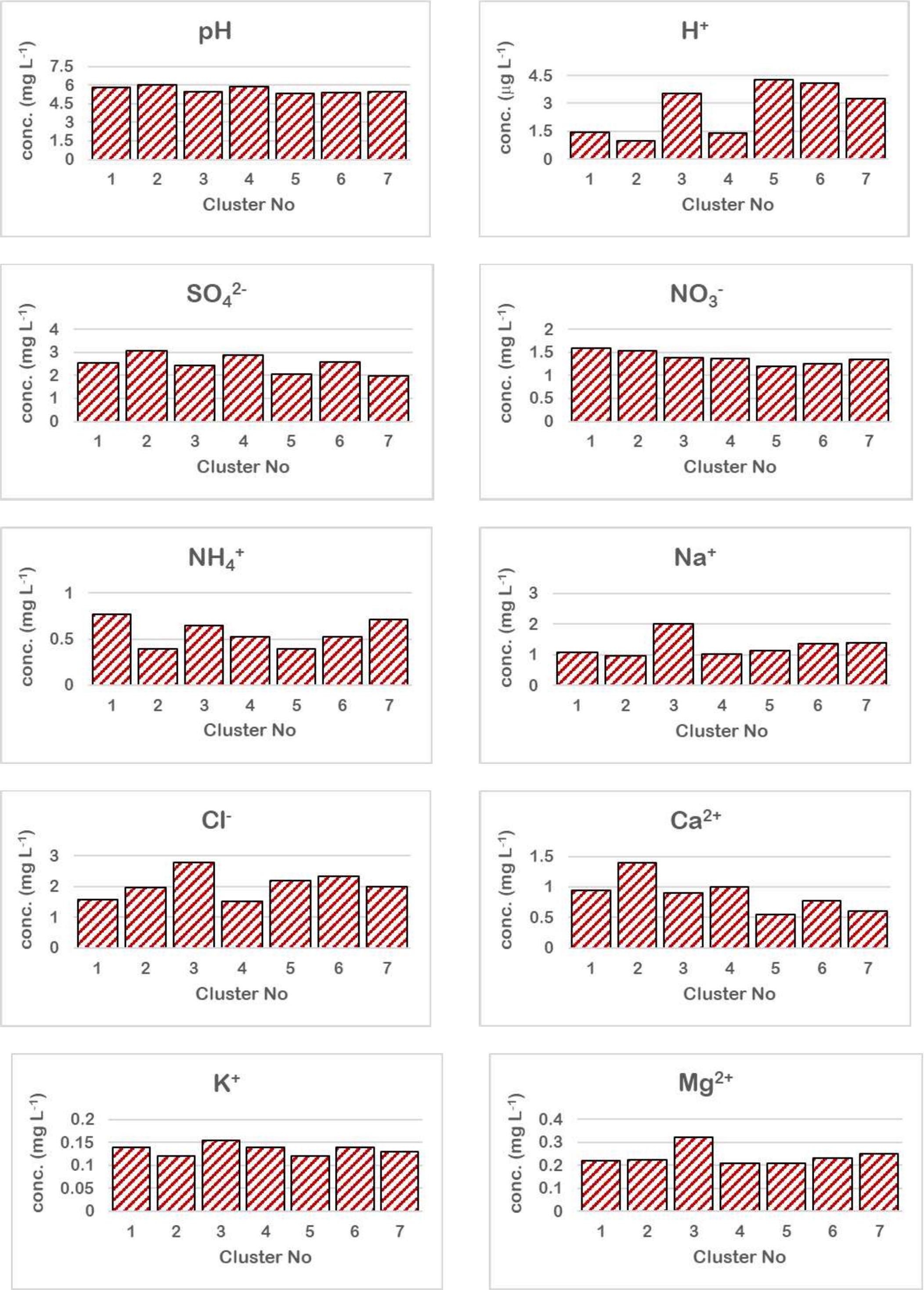

Figure 4.16 Median Concentration of Species (mg/L) for each Cluster

4.3. Ionic Composition of Wet Deposition

4.3.1. Ion Balance

Ion balance refers to the ratio of total anions to total cations which shows the completeness of the measured parameters. This ratio is expected to be unity if all anions and cations are measured. Deviation from unity (imbalance) implies that some ions are excluded.

The scatterplot of equivalent sum of total anions (SO_4^{2-}, NO_3^-, Cl^-) to equivalent sum of total cations (H^+, NH_4^+, Mg^{2+}, Na^+, Ca^{2+}, K^+) is shown in Figure 4.17.

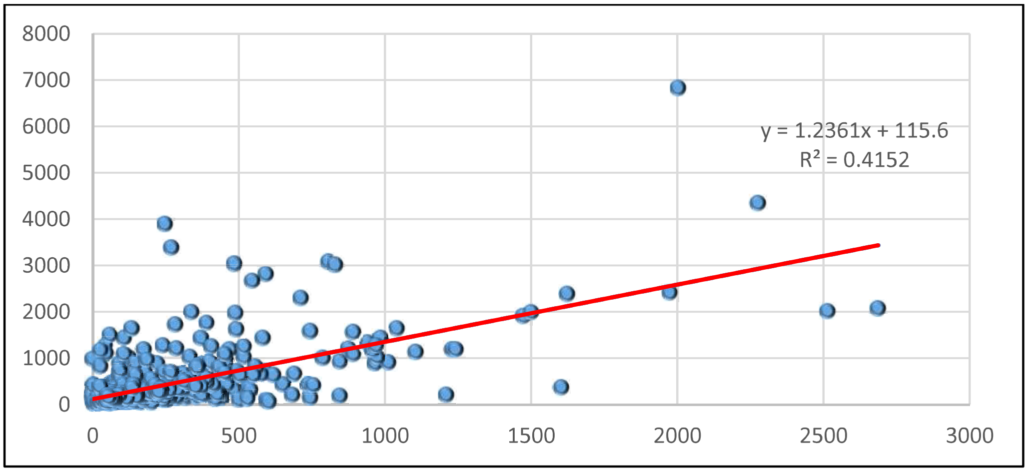

Figure 4.17 The scatterplot of the equivalent sum of anions to equivalent sum of cations.

Average of ∑anion/∑cation at Amasra station is 0.78±0.75 (median 0.65). This implicates that there is approximately 22% anion deficiency.

Similar anion deficiencies were reported in most of the rainwater studies in the Mediterranean region and attributed to lack of bicarbonate (HCO_3^-) measurements (Işıkdemir, 2006; Ding, et.al., 2013). Since organic acids are not measured in this study, exclusion of organic anions such as acetate ($HCOO^-$) and formate (CH_3COO^-) can also result in deficiency of anions. However, organic acids, primarily formic (HCOOH) and acetic (CH_3COOH), have been shown to influence rainwater chemistry substantially in tropical region having extensive forestry (Lacaux, et.al., 1992; Rodhe, et.al., 1988). Since this study is conducted at midlatitudes, where forestry is limited, anion deficiency can be explained by lack of HCO_3^- data, rather than organic anions.

HCO_3^- forms with the dissolution of atmospheric CO_2 in rain droplets. The concentration of HCO_3^- variates depending on the pH of the precipitation. Generally, as rainwater is more basic the effect of HCO_3^- on ion balance becomes much more imortant.

Theoretical relationship between pH and HCO_3^- is represented with the formula below (Das, et al., 2005; Tiwari, et al., 2006):

$$[HCO_3^-]=10^{(pH-5.05)}\mu eq/L \qquad \text{(Equation 4.2)}$$

When bicarbonate is calculated by using the equation above and added to the total anions the deficiency decreases from 22% to 15%. Therefore, the outcome supports that the cause of anion deficiency at Amasra station is at least partly due to lack of HCO_3^-data.

4.3.2. Contributions of Ions to Total Ion Mass

Contributions of ions to total ion mass for the period September 2005 to June 2016 is shown in Figure 4.18. As can be seen from Figure 4.18, the ion having the highest contribution is Cl^- (23%). which is followed by SO_4^{2-}(22%), Na^+(15%), NO_3^-(14%) and Ca^{2+}(12%). These five top contributors account for 85 % of total ion mass.

Total contribution of anthropogenic, crustal and marine ions to ionic mass are 45%, 38% and 17% respectively. SO_4^{2-} and NO_3^- are anthropogenic ions that are attributed to main cause of acidity observed in rainwater. Total contribution of these two ions to total ion mass is 36%. Rest of the anthropogenic contribution is due to NH_4^+ ion. Relatively high contribution of sea-salt ions (Na^+ and Cl^-) is due to proximity of the station to the coast. Although, contribution of H^+ ion to total ion mass is not high (0.76%), H^+ is important because it is a direct indicator of level of acidity in rainwater. Similarly, NH_4^+ and $Ca^{2+}$are also important, because they show the extend of neutralization in rainwater chemistry. Total contribution of these two ions is 21 %, indicating why neutralization is an important issue in the Eastern Mediterranean basin.

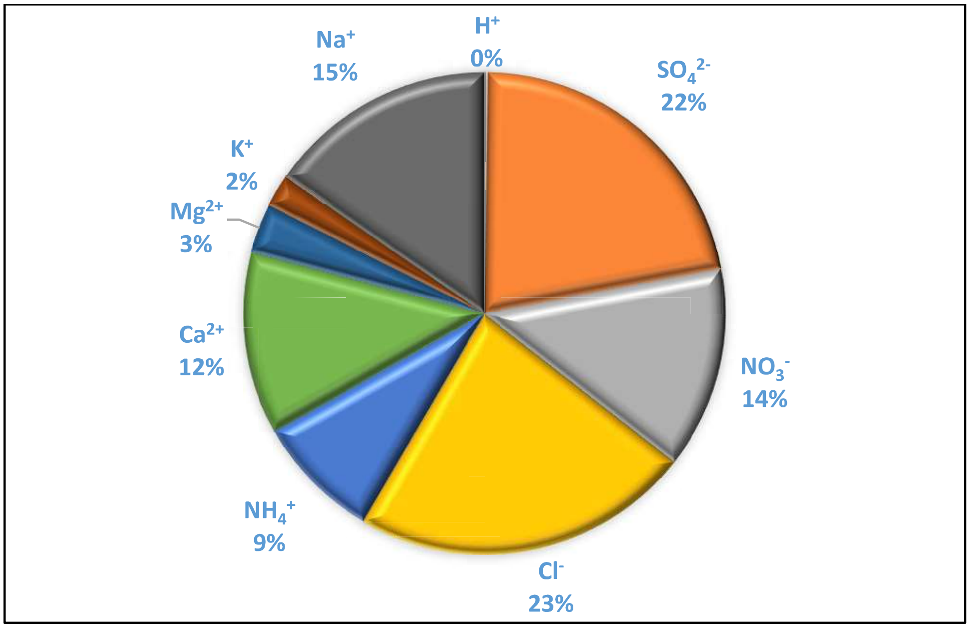

Figure 4.18 Contribution of Ions measured in Amasra Station to Total Ion Mass

Long-term variation in contribution of ions to total ion mass can be observed from Figure 4.19 where contribution of ions is presented for the years 2005 and 2016. Contributions of the ions for other years are given in the appendix. For the majority of ions, the change in contribution percentages is not significant. The only striking result is observed in NH_4^+ contribution. In 2005, the contribution is 16% whereas, in 2016 it is 6%. NH_4^+ is an anthropogenic ion that is introduced to the rainwater mainly by cattle breeding, fertilizer use and industrial processes (Wang and Han, 2011; Flues et al., 2002). Importance of ammonia emissions from agricultural regions on NH_4^+ concentrations in atmosphere is also noted in literature (Galloway et al., 1995: Wang and Han, 2011). Consequently, the decrease in contribution of NH_4^+ to total ion mass at Amasra region is probably due to changing habits of fertilizer application or changing fertilizer formulations in the Black Sea region.

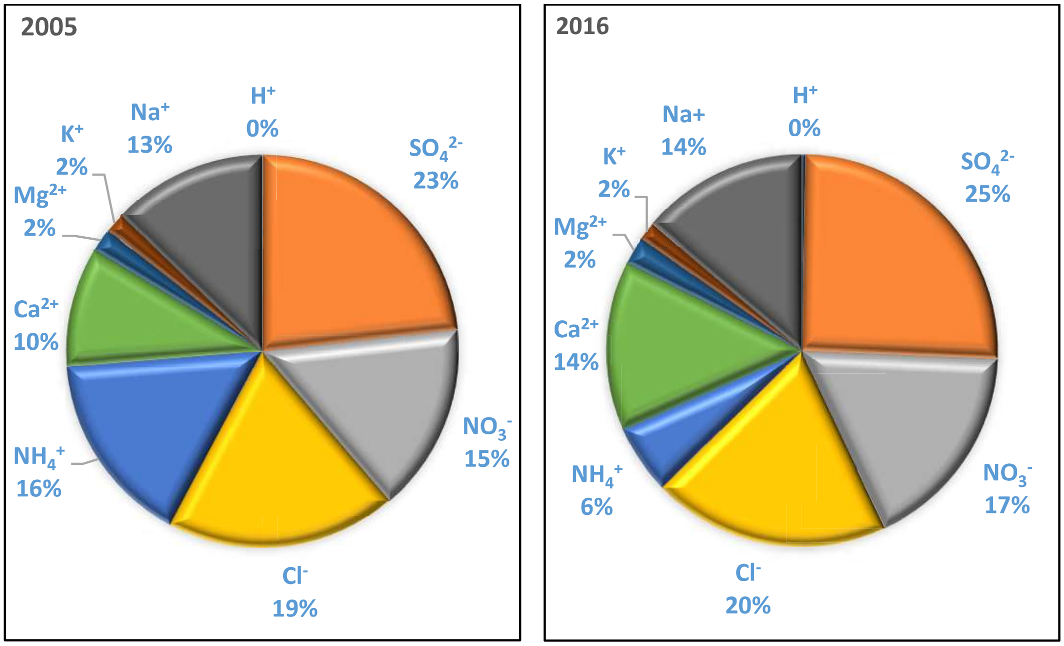

Figure 4.19 Variation of Ionic Contribution to Total Ionic Mass in Time

Seasonal variations in the contribution of ions to total ion mass are illustrated in Figure 4.20. The data was divided into two sets to represent the wet and dry seasons. From beginning of October throughout the end of March was considered as wet season and from the beginning of April throughout the end of September was considered as dry season.

According to Figure 4.20, the change of contribution between seasons of anthropogenic ions such as SO_4^{2-} and NO_3^- are not significant. On the other hand, contribution of the marine elements such as Na^+ and Cl^- is 13% and 18% in dry season and 17% and 26% in wet season respectively. The higher contribution of marine elements in wet season is because of the influence of more pronounced bubble-bursting process due to strong and persistent winds during winter season. Relatively calm conditions over the sea during dry season, significantly decreases the marine element generation thus resulting in lower contribution of these elements in summer months (Al-Momani, et al., 1997; Işıkdemir, 2006).

Contrarily, for crustal ions such as Ca^{2+}, Mg^{2+} and K^+ have higher contribution in dry season. This is because resuspension of soil particles during summer months is easier. Since the soil is damp during winter months the mobilization of soil particles is more difficult (Al-Momani, et al., 1997).

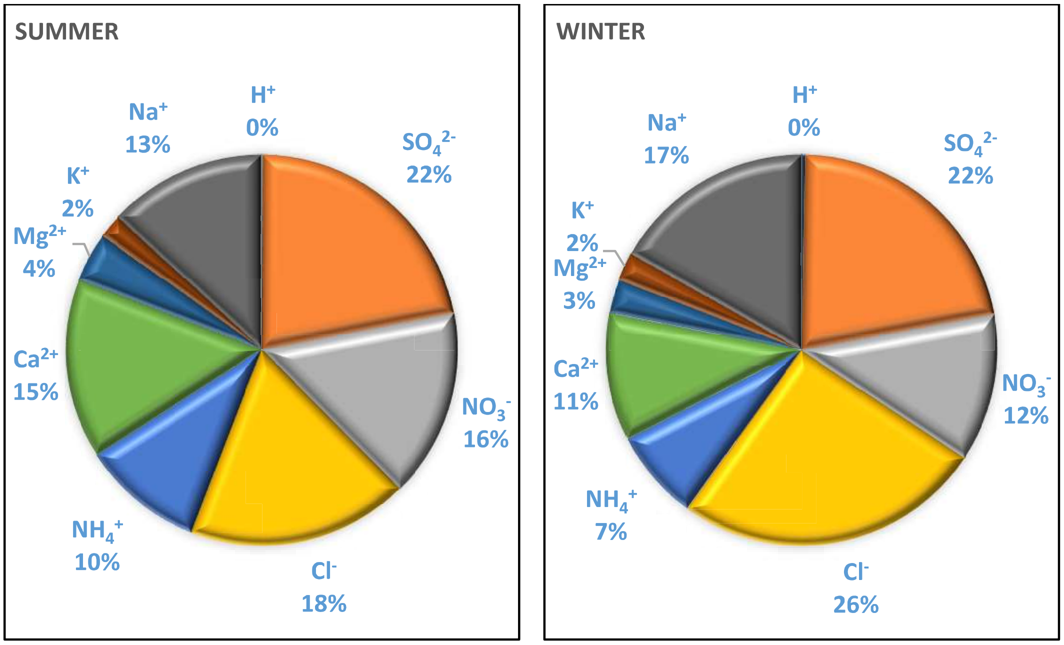

Figure 4.20 Seasonal Variation in Ionic Contributions to Total Mass

4.4. Acidity of Wet Deposition

4.4.1. pH of Rainwater

The natural acidity of rainwater is determined to be pH 5.6 by taking account that pure water in equilibrium with the atmospheric concentration of CO_2 which is 330 ppm. Generally, pH value of 5.6 is considered as the demarcation line for acidic precipitation. On the other hand, CO_2 is not the only constituent that influences the pH of precipitation. In the absence of compounds with basic nature such as NH_3 and $CaCO_3$ can be expected to be in the range of 5.0 to 5.6 due to presence of natural sulfur compounds alone (Gülsoy et.al., 1999; Charlson and Rodhe, 1982).

Annual, summer and winter frequency distribution graphs are shown in Figure 4.21. In the study, the measured pH ranges between 3.56 and 8.39. The annual average value is 5.57, whereas the median value is 5.62 which is approximately equal to natural acidity of rainwater. According to Figure 4.21, approximately 34% of the samples have pH lower than 5 and 19% have pH lower than 4.5. Approximately, 66% of the samples cannot be considered as acid rain.

Summer and winter histograms are also included in Figure 4.21. As can be seen from these histograms, higher pH values are observed in summer. During winter, on the other hand, frequency of occurrence shifts to lower pH values, indicating that rain is more acidic in winter season. In winter 55 % of the pH data is between 4 and 5.5. On the other hand, in summer 60% of the pH data lies between pH 5.5 and 7. These results indicate that neutralization extensively takes place in summer season., Which is not surprising, because acidity in rainwater is neutralized by $CaCO_3$ that has higher concentrations in atmosphere during summer. During winter, on the other hand, resuspension of soil containing $CaCO_3$ is more difficult form frozen or muddy soil.

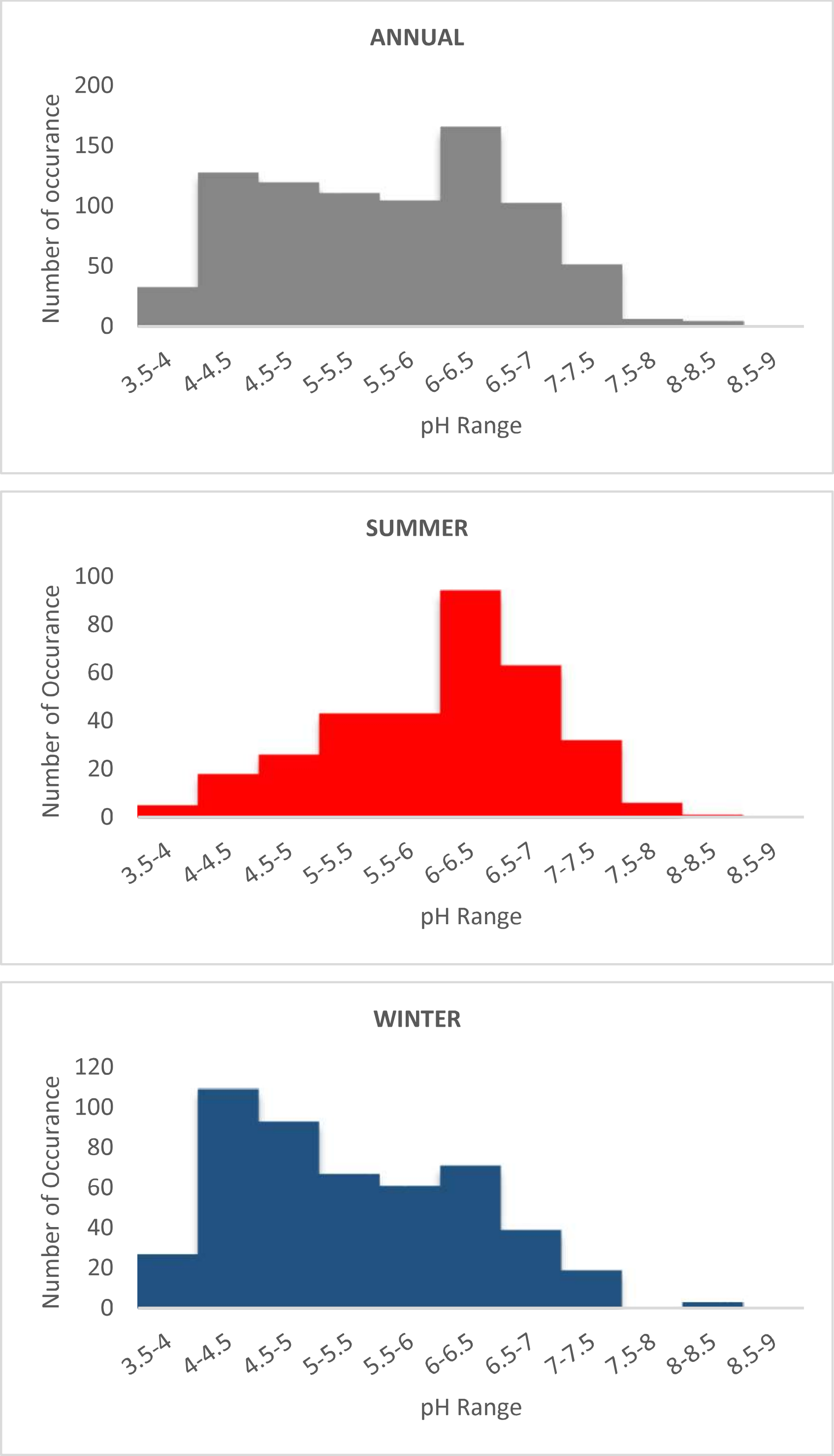

Figure 4.21 pH Frequency Distributions of pH in Amasra Station

4.4.2. Neutralization of Rainwater

The acidity of the precipitation originates primarily from H_2SO_4, and HNO_3. The monthly equivalent ratio of $[H^+]/([SO_4^{2-}] + [NO_3^-])$ is represented in Figure 4.22 for better understanding of the neutralization process. This ratio is expected to be unity if the free H^+ ions that results from H_2SO_4 and HNO_3 are not neutralized. If all H^+ ions are neutralized the ratio would become zero. As can be seen in the figure, neutralization is much more extensive in dry season. Throughout May to September strong neutralization occurs as the ratio almost approaches to zero. On the contrary, in wet season the neutralization is not as much as in dry period. The highest ratio is observed in January which is approximately 0.4, but even this highest ratio indicates that 60% of the H^+ is neutralized.

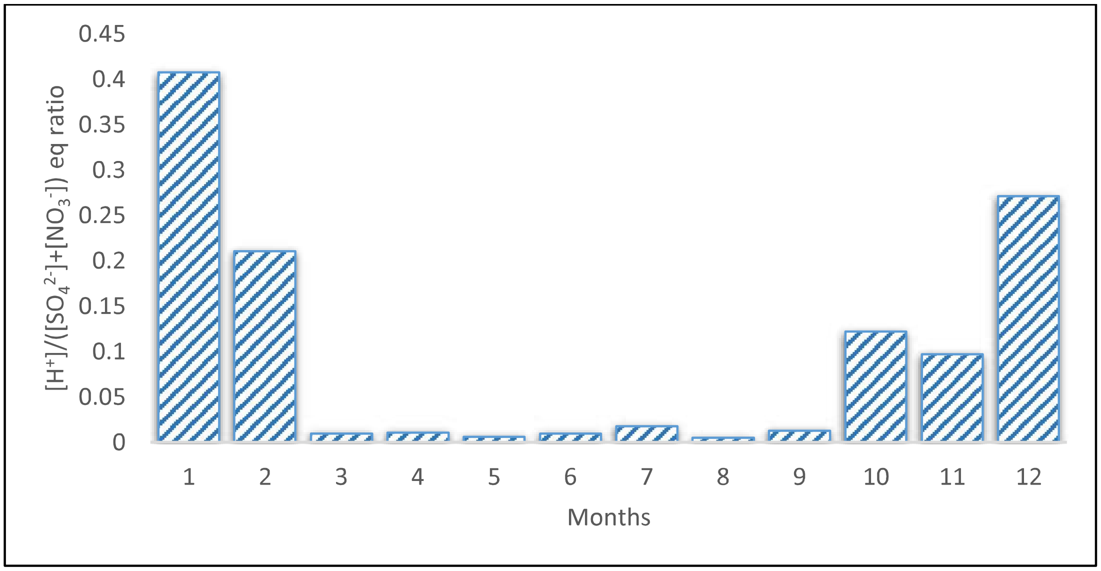

Figure 4.22 Monthly Variation of $[H^+]/([SO_4^{2-}] + [NO_3^-])$ Equivalent Ratio

Acids in the atmosphere can be neutralized by mainly two bases which are: NH_3 and $CaCO_3$ (Radojevic and Harrison, 1992). The main sources of NH_3 in rainwater are fertilizer applications in land or livestock farming (Al-Momani et al., 1997; Golobočanin et.al., 2008). On the other hand, neutralization by $CaCO_3$, is a local process, occurring by incorporation of $CaCO_3$ containing soil particles in rain primarily by below-cloud processes (Golobočanin et.al., 2008; Altwicker and Mahar, 1984). NH_4^+ concentrations measured in this and other studies in Eastern Mediterranean region demonstrated that the role of NH_3 in neutralization of acidity in rainwater is not very important when compared with neutralization by $CaCO_3$ in calcareous soil in the region. This can also be seen in Figure 4.23 where both Ca^{2+} and NH_4^+ ions are regressed against H^+ ion. Both NH_4^+ and Ca^{2+} showed weak, but statistically significant correlations with H^+ ion. Please note that chance correlation between two parameters depends not only the correlation coefficient, but also number of data points [P(r,n)]. When there is > 800 data, even very small R^2 values can become statistically significant. However, in the figure it is clear that Ca^{2+} correlates better with H^+ ion than NH_4^+.

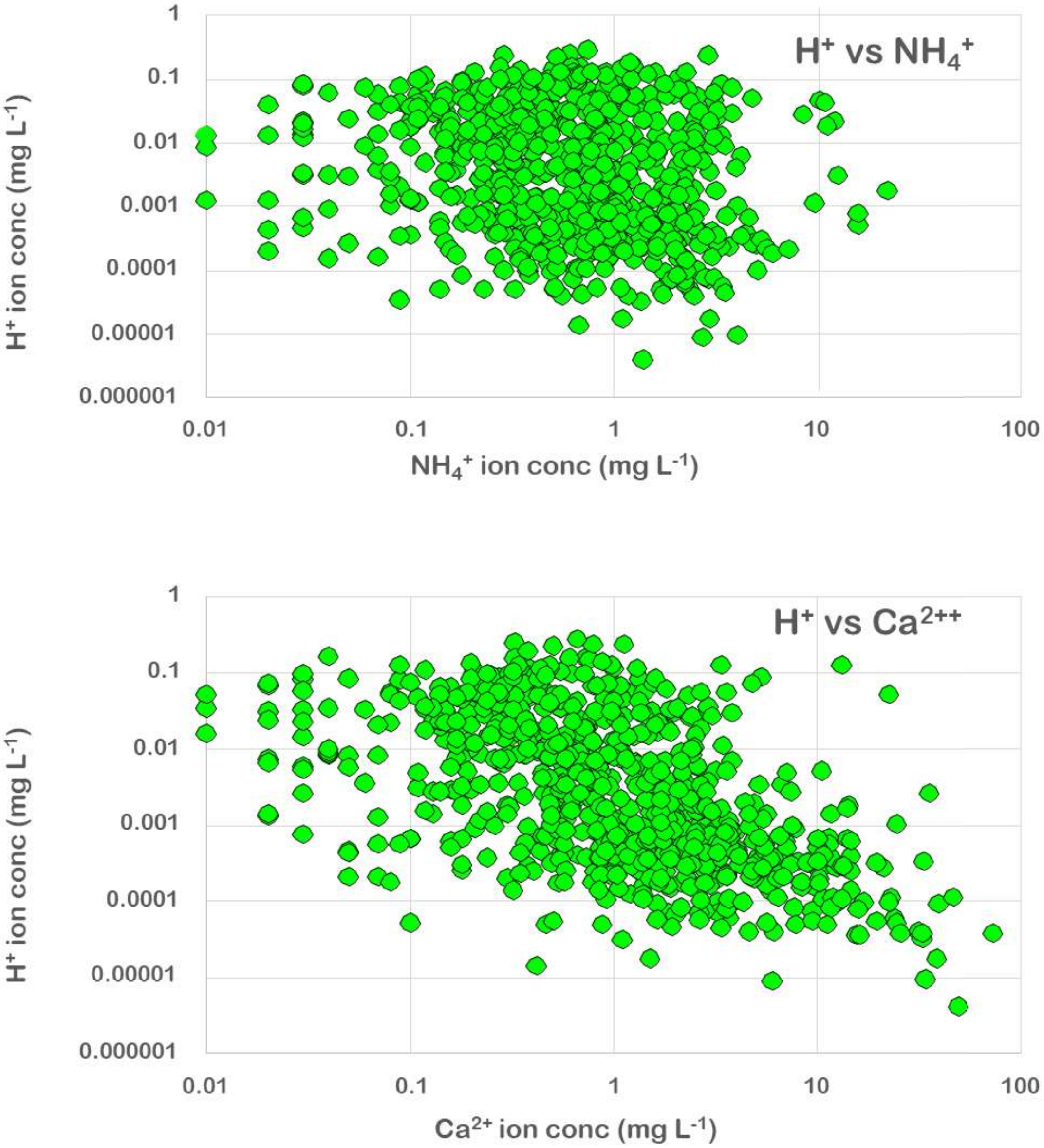

Figure 4.23 Regression of H^+ ion against Ca^{2+} and NH_4^+ ions

4.5. Temporal Variations

In urban atmosphere, it is important to understand temporal variability in data set to identify factors controlling variability in pollutant concentrations. Temporal variations in data set can be discussed as short-term variations (or episodic changes), diurnal changes, weekend-weekday changes seasonal changes and interannual changes (trends). Seasonal and interannual variations will be discussed in this manuscript, because diurnal and weekend-weekday variations are due to short term variations in pollutant emissions which are difficult to see in rural atmosphere which is not under direct influence of emission sources.

4.5.1. Seasonal Variations in Ion Concentrations

Seasonal variations observed in concentration of ion can be due to seasonal variation of transport pattern, and meteorology.

As discussed previously, seasons in this study was based on rainfall data since variation in precipitation amount is the main driver for variability in PM mass and ion concentrations. Monthly average rainfall data is provided in Figure 4.24 for Amasra Station between the years 1975 and 2016. Long-term average annual rainfall at Amasra is 990.3 mm, 392.7 mm (39%) of annual rainfall falls in Summer and 597.6 mm (61%) falls in winter. Based on the rainfall data, period between April to September selected as Summer and the rest of the year was selected as winter. As pointed in previous paragraph, 39% of the annual rainfall occurs in summer and remaining 61% in winter. This seasonal scheme was established in early 90s for the data generated at Antalya station (Al-Momani et al., 1998: Güllü et al., 1998). At Eastern Mediterranean region 20% of the rainfall occurs between April and September and 80% of the rainfall occurs in our winter season. The summer winter difference in Black Sea region is not as dramatic as that observed at the Eastern Mediterranean, but we wanted to keep that division, because it is being used in many years, and selection of a different seasonal division would make the comparison of data generated in this work with studies performed in our group, at different parts of Turkey difficult.

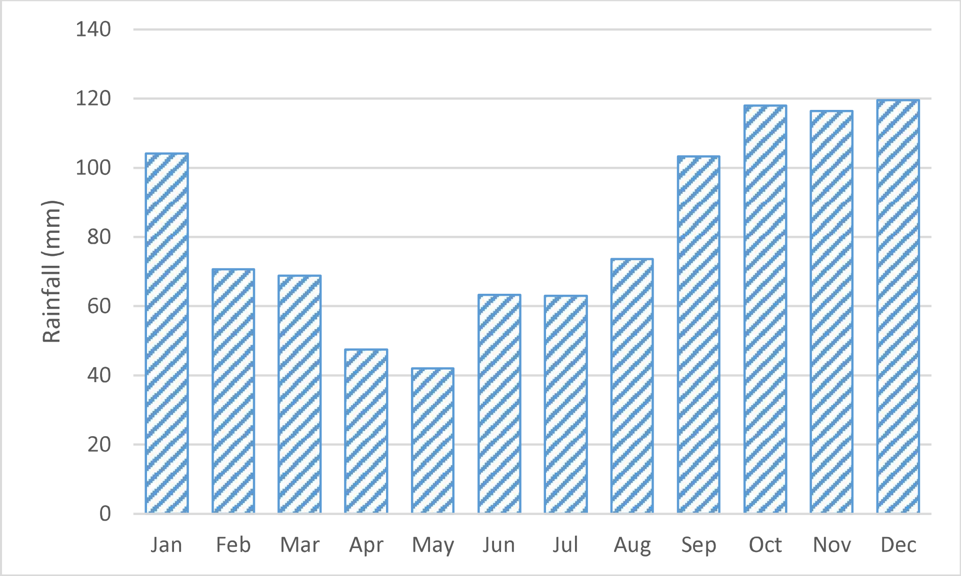

Figure 4.24 Average Monthly Variation of Rainfall (mm) at Amasra Station (1975-2016)

Monthly median concentrations of measured ions are illustrated in Figure 4.25 for anthropogenic ions and in Figure 4.26 for sea-salt and crustal ions. Anthropogenic ions such as SO_4^{2-}, NO_3^- and NH_4^+ have higher concentrations during summer months. Their summer to winter ratios are 1.35, 1.47 and 1.69, for SO_4^{2-}, NO_3^- and NH_4^+ ions, respectively. Higher summer season concentrations of secondary ions were observed in almost all rainwater studies performed in our group (and also around the world) and explained with more vigorous photochemical activity during summer, with increased solar flux (Meng, et al., 2014; Güllü et.al, 1998). Since gas-phase (photochemical) oxidation of SO_4^{2-}, NO_3^- and NH_4^+ ions are faster during summer season (Environment Agency, 2007) higher concentrations of these secondary ions in summer are higher is not surprising. For NH_4^+; higher volatility of NH_3 in summer also contributes for observed higher NH_4^+ concentrations in summer.

H^+ concentrations are much higher in winter months. This is due to the seasonal nature of neutralization process of acidity. The neutralization of acidity in Turkey is mainly governed by $CaCO_3$ content of the soil. Higher resuspension of this soil particle in the summer leads to occurrence of more extensive neutralization resulting in lower concentrations of hydrogen ion during this season.

Marine aerosol indicators Na^+ and Cl^- have higher concentrations in winter which is very typical. Key source of marine aerosol results from the breaking of waves in the Black Sea, a process that produces particles ranging from tens of nanometers to hundreds of micrometers in diameter (Blanchard and Woodcock, 1957; Clarke, et al., 2003; Russell and Singh, 2006). This process caused by breaking waves is called bubble bursting and production of bubbles increase with wind speed (Marks et.al., 2017). Therefore, extensive storm activity observed in winter months enhance the concentration of. Na^+ and Cl^- through bubble bursting process. Same observations are frequently reported in the literature (Güllü et.al., 1998; Yücel, 2019).

Similar to anthropogenic ions, crustal ions which are Ca^{2+}, Mg^{2+} and K^+ have higher atmospheric concentration during summer period. The main reason behind the higher concentrations observed in summer are related with the resuspension of soil. During winter season the resuspension is minimized due to high rainfall events dampening the soil which restricts the possibility of soil derived particles being released (Deshmukh et.al, 2011; Bhaskar and Mehta, 2010). On the contrary, in summer months soil becomes dry and crustal particles can become airborne much easier with moderate wind speeds. Please note that summer-winter difference inside of crustal elements is the highest for Ca^{2+}.Calcium is the only truly crustal element measured in this study. Other crustal ions, namely K^+ and Mg^{2+} have strong contribution from sea salt, which increases their winter concentrations and make the difference between summer and winter season concentration less pronounced than that of Ca^{2+}.

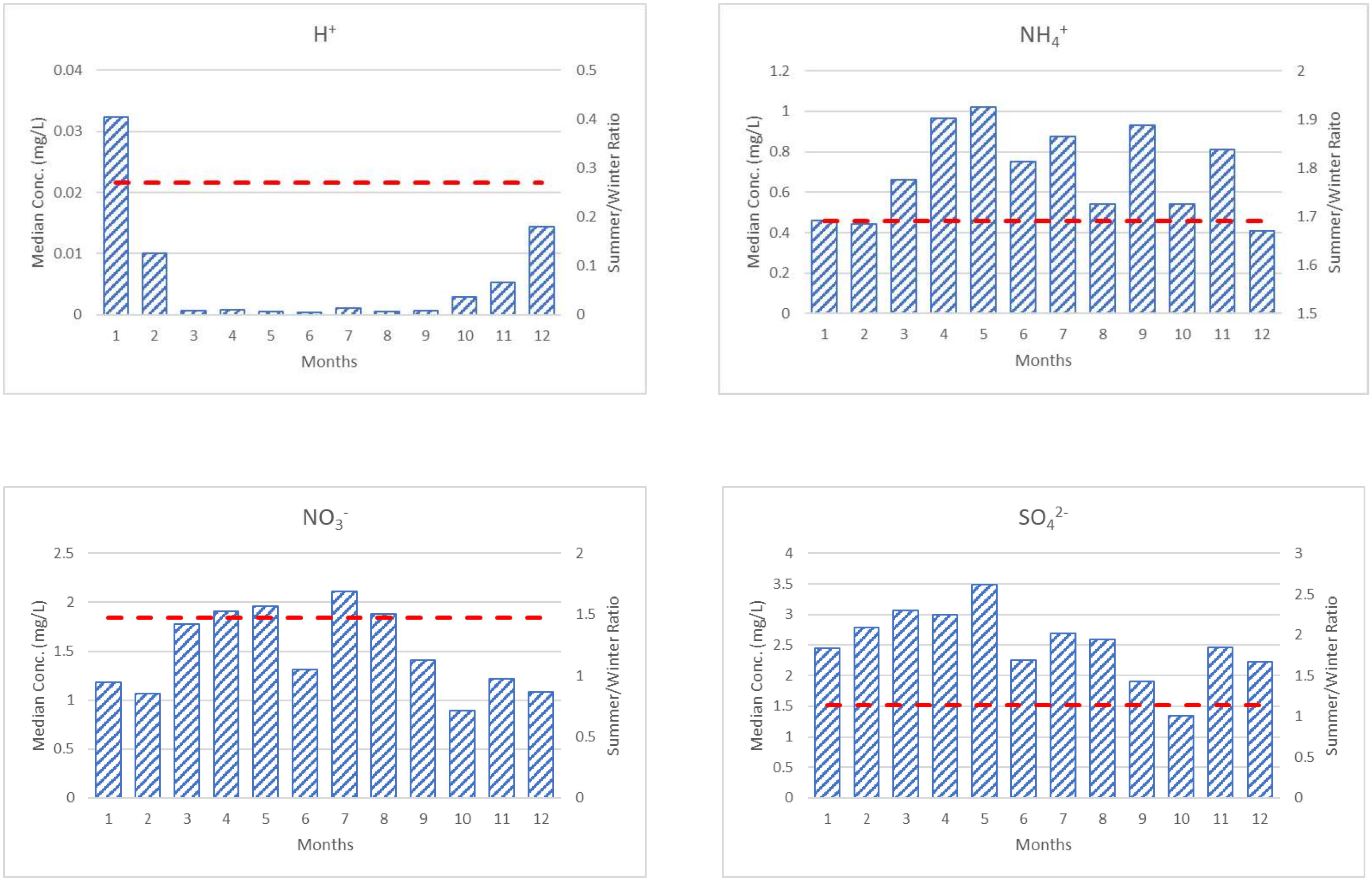

Figure 4.25 Monthly variation of Ion Concentrations and Summer to Winter Ratio of Anthropogenic Ions

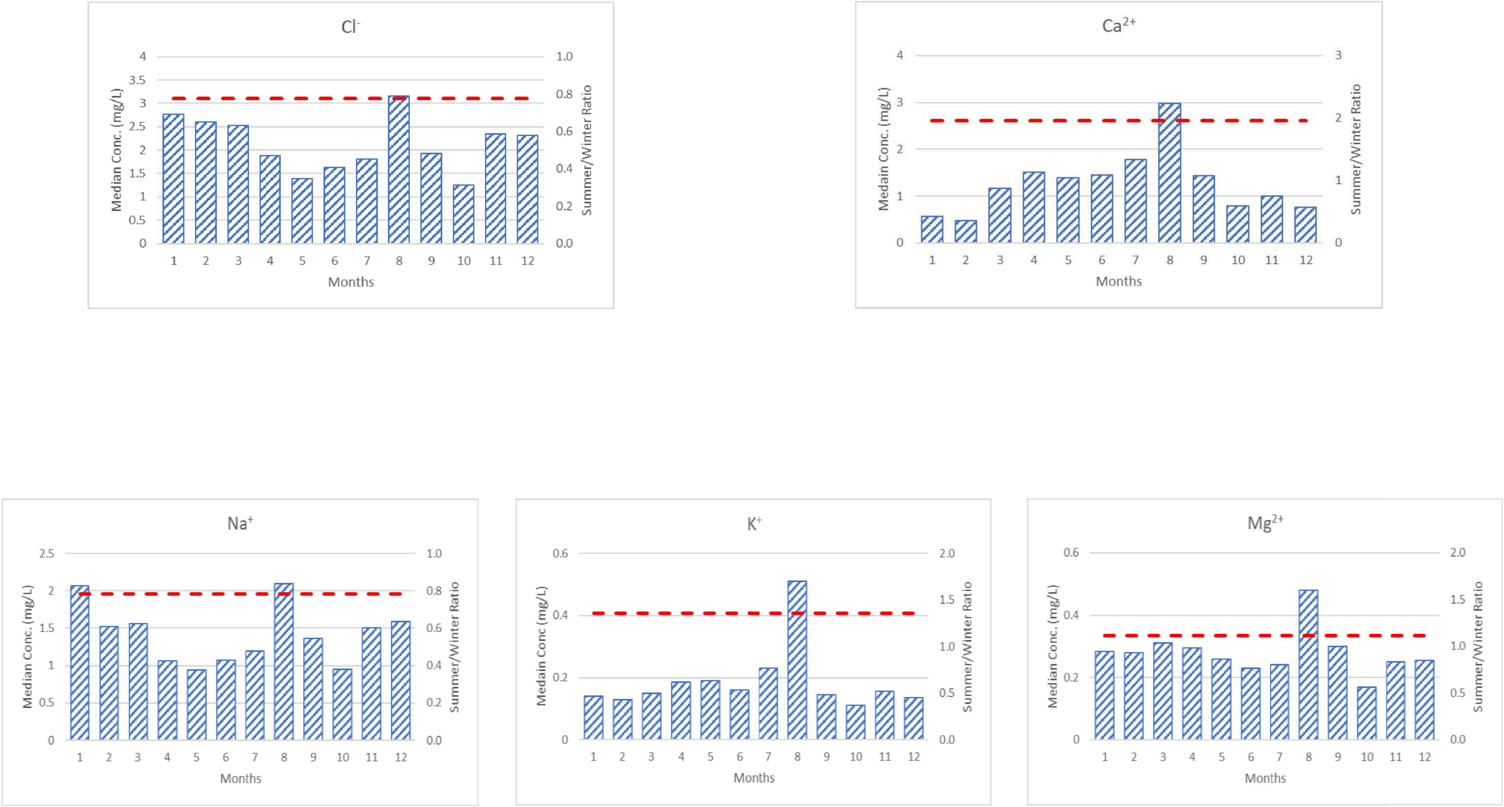

Figure 4.26 Monthly variation of Ion Concentrations and Summer to Winter Ratio of Natural Ions

Summer to winter ratio for each ion is represented in Figure 4.27. According to this figure, ratios for anthropogenic such as SO_4^{2-}, NO_3 and NH_4^+ and crustal ions such as Ca^{2+}, Mg^{2+} and K^+ are higher than 1. On the contrary, for H^+ ion and ions originating from sea salt such as Na^+ and Cl^- have ratios below 1. The main reasons are provided in the previous paragraphs of the manuscript.

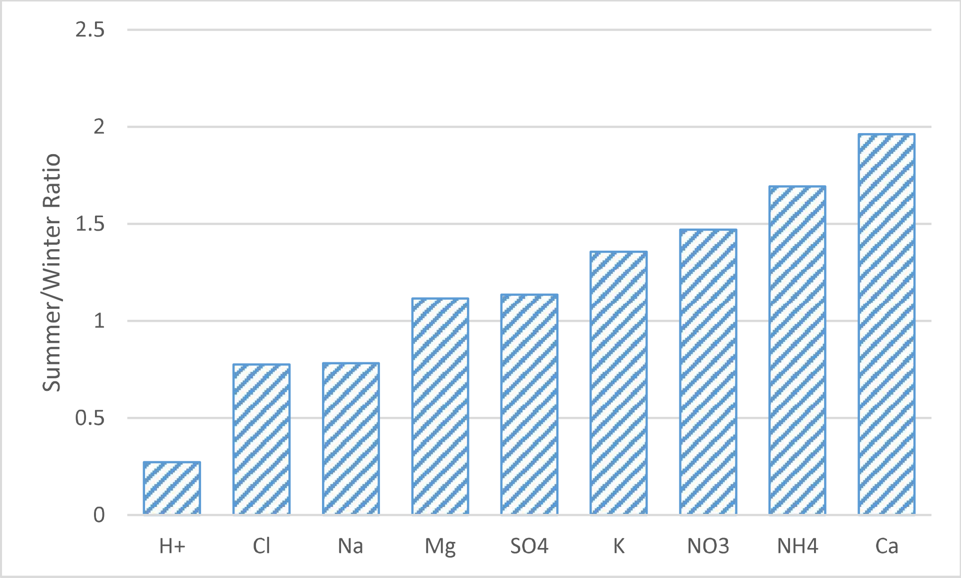

Figure 4.27 The Summer to Winter Ratio of Ions in Amasra Station

4.5.2. Interannual Variations in Ion Concentrations

Interannual variations in ion concentrations, is also known as long-term trends. Trends are important to assess results of actions taken to improve air quality. For example, most of the trend analysis demonstrated that rural SO_4^{2-} concentrations in Europe decreased by 70% since 1980, demonstrating success of actions taken to reduce SO_2 and NO_x emissions. It is not very difficult to detect a consistent increase or decrease in concentrations of parameters over years, but it is difficult to show observed decrease or increase in concentrations of a parameter is statistically significant or not.

Statistical tests are needed to validate statistical significance of an observed trend. Since distribution of element or ion concentrations is always right-skewed, tests have to be non-parametric. Today there are two, very widely used, statistical tools to test statistical significance of observed trends and to estimate its slope. These are "Man Kendall test", which tells whether an observed long-term change in concentration of a parameter is statistically significant or not. The second one is "Sens slope estimator", which gives slope of an increasing or decreasing trend-line.

In this part of the manuscript, interannual variations of the measured ions is discussed. Annual median concentrations of the measured parameters are given in Table 4.6.

As can be seen from the table, the highest median values are recorded for SO_4^{2-} in 2004 (3.205 mg L^{-1}) and lowest values are recorded for H^+ ion in 2005 (0.001 mg L^{-1}).

Annual variation of concentrations of pollution-derived ions are given in Figure 4.29 and for crustal and marine ions it is depicted in Figure 4.30. Concentrations of pollution-derived ions follow similar patterns between 2004 and 2016 at our Amasra station. Concentration of SO_4^{2-} decreased in time, particularly between the years 2006 and 2009. The concentration SO_4^{2-} increased in 2010 with respect to the previous years and showed a slight increasing trend until 2014 and decreased again in 2015. Concentration of NO_3^-, on the other hand decreased between 2004 and 2009 and remain the same, or even increased gradually between 2009 and 2016. Concentration of NH_4^+ showed a sudden drop after 2008 and gradually increased between 2009 and 2016, like NO_3^-. Furthermore, since fertilizer consumption is one of the sources for NH_4^+ in the atmosphere, annual fertilizer consumption data for Bartın province obtained from Plant Nutrition and Technology Development Department of the Ministry of Agriculture and Forestry is compared with the median concentrations of NH_4^+ measured in this study. The correlation and annual variation of fertilizer consumption in Bartın province and median concentration of NH_4^+ ion is depicted in Figure 4.28. As a result of this comparison it can be concluded that NH_4^+ regression against fertilizer consumption showed fairly good correlation with positive slope and R^2 value of 0.325.

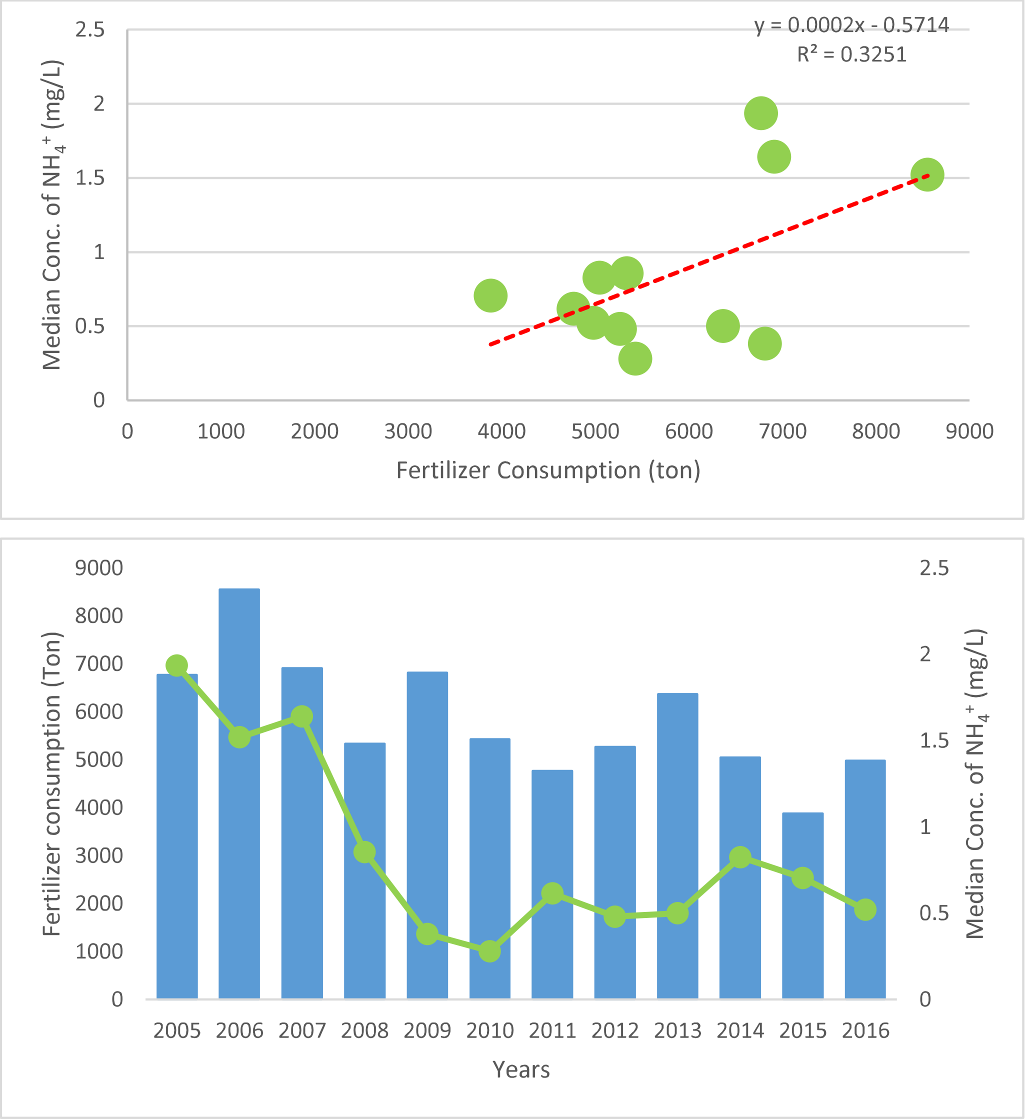

Figure 4.28 Correlation and Annual Variation of Fertilizer Consumption in Bartın Province and Median Concentration of NH_4^+ ion.

Concentration of H^+ ion remained low between 2004 -2009, increased between 2010 and 2013, then decreased again in 2014-2016 period. Statistical significance of these long-term patterns is discussed in following paragraphs.

No specific common increasing or decreasing trend is recorded for marine and crustal ions.

Table 4.6. *Annual Median Concentrations of Measured Major Ions (mg/L)*

	2004	**2005**	**2006**	**2007**	**2008**	**2009**	**2010**	**2011**	**2012**	**2013**	**2014**	**2015**	**2016**
H^+	0.002	0.001	0.001	0.000	0.001	0.001	0.005	0.017	0.011	0.017	0.001	0.006	0.004
SO_4^{2-}	3.205	2.790	2.795	3.110	2.745	2.005	2.345	2.770	2.335	2.690	2.730	0.890	2.670
NO_3^-	2.040	2.075	1.715	1.630	0.930	1.020	1.150	1.310	1.755	1.295	1.800	1.000	1.965
Cl^-	2.730	2.200	3.115	2.500	2.180	1.305	2.335	1.920	1.730	2.425	2.440	2.000	1.625
NH_4^+	-	1.935	1.520	1.640	0.855	0.380	0.280	0.615	0.480	0.500	0.825	0.705	0.520
Ca^{2+}	-	1.030	1.170	1.850	1.300	0.970	0.650	0.770	0.590	1.090	1.690	0.140	0.930
Mg^{2+}	-	1.010	0.350	0.310	0.285	0.315	0.190	0.230	0.190	0.320	0.340	0.365	0.250
K^+	-	0.160	0.200	0.215	0.240	0.140	0.120	0.150	0.130	0.140	0.150	0.110	0.130
Na^+	-	1.075	2.695	1.670	1.520	1.185	1.010	1.360	1.070	1.490	1.910	1.570	1.600

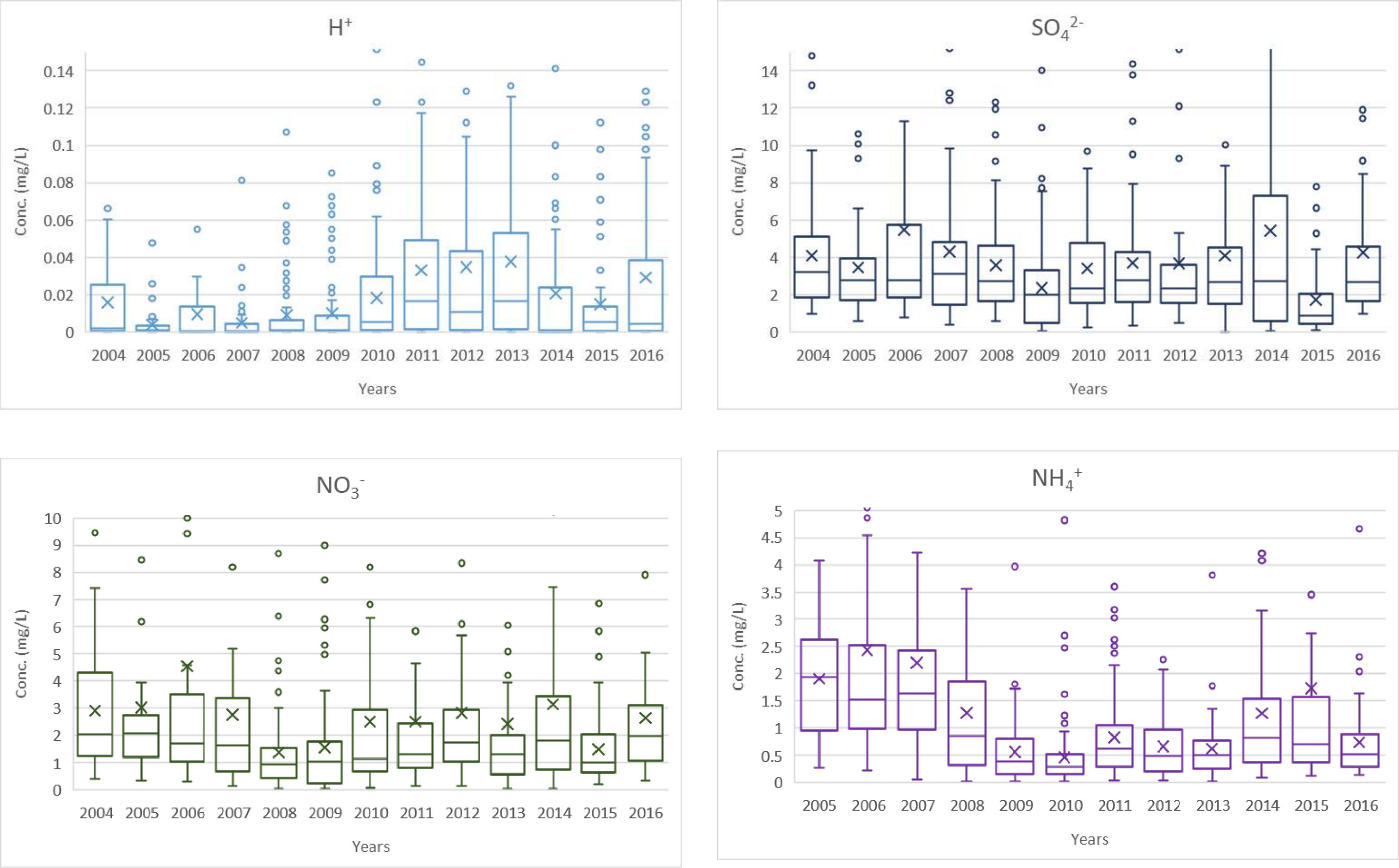

Figure 4.29 Interannual Variation Concentration Pollution-Derived Ions in Amasra Station

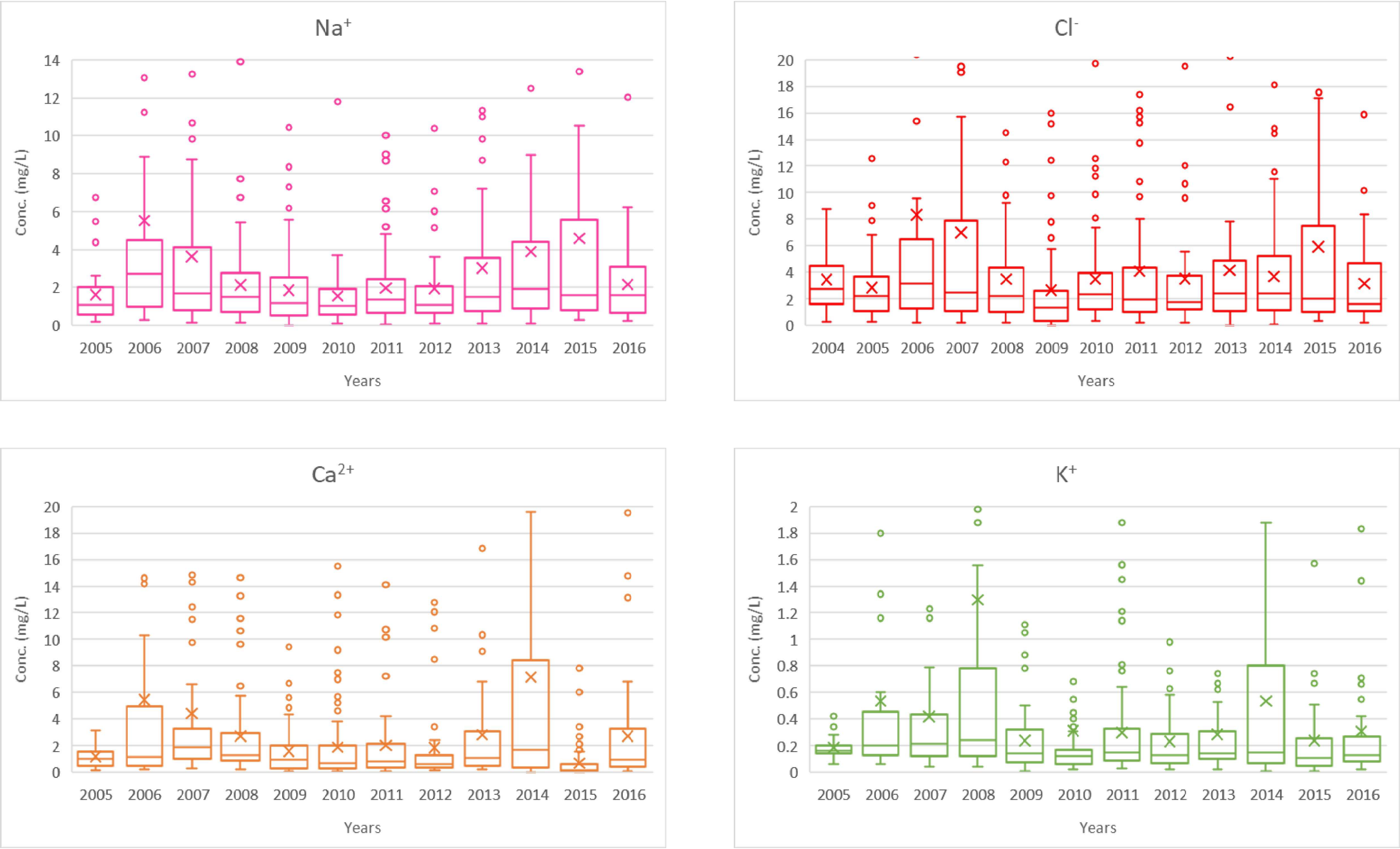

Figure 4.30 Interannual Variation Concentration Crustal and Marine Ions in Amasra Station

Mann – Kendal test was used to test statistical significance of long term variations in concentrations ion concentrations and Sens slope estimator was used to determine slope of the trend. These methods are frequently for trend analysis, particularly using meteorological data. They proved to be ideal for data sets which do not follow normal (Gaussian) distribution. As discussed in previous parts of this manuscript, ion concentrations measured in this work do not follow normal distribution, some of them fits lognormal distribution and some fits to other right-skewed distributions that are not lognormal. Since Mann-Kendall test and Sens slope estimator are independent of distribution type of the data set, they can be safely applied to data generated in this work.

The results of the Van Belle and Hughes homogeneity test, which were applied to our data are given in Table 4.7. In order to conduct this test, monthly averages were used, and 12 months of the year is taken as 12 seasons and they are set as the time periods. The calculated χ^2_{homog} values are found to be less than $\chi^2_{\mathrm{Critical}}$ (17.275) with d_f=12-1 and at the significance level of $\alpha = 0.1$. Hence, the null hypothesis of homogenous seasonal trends observed over time cannot be rejected. Since χ^2_{homog} values are not significant in this case, χ^2_{Trend} values are compared with $\chi^2_{\mathrm{Critical}}$ (2.706) with d_f=1 and at the same significance level. If the calculated $\chi_{\mathrm{Trend}} > \chi_{\mathrm{Critical}}$ for any parameter, then a global trend is present for that parameter in every season. According to this evaluation none of the parameters passed the homogeneity test. So, in this case it is more appropriate to apply Mann Kendall Test instead of Seasonal Mann Kendall Test.

Table 4.7. *Results of the Van Belle and Hughes Homogeneity Test*

	$X^2_{Homogen}$	$X^2_{Critical}$ $\alpha = 0.1$ df=11	X^2_{Trend}	$X^2_{Critical}$ $\alpha = 0.1$ df=1	X^2_{Total}
SO_4^{2-}	9.755	17.275	0.148	2.706	9.903
NO_3^-	10.265	17.275	0.156	2.706	10.420
Cl^-	3.309	17.275	0.050	2.706	3.359
NH_4^+	16.962	17.275	0.257	2.706	17.219
Ca^{2+}	13.377	17.275	0.203	2.706	13.580
Mg^{2+}	7.009	17.275	0.106	2.706	7.115
K^+	12.518	17.275	0.190	2.706	12.707
Na^+	5.893	17.275	0.089	2.706	5.982

In Mann-Kendall Test average values obtained for the months for each year are used as time period, since the test should be applied for every season individually as previously mentioned in the manuscript. The null hypothesis, H_0, which represents no trend versus alternative hypothesis, H_A of an upward or downward trend (two tailed test) was tested at a significance level of $\alpha = 0.1$. The critical value at this level of significance is 1.645. the two-sided null hypothesis of either an increasing or decreasing trend is statistically significant when the calculated absolute value of Z exceeds the $Z_{Critical}$ value. The summary of the Mann-Kendall Test is provided in Table 4.8.

Table 4.8. *Summary of the Results of the Mann-Kendall Test*

	Mann Kendall Statistic (S)	**Z**	**$Z_{Critical}$ α= 0.1**	**Trend**	**Trend Direction**
JANUARY					
SO_4^{2-}	-17	-1.323	1.645	Insignificant	↓
NO_3^-	**-23**	**-1.791**	**1.645**	**Significant**	↓
Cl^-	1	0.078	1.645	Insignificant	↑
NH_4^+	**-29**	**-2.594**	**1.645**	**Significant**	↓
Ca^{2+}	**-29**	**-2.594**	**1.645**	**Significant**	↓
Mg^{2+}	-5	-0.447	1.645	Insignificant	↓
K^+	**-37**	**-3.309**	**1.645**	**Significant**	↓
Na^+	-5	-0.447	1.645	Insignificant	↓
FEBRUARY					
SO_4^{2-}	-11	-0.983	1.645	Insignificant	↓
NO_3^-	-1	-0.089	1.645	Insignificant	↓
Cl^-	-3	-0.268	1.645	Insignificant	↓
NH_4^+	-2	-0.209	1.645	Insignificant	↓
Ca^{2+}	-4	-0.417	1.645	Insignificant	↓
Mg^{2+}	-2	-0.209	1.645	Insignificant	↓
K^+	-4	-0.417	1.645	Insignificant	↓
Na^+	0	0.000	1.645	-	-
MARCH					
SO_4^{2-}	17	1.520	1.645	Insignificant	↑
NO_3^-	11	0.984	1.645	Insignificant	↑
Cl^-	7	0.626	1.645	Insignificant	↑
NH_4^+	0	0.000	1.645	-	-
Ca^{2+}	0	0.000	1.645	-	-
Mg^{2+}	12	1.251	1.645	Insignificant	↑
K^+	4	0.417	1.645	Insignificant	↑
Na^+	-2	-0.209	1.645	Insignificant	↓
APRIL					
SO_4^{2-}	-3	-0.234	1.645	Insignificant	↓
NO_3^-	-17	-1.323	1.645	Insignificant	↓
Cl^-	1	0.078	1.645	Insignificant	↑
NH_4^+	2	0.209	1.645	Insignificant	↑
Ca^{2+}	6	0.626	1.645	Insignificant	↑
Mg^{2+}	10	1.043	1.645	Insignificant	↑
K^+	8	0.834	1.645	Insignificant	↑
Na^+	4	0.417	1.645	Insignificant	↑
MAY					
SO_4^{2-}	-1	-0.078	1.645	Insignificant	↓
NO_3^-	-9	-0.701	1.645	Insignificant	↓
Cl^-	-17	-1.323	1.645	Insignificant	↓
NH_4^+	2	0.209	1.645	Insignificant	↑
Ca^{2+}	-6	-0.626	1.645	Insignificant	↓
Mg^{2+}	-8	-0.834	1.645	Insignificant	↓
K^+	-6	-0.626	1.645	Insignificant	↓
Na^+	-10	-1.043	1.645	Insignificant	↓
JUNE					
SO_4^{2-}	-12	-0.732	1.645	Insignificant	↓
NO_3^-	6	0.366	1.645	Insignificant	↑
Cl^-	-10	0.610	1.645	Insignificant	↓
NH_4^+	-3	-0.234	1.645	Insignificant	↓
Ca^{2+}	-19	-1.479	1.645	Insignificant	↓
Mg^{2+}	-9	-0.701	1.645	Insignificant	↓
K^+	-5	-0.389	1.645	Insignificant	↓
Na^+	-9	-0.701	1.645	Insignificant	↓

Table 4.8. *Summary of the Results of the Mann-Kendall Test (continued)*

	Mann Kendall Statistic (S)	**Z**	**$Z_{Critical}$ $\alpha = 0.1$**	**Trend**	**Trend Direction**
JULY					
SO_4^{2-}	-10	-0.686	1.645	Insignificant	↓
NO_3^-	-14	-0.960	1.645	Insignificant	↓
Cl^-	-2	-0.137	1.645	Insignificant	↓
NH_4^+	2	0.209	1.645	Insignificant	↑
Ca^{2+}	5	0.447	1.645	Insignificant	↑
Mg^{2+}	13	1.163	1.645	Insignificant	↑
K^+	7	0.626	1.645	Insignificant	↑
Na^+	**21**	**1.878**	**1.645**	**Significant**	↑
AUGUST					
SO_4^{2-}	-6	-0.411	1.645	Insignificant	↓
NO_3^-	-8	-0.549	1.645	Insignificant	↓
Cl^-	-6	-0.411	1.645	Insignificant	↓
NH_4^+	-13	-1.163	1.645	Insignificant	↓
Ca^{2+}	-1	-0.089	1.645	Insignificant	↓
Mg^{2+}	7	0.626	1.645	Insignificant	↑
K^+	5	0.447	1.645	Insignificant	↑
Na^+	5	0.447	1.645	Insignificant	↑
SEPTEMBER					
SO_4^{2-}	-4	-0.274	1.645	Insignificant	↓
NO_3^-	8	0.549	1.645	Insignificant	↑
Cl^-	-8	-0.549	1.645	Insignificant	↓
NH_4^+	-19	-1.479	1.645	Insignificant	↓
Ca^{2+}	-1	-0.078	1.645	Insignificant	↓
Mg^{2+}	-3	-0.234	1.645	Insignificant	↓
K^+	-5	-0.389	1.645	Insignificant	↓
Na^+	3	0.234	1.645	Insignificant	↑
OCTOBER					
SO_4^{2-}	-7	-0.545	1.645	Insignificant	↓
NO_3^-	-1	-0.078	1.645	Insignificant	↓
Cl^-	-7	-0.545	1.645	Insignificant	↓
NH_4^+	**-25**	**-1.946**	**1.645**	**Significant**	↓
Ca^{2+}	-19	-1.479	1.645	Insignificant	↓
Mg^{2+}	-13	-1.012	1.645	Insignificant	↓
K^+	-3	-0.234	1.645	Insignificant	↓
Na^+	-9	-0.701	1.645	Insignificant	↓
NOVEMBER					
SO_4^{2-}	4	0.274	1.645	Insignificant	↑
NO_3^-	14	0.960	1.645	Insignificant	↑
Cl^-	6	0.411	1.645	Insignificant	↑
NH_4^+	-15	-1.168	1.645	Insignificant	↓
Ca^{2+}	1	0.078	1.645	Insignificant	↑
Mg^{2+}	11	0.856	1.645	Insignificant	↑
K^+	3	0.234	1.645	Insignificant	↑
Na^+	5	0.389	1.645	Insignificant	↑
DECEMBER					
SO_4^{2-}	**-25**	**-1.946**	**1.645**	**Significant**	↓
NO_3^-	-19	-1.479	1.645	Insignificant	↓
Cl^-	-3	-0.233	1.645	Insignificant	↓
NH_4^+	-15	-1.342	1.645	Insignificant	↓
Ca^{2+}	-17	-1.520	1.645	Insignificant	↓
Mg^{2+}	1	0.089	1.645	Insignificant	↑
K^+	-7	-0.626	1.645	Insignificant	↓
Na^+	-1	-0.089	1.645	Insignificant	↓

The Z values for pollution-derived and crustal and marine ions are given in Figure 4.31 and Figure 4.32, respectively. As can be seen from Figure 4.31, SO_4^{2-} shows a decreasing trend in the majority of the months. Increasing trends observed in March and November are not statistically significant. As for the months in which SO_4^{2-} shows a decreasing trend, the only month where observed trend is statistically significant is December. Furthermore, another pollution-derived ion NO_3^- similarly shows a decreasing trend in most of the months except for March, June, September and November. However, these increasing trends are not statically significant. The only month in which trend in which NO_3^- trend is statistically significant is January. NH_4^+ ion shows an increasing trend in April, May and July. The increasing trend observed in these months are not statistically significant. It showed a decreasing trend in the rest of the months. However, statistically significant deceasing trend was observed only in January and October.

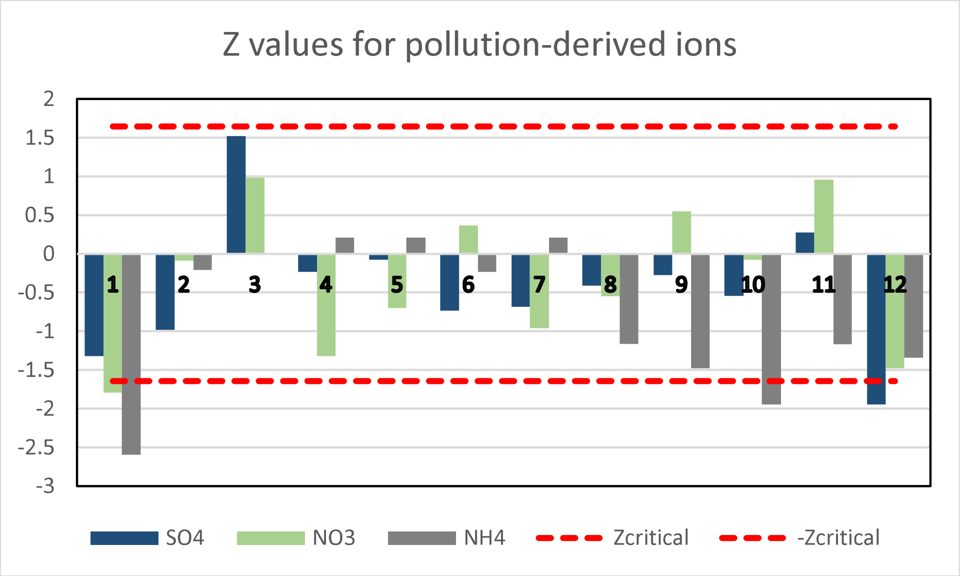

Figure 4.31 Z Values Calculated for Pollution-Derived Ions

As seen in Figure 4.32, marine and crustal ions generally do not show a statistically significant trend over time. Only in January, Ca^{2+} and K^+ show a significant decreasing trend and Na^+ shows a significant increasing trend in July.

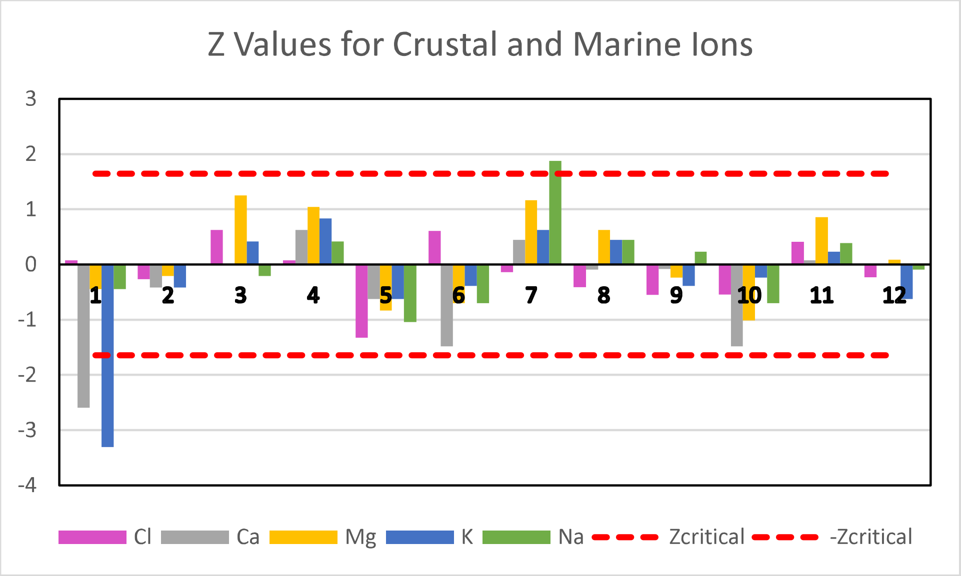

Figure 4.32 Z Values Calculated for Marine and Crustal Ions

Final analysis is done to determine the rate of change in the ion concentrations per time with Sen's Slope Estimator method.

The results of the Sen's Slope Estimator are given in Table 4.9.

Table 4.9. *Results of the Sen's Slope Estimator*

	Slope Estimate (μeq/L/yr)	90% Confidence Interval	
		Lower (μeq/L)	Upper (μeq/L)
JANUARY			
SO_4^{2-}	-5.221	-11.316	0.621
NO_3^-	**-1.734**	**-4.528**	**0.186**
Cl^-	0.597	-35.394	12.327
NH_4^+	**-6.451**	**-16.996**	**-1.079**
Ca^{2+}	**-7.250**	**-11.860**	**-2.553**
Mg^{2+}	-1.644	-12.301	1.992
K^+	**-1.260**	**-1.928**	**-0.622**
Na^+	-6.582	-57.143	12.858
FEBRUARY			
SO_4^{2-}	-3.322	-13.294	4.707
NO_3^-	-1.464	-3.361	2.401
Cl^-	-0.895	-19.221	17.110
NH_4^+	-1.026	-13.397	4.572
Ca^{2+}	-5.600	-46.507	9.695
Mg^{2+}	-0.743	-14.326	8.439
K^+	-0.174	-1.008	0.366
Na^+	-0.786	-46.365	17.764
MARCH			
SO_4^{2-}	3.082	-0.973	9.159
NO_3^-	1.544	-1.411	4.791
Cl^-	2.817	-6.751	16.026
NH_4^+	0.109	-15.930	6.248
Ca^{2+}	0.016	-27.625	25.100
Mg^{2+}	1.852	-3.280	5.799
K^+	0.039	-0.947	0.592
Na^+	-0.565	-8.540	37.142
APRIL			
SO_4^{2-}	-0.995	-7.967	7.168
NO_3^-	-0.923	-7.230	2.481
Cl^-	0.262	-3.561	4.714
NH_4^+	2.133	-6.481	15.427
Ca^{2+}	5.504	-23.286	46.540
Mg^{2+}	1.796	-2.529	4.564
K^+	0.149	-0.440	0.838
Na^+	4.369	-7.620	16.694
MAY			
SO_4^{2-}	-0.729	-13.442	14.241
NO_3^-	-4.751	-21.119	3.234
Cl^-	-5.745	-13.218	1.380
NH_4^+	1.471	-9.388	22.001
Ca^{2+}	-13.960	-66.785	37.457
Mg^{2+}	-5.831	-32.672	6.621
K^+	-0.845	-9.225	1.891
Na^+	-5.119	-20.748	15.783
JUNE			
SO_4^{2-}	-2.122	-13.697	6.248
NO_3^-	0.245	-2.339	7.063
Cl^-	-1.925	-14.167	9.434
NH_4^+	-2.426	-15.813	8.763
Ca^{2+}	-27.438	-61.020	3.984
Mg^{2+}	-3.090	-15.440	6.372
K^+	-0.325	-3.045	1.250
Na^+	-7.063	-33.646	13.591

Table 4.9. *Results of the Sen's Slope Estimator (continued)*

	Slope Estimate (μeq/L/yr)	**90% Confidence Interval**	
		Lower (μeq/L)	**Upper (μeq/L)**
JULY			
SO_4^{2-}	-4.510	-8.749	7.576
NO_3^-	-2.704	-9.258	2.544
Cl^-	-0.929	-13.609	23.202
NH_4^+	0.655	-7.376	7.554
Ca^{2+}	0.472	-55.846	52.086
Mg^{2+}	9.306	-8.049	18.178
K^+	0.328	-1.991	5.106
Na^+	**33.232**	**0.679**	**58.317**
AUGUST			
SO_4^{2-}	-2.114	-17.567	10.832
NO_3^-	-2.018	-16.736	6.237
Cl^-	-0.735	-15.567	12.164
NH_4^+	-9.074	-15.374	4.296
Ca^{2+}	-7.198	-51.582	74.022
Mg^{2+}	11.667	-13.678	29.333
K^+	0.653	-1.419	2.895
Na^+	6.667	-15.050	34.009
SEPTEMBER			
SO_4^{2-}	-2.556	-10.832	7.826
NO_3^-	0.723	-6.155	5.636
Cl^-	-4.829	-30.474	9.908
NH_4^+	-2.981	-13.765	0.886
Ca^{2+}	-1.083	-31.744	19.224
Mg^{2+}	-0.937	-7.816	2.136
K^+	-0.207	-1.200	0.523
Na^+	2.625	-24.360	13.995
OCTOBER			
SO_4^{2-}	-2.522	-6.550	2.890
NO_3^-	-0.204	-3.685	2.040
Cl^-	-1.403	-4.650	4.368
NH_4^+	**-9.213**	**-17.744**	**-0.436**
Ca^{2+}	-12.144	-24.398	2.804
Mg^{2+}	-1.477	-4.516	1.040
K^+	-0.011	-1.225	0.740
Na^+	-1.734	-7.312	4.025
NOVEMBER			
SO_4^{2-}	0.768	-4.220	5.158
NO_3^-	1.065	-1.412	2.729
Cl^-	3.404	-9.675	13.664
NH_4^+	-3.992	-10.558	3.976
Ca^{2+}	0.094	-13.016	30.734
Mg^{2+}	2.944	-2.121	10.641
K^+	0.278	-0.564	1.676
Na^+	2.283	-11.741	17.702
DECEMBER			
SO_4^{2-}	**-2.599**	**-7.641**	**-0.170**
NO_3^-	-2.117	-4.406	1.532
Cl^-	-3.488	-14.083	11.568
NH_4^+	-7.364	-14.744	2.990
Ca^{2+}	-4.592	-9.009	2.837
Mg^{2+}	0.428	-4.383	7.620
K^+	-0.401	-0.812	0.844
Na^+	-0.064	-8.998	33.678

Slopes found for trends that are found as statistically significant in Mann-Kendal test are indicated with bold fonts. Negative slopes were found for most of the ions in majority of the months, indicating that ion concentrations show a general decreasing trend in rainwater at the Central Black Sea region. However, these variations are not statistically significant in most of the months. The main reason for lack of statistical significance found in Mann-Kendal exercise is the small number of data points. Twelve year is generally long enough for a successful trend analysis, if data generated is daily, as in aerosol studies, or hourly as in meteorological data sets. More than 800 data for each ion unfortunately is not high enough. Uncertainty in monthly averages used in MK test becomes high when there is small number of data in them. This is particularly true in summer months when there are very few rain events.

The Mann-Kendall Test is also reapplied to the data set by taking each year as the time variable. It is conducted between the years 2005 to 2015 since this time period includes measurements for all ions included in this study. 2016 measurements were excluded from the data set since the measurements only continued in the first half of the year. The results of the test between 2005-2015 is given in Table 4.10 and ions having statistically significant trends are indicated by bold letters. H^+ ion shows statistically significant increasing trend whereas SO_4^{2-} and K^+ shows statistically significant decreasing trend at $\alpha=0.1$ significance level. It is interesting that H^+ ion shows increasing trend (positive Z value) while SO_4^{2-} and NO_3^- ions which are principle precursors of acidity show decreasing trends (negative Z value). Although the reasoning behind this result is not entirely clear, it is crucial to note that concentration of H^+ does not only depend on SO_4^{2-} and NO_3^-, it also depends on the neutralizers of acidity such as Ca^{2+} and NH_4^+ present in atmospheric environment as stated in the previous parts of the manuscript. Since both of these neutralizers are showing decreasing trends (negative Z values) this might be the reason behind increasing trend observed for H^+ throughout the years 2005-2015.

Table 4.10. *Summary of the Results of the Mann-Kendall Test between 2005-2015*

	Mann Kendall Statistic (S)	**Z**	**$Z_{Critical}$ α= 0.1**	**Trend**	**Trend Direction**
H^+	**28**	**2.186**	**1.645**	**significant**	↑
SO_4^{2-}	**-25**	**-1.946**	**1.645**	**significant**	↓
NO_3^-	-15	-1.168	1.645	insignificant	↓
Cl^-	-11	-0.856	1.645	insignificant	↓
NH_4^+	-19	-1.479	1.645	insignificant	↓
Ca^{2+}	-16	-1.249	1.645	insignificant	↓
Mg^{2+}	11	0.856	1.645	insignificant	↑
K^+	**-25**	**-1.946**	**1.645**	**significant**	↓
Na^+	-1	-0.078	1.645	insignificant	↓

Sen's slope estimator results between 2005-2015 is given in Table 4.11. Statistically significant results are indicated in bold letters. In 90% confidence interval the rate of change per time (slope estimator) for H^+ and SO_4^{2-} are 0.639 μeq/L/yr and -1.131 μeq/L/yr, respectively.

Table 4.11. *Results of the Sen's Slope Estimator between 2005-2015*

	Slope Estimate (μeq/L/yr)	**90% Confidence Interval**	
		Lower (μeq/L)	**Upper (μeq/L)**
H^+	**0.639**	**0.042**	**2.295**
SO_4^{2-}	**-1.131**	**-4.03**	**-0.101**
NO_3^-	-0.403	-2.062	1.016
Cl^-	-1.786	-4.159	1.015
NH_4^+	-6.265	-10.703	1.198
Ca^{2+}	-3.5	-7.756	2.888
Mg^{2+}	0.556	-0.379	1.68
K^+	**-0.256**	**-0.386**	**-0.04**
Na^+	-0.031	-6.257	3.207

4.6. Positive Matrix Factorization

Ionic composition of precipitation at our Amasra Station are determined by source regions in and out of Turkey. A two-step approach was used to identify sources and source regions affecting composition of rainwater at Central Black Sea region. In the first step, a multivariate statistical tool namely, positive matrix factorization (PMF) is used to identify the source types which affect the composition of precipitation at Amasra Station. In the second part of the exercise, factor scores calculated for the anthropogenic factor in PMF was used as an input data set in potential source contribution function approach (PSCF) to identify source regions where those anthropogenic sources are located.

PMF requires two data files which are a datafile containing information on measured concentrations and an uncertainty file that consists of uncertainties assigned to each datum. In relation to these two input files PMF analysis assigns categories to each specie depending on their signal-to-noise ratios (S/N). there are three categories that PMF analysis assigns which are “Bad”, “Weak” and “Strong”. Species that are assigned as “Bad” have S/N below 0.5 and they are excluded from PMF analysis entirely. Species that are assigned as “Weak” have S/N value between 0.5 and 1. In this category, the uncertainties associated to these ions are multiplied by three, which means that they are included in PMF, but they don’t play a role in the fit.

Lastly, species that are assigned as “Strong” have S/N value greater than 1 and their uncertainties stay as provided in the beginning. These are the parameters that are used in the PMF fit.

The S/N values in this study and the assigned categories for each specie are given in Table 4.12.

Table 4.12. *Categories and Signal-to-Noise Raitos (S/N) of the Ions*

Species	Category	S/N
SO_4^{2-}	Strong	8.9
NO_3^-	Strong	8.7
Cl^-	Strong	8.8
NH_4^+	Strong	7.9
Ca^{2+}	Strong	8.0
Mg^{2+}	Strong	8.2
K^+	Strong	8.1
Na^+	Strong	8.3

As can be seen from the table all ions measured in this study have fairly high S/N ratios and assigned as "strong" variables.

The most challenging part of PMF is the selection of optimum number of factors as it is left to the user. There are some guidelines on selecting the optimum number factors. First and the most important guideline is to minimize the "object function" Q. Q_{robust}, values are calculated by the PMF model for each factor number. These values are compared with $Q_{theoretical}$ value. Definition for the Q values are discussed in section 2.3.2.3. of this manuscript. The difference between these two Q values must be minimized by changing a number of parameters in PMF. The number of factors having the minimum ΔQ is selected as the optimum number of factors. Other criteria for selecting number of factors can be listed as scaled residuals, observed and predicated concentrations of species and correlations between factor contributions.

In order to decide on the number of factors the analysis was carried out and examined starting from 3 factors to 7 factors. The optimum was selected as 4 factors. For 4 factors, the calculated Q_{robust} by the PMF software was 4833.69 and the $Q_{theoretical}$ is calculated as 3248 by using Equation 3.5. These two Q values was accepted as sufficiently close and thus four factors were considered as the optimum number of factors.

It should be noted that number of ions analyzed in this study was too small for PMF to be successful. The resulting four factors in this study is not a direct indication that there are only four source types in rainwater. Larger number of factors could be extracted from PMF analysis if other parameters such as trace elements POPs or carbon fractions were also measured.

As stated in previous paragraphs, four factors were selected as optimum. These four factors are briefly discussed in following sections.

Factor 1:

Diagnostic figures, including factor loadings, percent contribution of factor 1 on measured ion concentrations and monthly median values of factor scores for factor 1 are given in Figure 4.33. Factor 1 explains approximately 95% of the measured NH_4^+ concentration as well as 12% and 6.5% of the measured K^+ and Mg^{2+} concentrations, respectively. In many PMF studies conducted in Turkey, a factor consisting of only NH_4^+ was encountered (Ayaklı, 2014; Güllü et.al, 2005; Yücel, 2019). Factor 1 scores are relatively lower in winter (October–March) and higher during summer (April-September). This supports the fertilizer source since NH_4^+ is present in synthetic fertilizers such as $(NH_4)_3PO_3$ and $(NH_4)_2SO_4$ which are applied at spring and some of the NH_4^+ in fertilizer is reduced to NH_3 and evaporates to atmosphere, where it is oxidized back to NH_4^+. Therefore, factor 1 is identified as fertilizer factor.

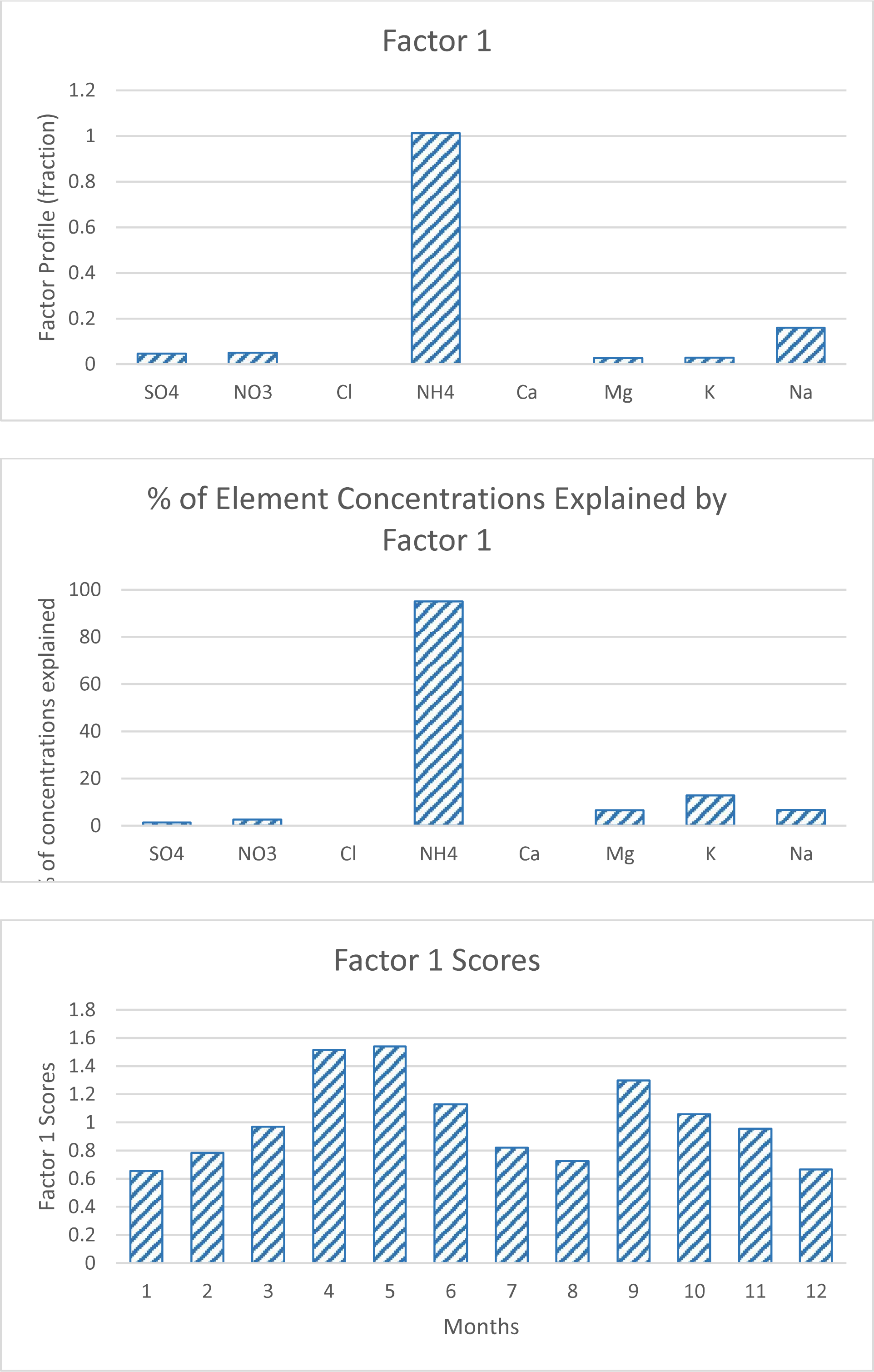

Figure 4.33 Factor 1 Diagnostics: (a) factor loadings, (b) fractions of ion concentrations explained by factor 1 and (c) monthly variations of factor scores

Factor 2:

Factor loadings, percent contribution of factor 2 on measured ion concentrations and monthly median values for factor scores for factor 2 are depicted in Figure 4.34. Factor 2 is identified as “crustal” factor, because it accounts for 87.5% of measured concentration of Ca^{2+} and 49%, 39% of measured concentrations of K^{+}, and Mg^{2+} respectively. These are all crustal ions. This factor represents the soil particles present in the atmosphere which are washed out from the atmosphere by below-cloud processes. Factor 2 scores are higher in the summer months. This typical monthly variation observed in most crustal elements.

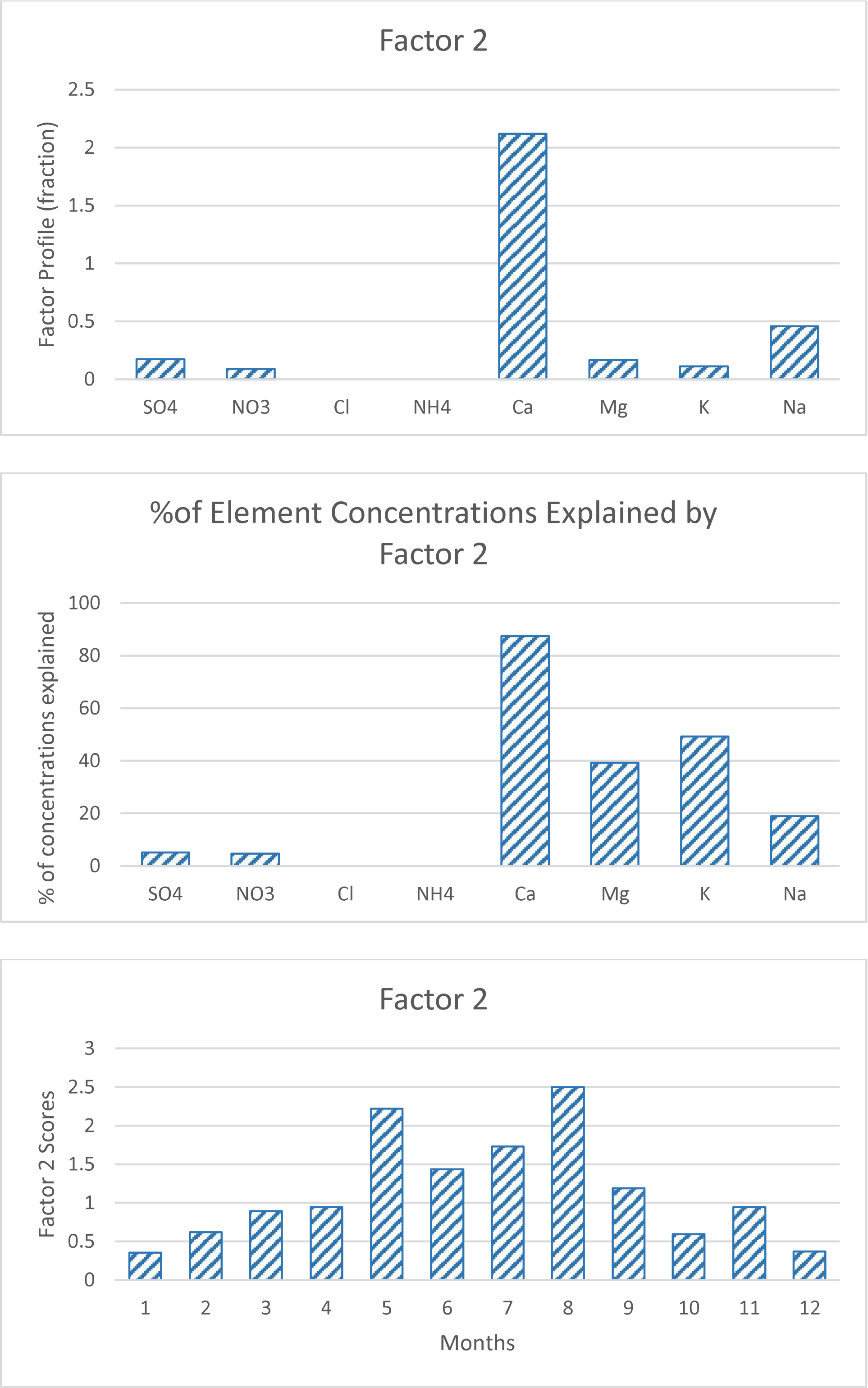

Figure 4.34 Factor 2 Diagnostics: (a) factor loadings, (b) fractions of ion concentrations explained by factor 2 and (c) monthly variations of factor scores

Factor 3:

Diagnostic figures for factor 3 is given in Figure 4.35. The factor has high loadings of secondary anthropogenic ions SO_4^{2-} and NO_3^-. Factor 3 accounts for 91% and 93% of measured concentrations of SO_4^{2-} and NO_3^-, respectively. This factor is identified as "Long-range transport" factor as it represents anthropogenic components. Factor 3 has higher scores in summer months. This can also be an indication of long-range transport of the species as pollutants cannot be transported over large distances in winter due increased wet scavenging of pollutants from atmosphere in winter (Işıkdemir, 2006).

PSCF distribution map of the Factor 3 scores are given in Figure 4.36. According to this distribution map the source areas can be identified as NE Mediterranean coast of Libya and Algeria, Middle East, Russia, NW coast of Caspian Sea, Azerbaijan, Georgia, Western Turkey and central Black Sea region of Turkey.

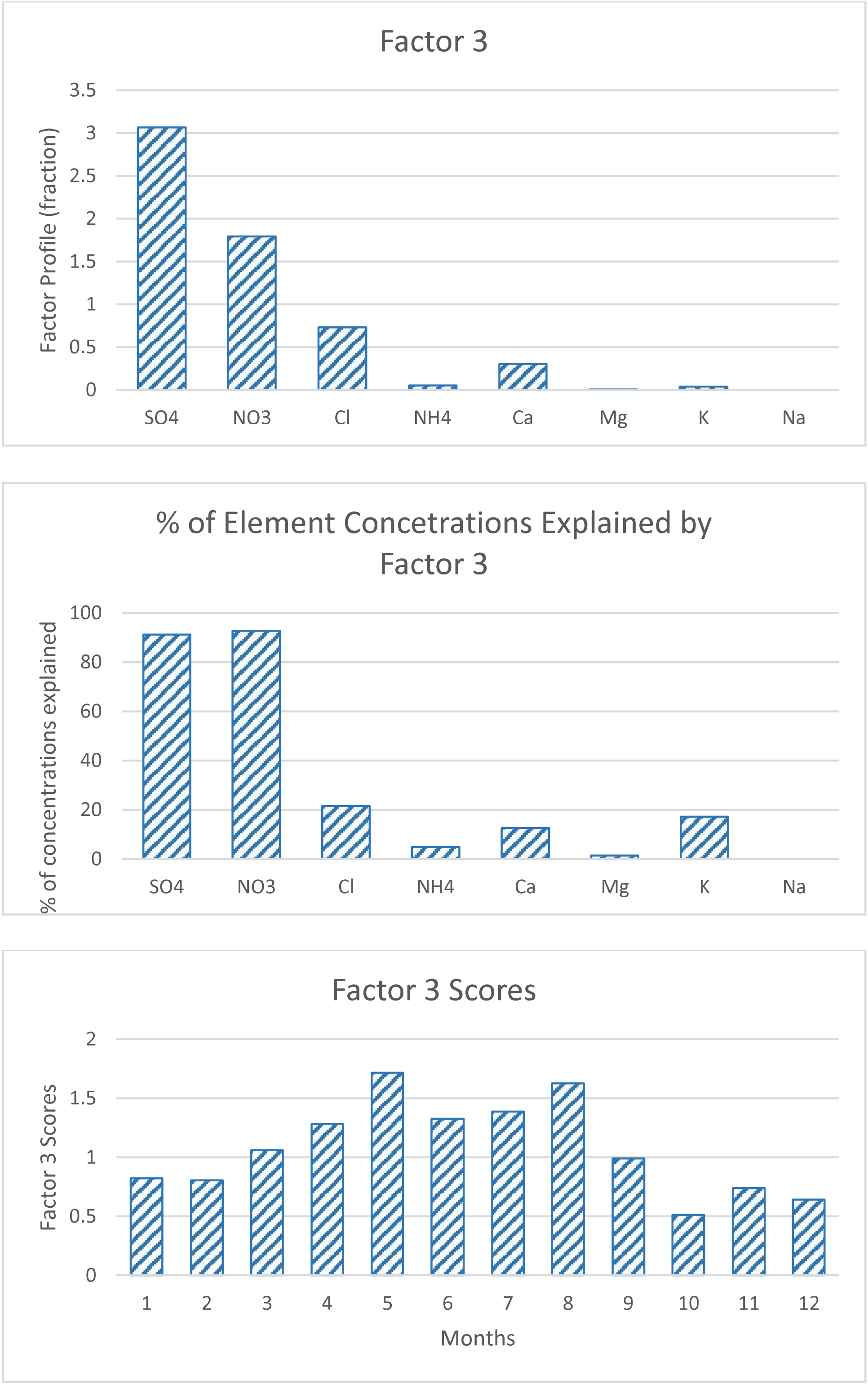

Figure 4.35 Factor 3 Diagnostics: (a) factor loadings, (b) fractions of ion concentrations explained by factor 3 and (c) monthly variations of factor scores

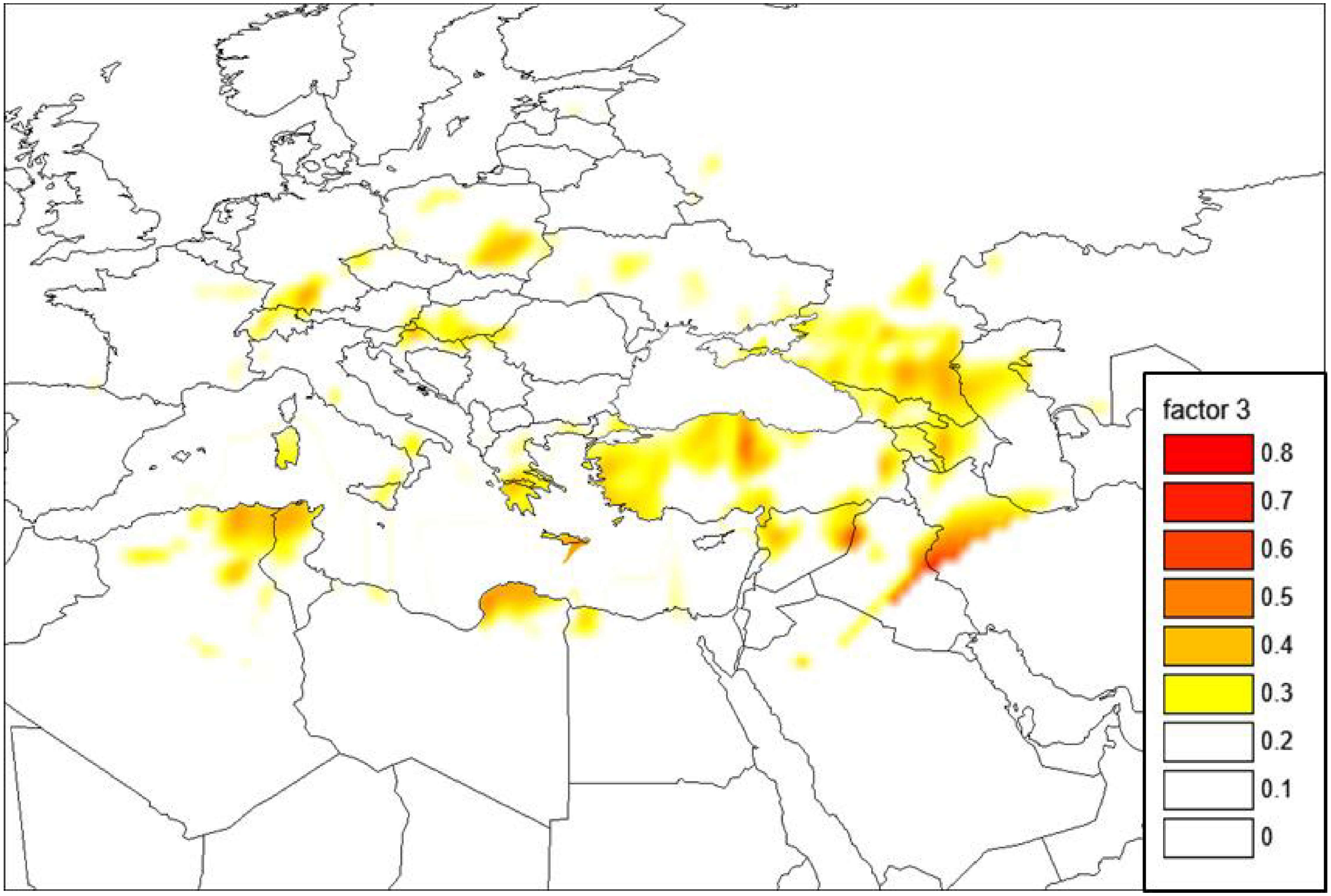

Figure 4.36 Distribution of PSCF Values Using Factor 3 Scores

Factor 4:

Diagnostics for Factor 4 is represented in Figure 4.37. Factor 4 is a typical marine factor as it is dominated by Na^+ and Cl^-. Factor 4 accounts for approximately 75-80% of the measured concentrations of Na^+ and Cl^-. Following these two abundant species, SO_4^{2-}, Mg^{2+} and K^+ constitute 7,5%, 3.7% and 1.1% of the total dissolved solids in sea water (Mero, 1965). This factor also accounts for 2.3%, 53% and 21% of measured concentrations of SO_4^{2-}, Mg^{2+} and K^+, respectively.

Unlike the other factors, Factor 4 has higher scores in winter months especially in January. The formation of sea salt aerosol is impacted by various meteorological and environmental aspects such as wind speed, temperature of the sea surface and precipitation. The main process by which the sea salt aerosol is introduced to the atmosphere is the wind stress on the sea surface. Generally, this occurs by a mechanism called bubble bursting when air is mixed into the water by breaking waves (Lundgren, 2010). The higher PMF scores in winter for this factor suggests extensive and frequent storm activities which supports the bubble bursting mechanism and further explains this factor being a marine factor. Please note that monthly variation in Factor 4 scores are very similar to monthly variation in concentrations of Na and Cl which were discussed in previous sections of the manuscript.

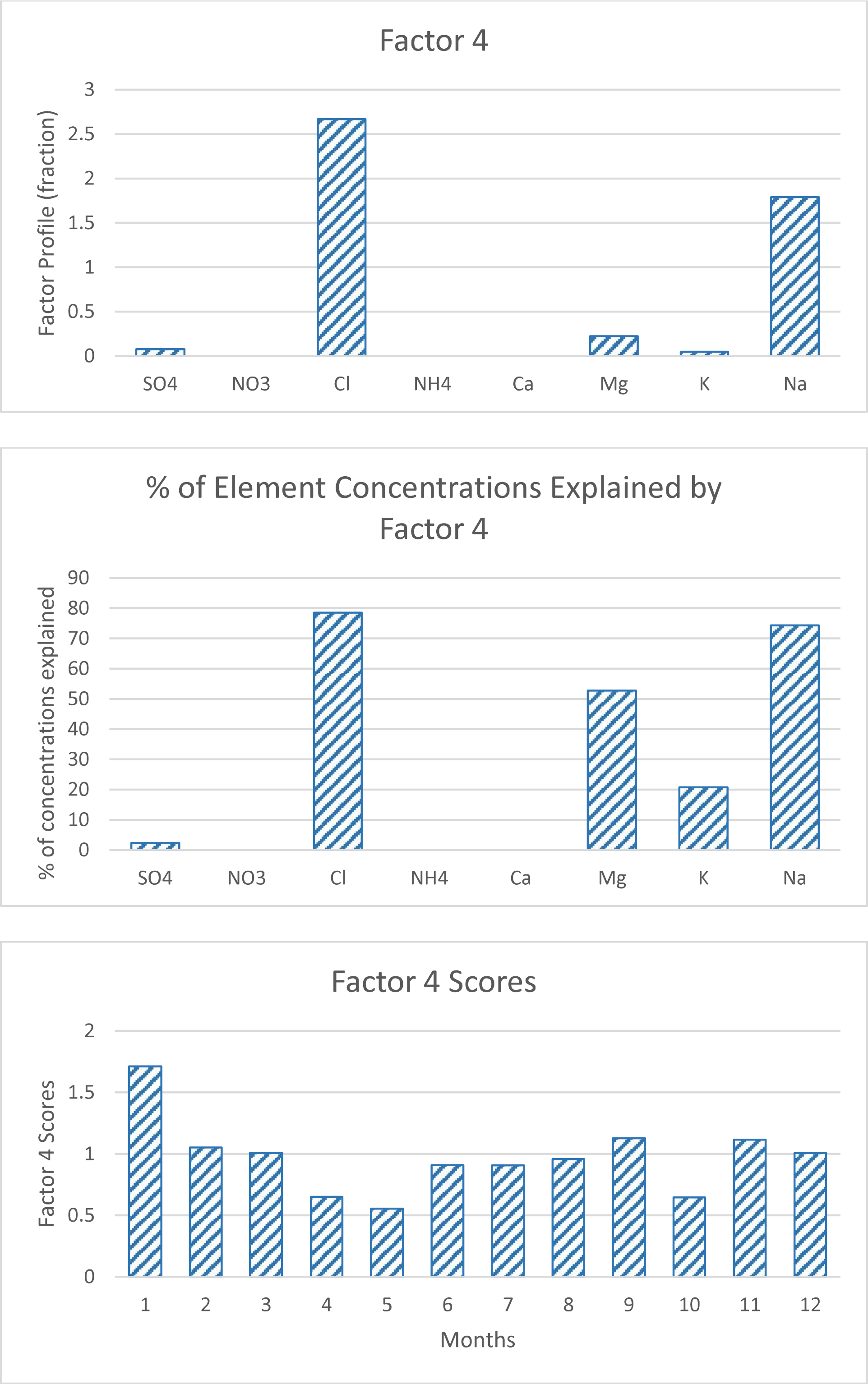

Figure 4.37 Factor 4 Diagnostics: (a) factor loadings, (b) fractions of ion concentrations explained by factor 4 and (c) monthly variations of factor scores

4.7. Deposition Fluxes

Natural deposition is a mechanism that cleans the atmosphere. In contrast, this mechanism also provides a pathway for nutrients and contaminants present in air to reach aquatic and terrestrial ecosystems (Pan and Wang, 2015). Thus, atmospheric deposition can be an important source for transfer of pollutants from atmosphere to marine and terrestrial environment (Buehler and Hites, 2002; Sakata and Marumoto, 2005).

Wet deposition fluxes of ions and other parameters are calculated by multiplying measured concentration data (mg/L) with rainfall (mm) recorded for each event and then summing the calculated event-based fluxes monthly or annually dependeding on the time interval that is desired. This standard procedure requires consistent collection of data throughout the study period for all rain events. Unfortunately, for this study, number of missed events (rain events which were not sampled) was too high in order to conduct this method. To avoid underestimation of deposition fluxes related to missed rain events, wet deposition fluxes of ions were calculated by multiplying median concentrations of ions in each month with long-term average monthly rainfall data obtained for the Amasra Station. Monthly fluxes were then summed up to obtain seasonal and annual fluxes. This approach is used in other studies in our group (Işıkdemir, 2006; Ayaklı, 2014).

The monthly variation of deposition fluxes is represented in Figure 4.38 for pollution-derived ions and in Figure 4.39 for marine and crustal ions. Also, seasonality of the data is represented in Table 4.13 with winter to summer ratios.

As discussed in the previous sections in the manuscript 60% of the total annual rain occurs during the winter months (October to March) and the 40% occurs in the summer months (April to September). Thus, higher fluxes are expected in winter months due to higher percentage of rainfall is recorded in the winter months. In Table 4.9 the winter to summer ratio was highest for H^+ ion with a value of 25.6 and lowest ratio was recorded for Ca^{2+} ion with a value of 0.67. Also, from the table it can be seen that the situation of higher flux values expected for winter months is valid for all ions except Ca^{2+} higher wet deposition fluxes in winter months, as expected. As pointed earlier in the manuscript, Ca^{2+} has the highest summer – winter difference in its concentration. Although summer rainfall amount is smaller than winter rainfall amount at Amasra, Ca^{2+} flux is higher in summer due to its very high summer concentration.

A similar pattern in wet deposition fluxes of ions (and also elements) was observed in a previous study at Amasra by our group (Alagha and Tuncel, 2003). The highest winter to summer ratio flux is recorded for H^+. In Figure 4.38 it can be also seen that the flux is significantly lower than those obtained in winter months. This can be related to neutralizing effect being much more extensive at summer months. The monthly variation of wet deposition fluxes for marine ions show a well-defined pattern being higher in winter months and lower in summer months as expected.

Figure 4.38 Monthly variation of Deposition Fluxes for pollution-derived Ions

Figure 4.39 Monthly variation of Deposition Fluxes for Marine and Crustal Ions

Table 4.13. *Seasonal Fluxes of Major Ions and Their Winter to Summer Ratios*

	Winter	**Summer**	**Winter/Summer**
H^+	96.4	3.8	25.59
SO_4^{2-}	19464.4	13982.6	1.39
NO_3^-	9871.1	9525.4	1.04
NH_4^+	4696.3	4629.7	1.01
Na^+	12844.8	7472.0	1.72
Cl^-	18997.3	11246.5	1.69
Ca^{2+}	6693.4	9925.6	0.67
Mg^{2+}	2129.5	1711.7	1.24
K^+	1150.1	1016.6	1.13

The annual variation of the deposition fluxes for Amasra Station was provided between the years 2005 to 2015 in Figure 4.40 and 4.41. Measurements of some of the ions has started in 2005 so starting year for deposition flux calculation is taken as 2005. In 2016 there is only data recorded until June so since the half of the year is missing, thus 2016 is excluded from the calculation. This is an important information and demonstrate that acidity of rainwater on our Black Sea coast is increasing while it is decreasing in most of the Europe.

Sulfate flux started to increase between the years 2005 to 2008. After showing a decrease in 2009 sulfate flux started increasing between the years 2009 and 2011. After 2011 until 2015 it showed a slight decreasing trend. Similar situation was recorded for Nitrate wet deposition flux. It decreased between 2005 and 2009. Then showed an increase 2010 and 2011. After this increase it followed a decreasing trend between 2011 and 2015. NH_4^+ ion on the other hand does not have a well-defined variation throughout the years. Variability in NH_4^+ flux may reflect variations in fertilizer use patterns in the region.

As depicted in Figure 4.40, crustal and marine ions do not show a well-defined trend in deposition fluxes throughout the years.

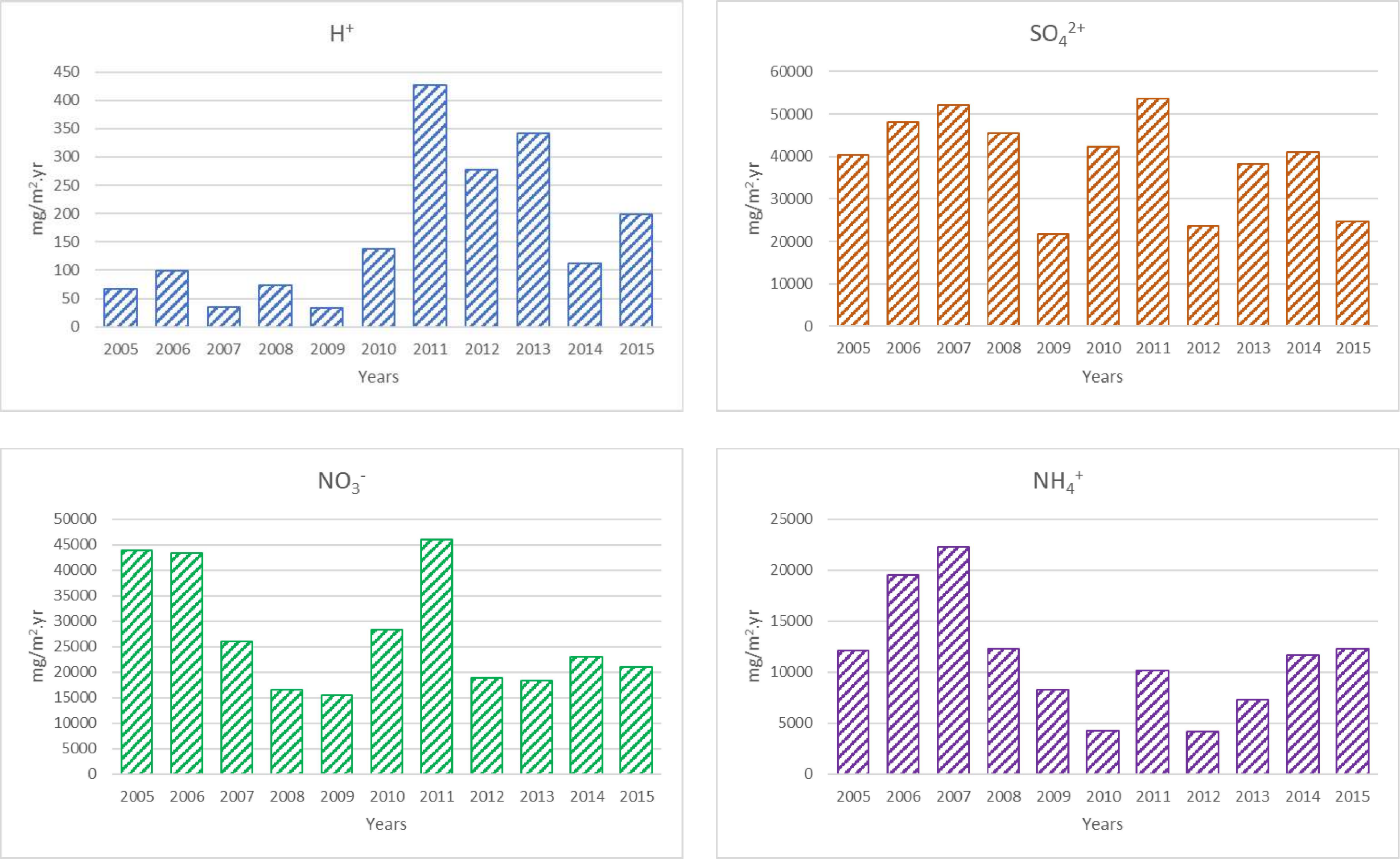

Figure 4.40 Annual variation of Deposition Fluxes for pollution-derived Ions

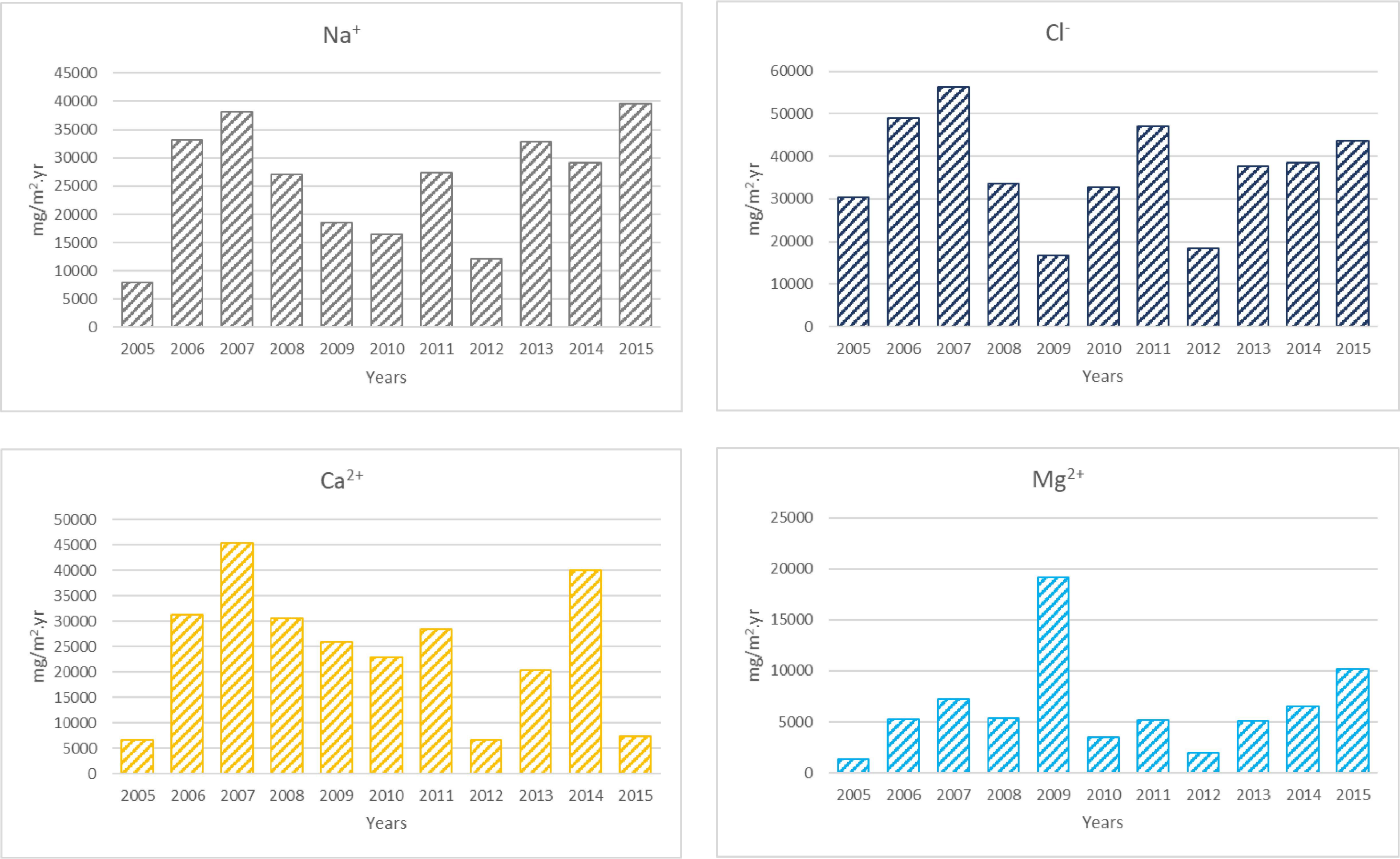

Figure 4.41 Annual variation of Deposition Fluxes for Marine and Crustal Ions

The episodic nature of wet deposition fluxes is another important topic. The percentage of events accounting for 90% of wet deposition fluxes of each ion is depicted in Figure 4.42. Rainfall has an episodic nature thus; wet deposition is also episodic by nature. As seen from Figure 4.42, the ion having the most episodic nature is H^+ in which 24.4% of the events accounted for 90% of this ions deposition. On the other hand, for the rest of the ions approximately 44%-60% of rain events accounted for 90% of their deposition. For this study, at Amasra Station 61% of events account for 90% of the annual deposition. Other than the episodic nature of rainfall another reason effecting the highly episodic nature of H^+ deposition flux is the neutralization effect of ions like Ca^{2+}. Therefore, hydrogen ion becomes much more episodic than other measured ions.

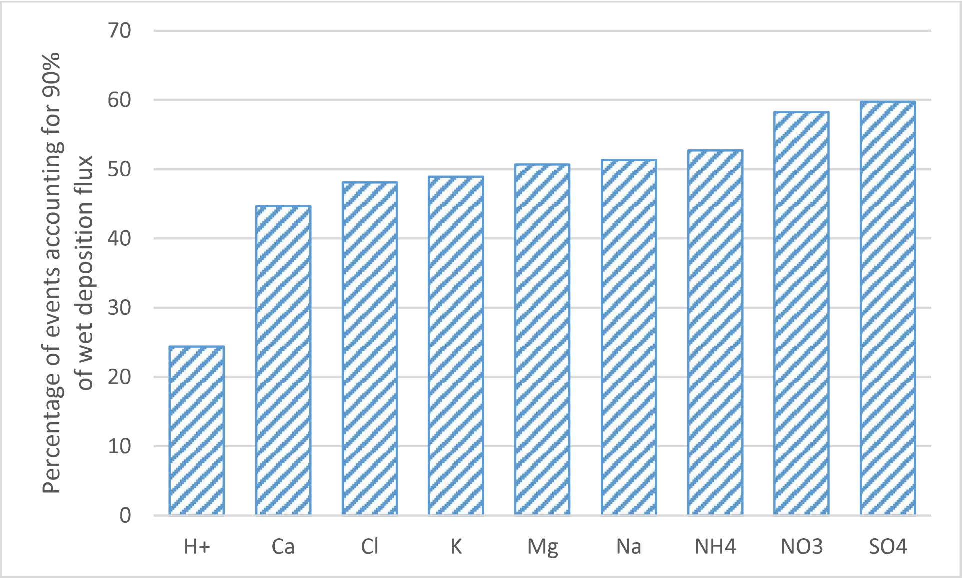

Figure 4.42 Episodic Nature of Wet Deposition Fluxes: Percentage of Rain Events Accounting for 90% of Wet Deposition Fluxes of Ions

CHAPTER 5

CONCLUSION

In this study, major ions in collected rainwater samples from Amasra Station was measured by ion chromatography between the years 2004 and 2016. The total number of samples analyzed in this work was 820.

The frequency histograms revealed all ions in this study have a right-skewed distribution. Only, NH_4^+, Ca^{2+}, Na^+ showed log-normal distribution.

Ionic balance of samples was investigated by calculating the ratio of sum of anions to sum of cations. The outcome was presented on a scatter graph. Sum of anion to sum of cation ratios were found to be lower than 1.0 for Amasra Station, which indicates that there is anion deficiency. This deficiency was linked to unmeasured HCO_3^- concentration.

Highest contribution to the total ions mass was Cl^- (23%). Cl^- was followed by SO_4^{2-} (22%), Na^+(15%), NO_3^-(14%) and Ca^{2+}(12%). These five top contributors accounted for 85 % of total ion mass. Na^+ and Cl^-together had a total contribution of 38% to total ion mass. This high contribution is attributed to Amasra Station being located near the Black Sea coast of Turkey.

The annual average value for pH was found to be 5.57 for samples collected at Amasra Station which is approximately equal to natural acidity of rainwater. Approximately, 34% of the samples had pH lower than 5 and 19% had pH lower than 4.5. Approximately, 66% of the samples cannot be considered as acid rain. In summer higher pH values were observed, whereas in winter the frequency of occurrences shifted to lower pH values in winter. Results indicated that neutralization extensively takes place in summer season. $CaCO_3$ was found to be the main driver of neutralization taking place in the study area.

The trajectory analysis is conducted between the years 2004 to 2016 namely 13 years by calculating 5-day long back trajectories with starting altitudes 500 m, 1000 m and 1500 m for each day. Residence time analysis revealed that the locations the air masses spend the majority of time are the western half of Turkey, Balkan countries which have a coast on the Black Sea such as Bulgaria and Romania and other countries that have coast on the Black Sea particularly Ukraine and Russia. Residence times were also investigated in terms of dry and wet seasons. In dry season it is found that the air masses spend more time in North and North eastern part of the study area. On the other hand, in wet season, Western half of Turkey and Western Europe were the regions where the air masses were found to spend the majority of the time. Sector- based flow climatology showed similar results as sectors that the air masses spend longer time are N, NE, W and NW. In summer, significantly longer residence times are observed in N, NE and E sectors whereas in winter significantly longer residence times are observed in SE, S, SW and W. In sector NW the results are similar for both seasons. Cluster analysis was also carried out as part of flow climatology and 7 clusters were selected as optimum to group the trajectories.

The chemical composition of precipitation in Amasra was compared with similar stations located at rural sites in Turkey. Moreover, ion concentrations measured in this study were compared with the EMEP database for same years with this study. As a result of the comparison, all pollution derived ions such as SO_4^{2-} , NO_3^- and NH_4^+ are found to be higher than Europe. This is attributed to the station being close to high emission sites like Ukraine and Russsia. Crust originated ion Ca^{2+} concentrations are also found to be higher than Europe which is attributed to calcareous nature of soil in Turkey.

PMF model revealed four factors consisting of two anthropogenic, one marine and one crustal factor. PSCF applied to scores of anthropogenic factor and potential source areas were identified as NE Mediterranean coast of Libya and Algeria, middle of Iran-Iraq boundary line, Russia, NW coast of Caspian Sea, Azerbaijan, Georgia and central Black Sea region of Turkey.

CHAPTER 6

RECOMMENDATIONS FOR FUTURE RESEARCH

Major ions were included and evaluated in this study. However, trace elements, bicarbonate ion and organic compounds were not measured and the measurements should be included in further studies in order to fully understand the composition of rainwater samples.

The PMF analysis was conducted only for major ions. Since more specific source indicators such as trace elements and organic compounds were excluded, all anthropogenic ions coincided into one factor. If specific indicators are also included in further research, more than one group can be determined in the PMF analysis.

Additionally, dry deposition data can be collected in future works at one station in order compare with the wet deposition. The evaluation of effect of two types of deposition can be investigated by this manner.

Finally, the samplings should continue in the upcoming years in order to have more data for the trend analysis and obtain much more robust results.

REFERENCES

Al-Momani, F., Güllü, G., Ölmez, I., Eler, Ü., Örtel, E., Şirin, G., & Tuncel, G. (1997). Chemical composition of eastern Mediterranean aerosol and precipitation: Indications of long-range transport. *Pure & App. Chem, 69*, 41-46.

Brook, J., Vega, E., & Watson, J. (2008). *Receptor Methods.*

Abdulmogith, S., & Harrison, R. M. (2005). *The Use of Trajectory Cluster Analysis to Examine the Long-Range Transport of Secondary Inorganic Aerosol in the UK.* Birmingham, United Kingdom: Division of Environmental Health & Risk Management School of Geography, Earth & Environmental Sciences The University of Birmingham.

Alagha, O., & Tuncel, G. (2003). Evaluation of air quality over the Black Sea: Major ionic composition of rainwater. *Water, Air, & Soil Pollution*, 87-96.

Al-Khashman, O. (2005). Study of chemical composition in wet atmospheric precipitation in Eshidiya area, Jordan. *Atmospheric Environment, 39*, 6175–6183.

Al-Momani, I. F., Aygun, S., & Tuncel, G. (1998). Wet deposition of major ions and trace elements in the eastern Mediterranean basin. *Geophys. Res., 103*, 8287-8299.

Altwicker, E. R., & Mahar, J. T. (1984). NH4/Ca ratios in different forms of atmospheric deposition: Interpretive potential. *Atmospheric Environment, 18*, 1875-1888.

Amato, F., Pandolfi, M., Viana, M., Querol, X., Alastuey A., & Moreno, T. (2009). Spatial and chemical patterns of PM10 in road dust deposited in urban environment. *Atmospheric Environment*, 1650-1659.

Anttila, P., Paatero, P., Tapper, U., & Jarvinen, O. (1995). Source identification of bulk wet deposition in Finland by positive matrix factorization. *Atmospheric Environment, 29*, 1705-1718.

Aron, J. L., & Patz, J. A. (2001). *Ecosystem Change and Public Health: A Global Perspective.* The Johns Hopkins Press.

Ayaklı, G. (2014, February). Chemical Composition of Precipitation in Different Parts of Turkey. *M. Sc. Thesis*. Ankara: Middle East Technical University.

Bakan , G., & Büyükgüngör, H. (2000). The Black Sea. *Marine Pollution Bulletin*, 24-43.

Balcılar, İ. (2018). *Chemical Composition of Atmospheric Particles as a Tool to Identify Sources Affecting Aerosol Population in the Eastern Black Sea Atmosphere.* Ph.D. Thesis, Department of Environmental Engineering: Middle East Technical University, Ankara.

Balcılar, İ., Zarasız, A., Kalaycı, Y., Doğan, G., & Tuncel, G. (2014). Chemical composition of eastern black sea aerosol-preliminary results. *Science of the Total Environment*, 422-428.

Bhargava, S., & Bhargava, S. (2013). Ecological Consequences of the Acid Rain. *IOSR Journal of Applied Chemistry*, 19-24.

Bhaskar, B. V., & Mehta, V. M. (2010). Atmospheric Particulate Pollutants and their Relationship with Meteorology in Ahmedabad. *Aerosol Air Qual. Res., 10*, 301–315.

Biegalski, S., & Hopke, P. K. (2004). Total Potential Source Contribution Function Analysis of Trace Elements Determined in Aerosol Samples Collected near Lake Huron. *Environmental Science Technology, 38*, 4276-4284.

Blanchard, D. C., & Woodcock, A. H. (1957). Bubble Formation and Modification in the Sea and its Meteorological Significance. *Tellus, 9*, 145–158.

Bricker, O. P., & Rice, K. C. (1993). Acid Rain. *Annual Review of Earth and Planetary Sciences, 21*, 151-174.

Buehler, S. S., & Hites, R. A. (2002). The Great Lakes integrated atmospheric deposition network. *Environmental Science and Technology*, 354A–359A.

Burns, D. A. (2016). Acid Rain and its Environmental Effects: Recent Scientific Advances. *Atmospheric Environment*, 1-4.

Carroll, D. (1962). *Rainwater as a Chemical Agent of Geologic Processes A Review.* Washington: United States Goverment Printing Office.

Charlson, R. J., & Rodhe, H. (1982). Factors controlling the acidity of natural rainwater. *Nature, 295*, 683-685.

Chiapello, I., Bergametti, G., Chatenet, B., Bousquet, P., Dulac, F., & Santos Soares, E. (1997). Origins of African dust transported over the northeastern tropical Atlantic. *Journal of Geophysical Research* , 701-709.

Clarke, A., Kapustin, V., Howell, S., Moore, K., Lienert, B., Masonis, S., . . . Covert, D. (2003). Sea-Salt Size Distributions from Breaking Waves: Implications for Marine Aerosol Production and Optical Extinction Measurements during SEAS. *J. Atmos. Ocean. Technol.*, 1362–1374.

Claudio, A. B., Larsen, B., Amato, F., El Haddad, I., Favez, O., Harrison, R. M., . . . Viana, M. (2014). *European Guide on Air Pollution Source Apportionment with Receptor Models.* Ispra, Italy: Joint Research Center.

Comero, S., Capitani , L., & Gawlik, B. (2009). *Positive Matrix Factorisation (PMF).* JRC Scientific and Technical Reports.

Cooper, J. A., & Watson Jr., J. G. (2012). Receptor Oriented Methods of Air Particulate Source Apportionment. *Journal of the Air Pollution Control Association, 30*, 1116-1125.

Das, R., Das, S. N., & Misra, V. N. (2005). Chemical composition of rainwater and dustfall at Bhubaneswar in the east coast of India. *Atmospheric Environment*, 5908–5916.

Deshmukh, D. K., Deb, M. K., Tsai, Y. I., & Mkoma, S. L. (2011). Water Soluble Ions in PM2.5 and PM1 Aerosols in Durg City, Chhattisgarh, India. *Aerosol and Air Quality Research, 11*, 696–708.

Ding, H., Lang, Y.-C., Liu, C.-Q., & Liu, T.-Z. (2013). Chemical characteristics and δ34S–SO4 of acid rain: Anthropogenic sulfate deposition and its impacts on CO2 consumption in the rural karst area of southwest China. *Geochemical Journal, 47*, 625-638.

Doğan, G. (2005). *Comparison of the rural atmosphere aerosol compositions at different parts of Turkey.* M.Sc. Thesis, Department of Environmental Engineering: Middle East Technical University, Ankara.

Dutton, J. A. (1986). *The Ceaseless Wind an Introduction to the Theory of Atmospheric Motion.* Dover, New York.

Eldin , A., & Ramadan , K. (2004). Acid Deposition Phenomena. *TESCE, 30*, 1369-1389.

EMEP. (n.d.). *EMEP*. Retrieved July 18, 2019, from EMEP Web Site: https://www.emep.int/

Environment Agency. (2007). *Processes and parameters influencing the oxidation of SO2 and NOX in plumes.* Bristol: Environment Agency.

EPA. (2004). *Acid Rain—why it is a concern.*

EPA. (2017). *United States Environmental Protection Agency.* Retrieved April 06, 2019, from United States Environmental Protection Agency Web Site: https://www.epa.gov/acidrain/what-acid-rain

Flues, M., Hama, P., Lemes, M., Dantas, E., & Fornaro, A. (2002). Evaluation of the rainwater acidity of a rural region due to a coal-fired power plant in Brazil. *Atmospheric Environment, 36*, 2397–2404.

Francy, D. S., Jones, A. L., Myers, D. N., Rowe, G. L., Eberle, M., & Sarver, K. M. (1998). *Quality-Assurance/Quality-Control Manual for Collection and Analysis of Water-Quality Data in the Ohio District, U.S. Geological Survey.* Ohio: USGS.

Galloway, J. N. (1995). Acid deposition: Perspectives in time and space. *Water, Air & Soil Pollution, 85*, 15-23.

Gao, N., Cheng , M.-D., & Hopke, P. K. (1993). Potential source contribution function analysis and source apportionment of sulfur species measured at Rubidoux CA during the Southern California Air Study. *Analytica Chimica Acta, 277*, 369-380.

Giardina, M., & Buffa, P. (2018). A new approach for modeling dry deposition velocity of particles. *Atmospheric Environment*, 11-22.

Gilbert, R. O. (1987). *Statistical Methods for Environmental Pollution Monitoring.* John Wiley & Sons Inc.

Golobočanin, D., Žujić , A., Milenković , A., & Miljević, N. (2008). Precipitation composition and wet deposition temporal pattern in Central Serbia for the period from 1998 to 2004. *Environ Monit Assess, 142*, 185-198.

Gorham, E. (1961). Factors influencing supply of major ions to inland waters, with special reference to the atmosphere. *Geol. Soc. Am. Bull.* , 795-840.

Grantza, D. A., Garnerb, J., & Johnson, D. W. (2003). Ecological effects of particulate matter. *Environment International, 29*, 213-239.

Gugamsetty, B. (2012). Source characterization and apportionment of PM10, PM2.5 and PM0.1 by using positive matrix factorization. *Aerosol and Air Quality Research, 12*, 476-491.

Güllü, G., Doğan, G., & Tuncel, G. (2005). Atmospheric trace element and major ion concentrations over the eastern Mediterranean Sea: Identification of anthropogenic source regions. *Atmospheric Environment, 39*, 6376–6387.

Güllü, G., Ölmez, İ., & Tuncel, G. (1998). Atmospheric trace element concentrations over the eastern Mediterranean Sea: Factors affecting temporal variability. *Journal of Geophysical Research*, 21943-21954.

Gülsoy, G., Tanyaç , M., & Ertürk, F. (1999). Chemical analyses of the major ions in the precipitation of Istanbul, Turkey. *Environmental Pollution, 105*, 273-280.

Hopke, P. K. (2009). Air Quality and Ecological Impacts: Relating Sources to Effects. *Developments in Environmental Science*.

Hüttl, R. F., & Schaaf, W. W. (1997). *Magnesium Deficiency in Forest Ecosystems.* Cottbus, Germany: Springer Science.

Işıkdemir, Ö. (2006). *Investigation of 8-year long composition record in the Eastern Mediterranean precipitation.* M.Sc. Thesis, Department of Environmental Engineering: Middle East Technical University, Ankara.

IUPAC. (1995). *NOMENCLATURE IN EVALUATION OF ANALYTICAL METHODS INCLUDING DETECTION AND QUANTIFICATION CAPABILITIES* . Great Britain: IUPAC.

Jackson, P. E. (2000). Ion Chromatography in Environmental Analysis. *Encyclopedia of Analytical Chemistry*, 2779-2801.

Jacob, D. J. (1999). *Introduction to Atmospheric Chemistry.* Chichester: Princeton University Press.

Jia, J., & Gao, Y. (2017). Acid deposition and assessment of its critical load for the environmental health of waterbodies in a subtropical watershed, China. *Journal of Hydrology*, 155-168.

Kalaiarasan, G., Balakrishnan, R. M., Sethunath, N. A., & Manoharan, S. (2018). Source apportionment studies on particulate matter (PM10 and PM2.5) in ambient air of urban Mangalore, India. *Journal of Environmental Management, 217*, 815-824.

Kotz, J., Treichel, P., & Townsend, J. (2009). *Chemistry and Chemical Reactivity.* Belmont, USA: Thomson Higher Education.

Lacaux, J. P., Delmas, R., Kouadio, G., Cros, B., & Andreae, M. O. (1992). Precipitation Chemistry in the Mayomb Forest of Equatorial Africa. *Journal of Geophysical Research*, 6195-6206.

Lee, E., Chan, C. K., & Paatero, P. (1999). Application of positive matrix factorization in source apportionment of particulate pollutants in Hong Kong. *Atmospheric Environment, 33*, 3201-3212.

Liang, J. (2013). *Chemical Modeling for Air Resources: Fundamentals, Applications and Corroborative Analysis.* Academic Press.

Likens, G. E., & Bormann, F. H. (1974). Acid rain: a serious regional environmental problem. *Science*, 1176-1179.

Lundgren, K. (2010). *Direct Radiative Effects of Sea Salt on the Regional Scale.* Karlsruhe: KIT Scientific Publishing.

Marks, R., Górecka, E., Mc Cartney, K., & Borkowski, W. (2017). Rising bubbles as mechanism for scavenging and aerosolization of diatoms. *Ocean Sci. Discuss.*, 7-19.

Meng, Z., Zhang, R., Lin, W., Jia, X., Yu, X., Yu, X., & Wang, G. (2014). Seasonal Variation of Ammonia and Ammonium Aerosol at a Background Station in the Yangtze River Delta Region, China. *Aerosol and Air Quality Research, 14*, 756-766.

Menz, F. C., & Seip, H. M. (2004). Acid rain in Europe and the United States: an update. *Environmental Science & Policy, 7*, 253-265.

Mero, J. L. (1965). *The mineral resources of the sea.* California: Elsevier Publishing Company.

Migliavacca, D., Teixeira, E. C., Wiegand, F., Machado, A. C., & Sanchez, J. (2005). Atmospheric precipitation and chemical composition of an urban site, Guaíba hydrographic basin, Brazil. *Atmospheric Environment, 39*, 1829-1844.

Moody, J. L., & Samson, P. J. (1989). The influence of atmospheric transport on precipitation chemistry at two sites in the Midwestern United States. *Atmospheric Environment, 23*, 2117-2132.

National Academy of Engineering and National Research Council. (2008). *Energy futures and urban air pollution.* Washington D.C.: The National Academies Press.

National Atmospheric Deposition Program. (2019). *NADP.* Retrieved April 2019, from NADP Web site: http://nadp.slh.wisc.edu/educ/sample.aspx

OSU. (2011). *Ion Chromatography- Theory*. Retrieved April 11, 2019, from The Ohio Consortium for Undergraduate Research Web Site: https://research.cbc.osu.edu/reel/research-modules/environmental-chemistry/instrumentation/instrument-calibration/ion-chromatography-theory/

Özsoy, T., Türker, P., & Örnektekin , S. (2008). Precipitation chemistry as an indicator of urban air quality in Mersin Northeastern Mediterranean Region. *Water, Air, and Soil Pollution*, 69-83.

Öztürk, F., Zararsız , A., Dutkiewicz, V. A., Husain, L., Hopke, P. K., & Tuncel, G. (2012). Temporal variations and sources of eastern Mediterranean aerosols based on a 9-year observation. *Atmospheric Environment, 61*, 463-475.

Paatero, P., & Tapper , U. (1994). Positive Matrix Factorization: a non-negative factor model with optimal utilization of error estimates of data values. *Environmetrics, 5*, 111-126.

Pan, Y. P., & Wang, Y. S. (2015). Atmospheric wet and dry deposition of trace elements at 10 sites in Northern China. *Atmospheric Chemistry and Physics*, 951-972.

Pant, P., & Harrison, R. M. (2013). Estimation of the contribution of road traffic emissions to particulate matter concentrations from field measurements: a review. *Atmospheric Environment, 77*, 78-97.

Peden, M. E., Bachman, S. R., Kenni , O. J., Demir, B., James, K. O., Kaiser, B. W., . . . Slater , M. J. (1986). *Methods for Collection and Analysis of Precipitation.* Illinois.

Polissar, A. V., Hopke, P. K., Malm, W. C., & Sisler, J. (1996). The ratio of aerosol optical absorption coefficient to sulfur concentrations, as an indicator of smoke from forest fires when sampling in polar regions. *Atmospheric Environment, 30*, 1147-1157.

Radojevic, M., & Harrison, R. M. (1992). *Atmospheric Acidity: Sources, Consequences and Abatement.* Essex, England: Elsevier Applied Sciences.

Rauf, M. A., & Hanan, A. (2009). Quality Assurance Considerations in Chemical Analysis,. *Qual Assur J*, 16-21.

Rodhe , H. (1972). A study of lhe sulfur budget for the atmosphere over Northern Europe. *Tellus*, 128-138.

Rodhe, H., Cowling, E., Galbally, I., Galloway , J., & Herrera, R. (1988). *Acidification in Tropical Countries.* Chichester, England: John Wiley & Sons Ltd.

Russell , L. M., & Singh, E. G. (2006). Submicron Salt Particle Production in Bubble Bursting. *Aerosol Science and Technology*, 664-671.

Sakata, M., & Marumoto, K. (2005). Wet and dry deposition fluxes of mercury in Japan. *Atmospheric Environment, 39*, 3139-3146.

Salve, P. R., Maurya, A., Wate, S. R., & Devotta, S. (2008). Chemical Composition of Major Ions in Rainwater. *Bulletin of Environmental Contamination and Toxicology, 80*, 242–246.

Santos, P. S., Otero, M., Santos, E. B., & Duarte, A. C. (2011). Chemical composition of rainwater at a coastal town on the southwest of Europe: What changes in 20 years? *Science of the Total Environment*, 3548–3553.

Sarkodie, S. A., Strezov, V., Jiang, Y., & Evans, T. (2019). Proximate determants of particulate matter (PM 2.5) emission, mortality and life expectancy in Europe, Central Asia, Australia, Canada and the US. *Science of the Total Environment, 683*, 489-497.

Singh, A., & Agrawal, M. (2008). Acid rain and its ecological consequences. *Journal of Environmental Biology*, 15-24.

Sivaramanan, S. (2015, April 24). Acid rain, causes, effects and control strategies. Battaramulla, Sri Lanka.

Smith , S., Hewitt , C. N., Pollard , S., Kinniburgh , J., Salmond, J., & Kibblewhite , M. G. (2015). *An Introduction to Pollution Science.* (R. M. Harrison, Ed.) Royal Society of Chemistry.

Smith, R. A. (1872). *Air and Rain: The Beginnings of a Chemical Climatology.* London: Longmans, Green and Co.

Steinacker, R. (1984). Airmass and frontal movement around the Alps. *Rivista di Meteorologia Aeronautica, 44*, 85-93.

Stohl, A. (1998). Computation, accuracy and applications of trajectories—a review and bibliography. *Atmospheric Environment, 32*, 947–966.

Stohl, A., Eckhardt, S., Forster, C., James, P., Spichtinger, N., & Seibert, P. (2002). A replacement for simple back trajectory calculations in the interpretation of atmospheric trace substance measurements. *Atmospheric Environment, 36*, 4635–4648.

Thibodeaux, L. J., & Mackay, D. (2011). *Handbook of Chemical Mass Transport in the Environment.* New York: CRC Press.

Tiwari, S., Ranade, A., & Singh, D. (2006). Study of Chemical species in rainwater at Ballia, a rural environment in Eatern Uttar Pradesh, İndia,. *Indian Journal of Radio & Space Physics*, 35-41.

Tokgöz, D. D. (2013). *Temporal Variation in Aerosol Composition at Northwestern Turkey.* Ph.D. Thesis, Department of Environmental Engineering : Middle East Technical University, Ankara.

Tokgöz, D. D., & Tuncel, G. (2015). Ionic composition of aerosols in northwestern Turkey. *International Journal of Global Warming, 7*, 161-172.

United States Environmental Protection Agency. (2009, April 27). *EPA* . Retrieved from EPA Web site: https://www.epa.gov/sites/production/files/2015-06/documents/blanks.pdf

Valenta, P., Nguyen, V. D., & Norburg, H. W. (1986). Acid and heavy metal pollution by wet deposition. *Sci. Tot. Environ.*, 311-320.

Vet, R., Artz, R. S., Carou, S., Shaw, M., Ro, C.-U., Aas, W., . . . Reid, N. W. (2014). A global assessment of precipitation chemistry and deposition of sulfur, nitrogen, sea salt, base cations, organic acids, acidity and pH, and phosphorus. *Atmospheric Environment, 93*, 3-100.

Wang, H., & Han, G. (2011). Chemical composition of rainwater and anthropogenic influences in Chengdu, Southwest China. *Atmospheric Research, 99*, 190-196.

Wang, Y. Q., Zhang, X. Y., & Draxler, R. R. (2008). *TrajStat: GIS-based software that uses various trajectory statistical analysis methods to identify potential sources from long-term air pollution measurement data.* Beijing, China: Center for Atmosphere watch and services, Chinese Academy of Meteorological Sciences .

Wang, Z.-s., Wu, T., Shi, G.-l., Fu, X., Tian, Y.-z., Feng, Y.-c., . . . Zhang, W.-j. (2012). Potential Source Analysis for PM10 and PM2.5 in Autumn in a Northern City in China. *Aerosol and Air Quality Research, 12*, 39-48.

Worthy, D. E., Chan, E., Ishizawa, M., Chan, D., Poss, C., Dlugokencky, E. J., & Levin, I. (2009). Decreasing anthropogenic methane emissions in Europe and Siberia inferred from continuous carbon dioxide and nethane observations at alert, Canada. *Journal of Geophysical Research: Atmospheres, 114*.

Yatkın, S., & Bayram, A. (2008). Source apportionment of PM10 and PM2.5 using positive matrix factorization and chemical mass balance in Izmir. *Science of the Total Environment, 390*, 109-123.

Yılmaz, R. F. (2010, May). *Development of GIS Based Trajectory Statistical Analysis Method to Identify Potential Sources of Regional Air Pollution.* M.Sc. Thesis, Department of Geodetic and Geographic Information Technologies: Middle East Technical University, Ankara.

Yu, H., He, N., Wang , Q., Zhu, J., Gao, Y., Zhang, Y., . . . Yu, G. (2017). Development of atmospheric acid deposition in China from the 1990s. *Environmental Pollution*, 182-190.

Yücel, G. (2019). Ionic Composition of Precipitation in Marmaris Station. Ankara: Middle East Technical University, Department of Environmental Engineering.

Zhao, M., Li , L., Liu, Z., Chen, B., Huang, J., Cai, J., & Deng, S. (2013). Chemical Composition and Sources of Rainwater Collected at a Semi-Rural Site in Ya'an, Southwestern China. *Atmospheric and Climate Sciences*, 486-496.